FLEXIBLE ELECTRONICS: MATERIALS and DEVICE FABRICATION

by

Nurdan Demirci Sankır

Dissertation submitted to the Faculty of
Virginia Polytechnic Institute and State University
In partial fulfillment of the requirements for the degree of

DOCTOR OF PHILOSOPHY
in
Materials Science and Engineering

APPROVED:

Richard O. Claus, Chairman
Sean Corcoran
Guo-Quan Lu
Daniel Stilwell
Dwight Viehland

December 7, 2005
Blacksburg, Virginia

Keywords: flexible electronics, organic electronics, organic semiconductors, electrical conductivity, line patterning, inkjet printing, field effect transistor.

FLEXIBLE ELECTRONICS: MATERIALS and DEVICE FABRICATION

by

Nurdan Demirci Sankır

ABSTRACT

This dissertation will outline solution processable materials and fabrication techniques to manufacture flexible electronic devices from them. Conductive ink formulations and inkjet printing of gold and silver on plastic substrates were examined. Line patterning and mask printing methods were also investigated as a means of selective metal deposition on various flexible substrate materials. These solution-based manufacturing methods provided deposition of silver, gold and copper with a controlled spatial resolution and a very high electrical conductivity. All of these procedures not only reduce fabrication cost but also eliminate the time-consuming production steps to make basic electronic circuit components. Solution processable semiconductor materials and their composite films were also studied in this research. Electrically conductive, ductile, thermally and mechanically stable composite films of polyaniline and sulfonated poly (arylene ether sulfone) were introduced. A simple chemical route was followed to prepare composite films. The electrical conductivity of the films was controlled by changing the weight percent of conductive filler. Temperature dependent DC conductivity studies showed that the Mott three dimensional hopping mechanism can be used to explain the conduction mechanism in composite films. A molecular interaction between polyaniline and sulfonated poly (arylene ether sulfone) has been proven by Fourier Transform Infrared Spectroscopy and thermogravimetric analysis. Inkjet printing and line patterning methods also have been used to fabricate polymer resistors and field effect transistors on flexible

substrates from poly-3-4-ethyleneoxythiophene/poly-4-sytrensulfonate. Ethylene glycol treatment enhanced the conductivity of line patterned and inkjet printed polymer thin films about 900 and 350 times, respectively. Polymer field effect transistors showed the characteristics of traditional p-type transistors. Inkjet printing technology provided the transfer of semiconductor polymer on to flexible substrates including paper, with high resolution in just seconds.

To my dad, Late Mr. Enver Demirci

would have been very proud to see this day...

and

To my husband, Dr. Mehmet Sankır

Thank you for being with me in this long journey

and lighting up my life

ACKNOWLEDGEMENTS

I would like to give grateful acknowledegements to following all individuals and institutions enabled me to pursue and complete this research work:

Prof. Richard O. Claus, my advisor at the completion of this degree, for all his time, advice, constant encouragement, and support throughout this research project.

Members of my advisory committee, Prof. Sean Corcoran, Prof. Guo-Quan Lu, Prof. Daniel Stilwell and Prof. Dwight Viehland, for their time and guidance for developing this dissertation.

Prof. Richard M. Goff for his providing a wealth of information, and for conducting the mechanical tests.

Dr. Jeffrey B. Mecham for the helpful discussions and sharing his experience with me in polymer science and technology.

Dr. Jennifer K. Lalli for giving me the chance work at NanoSonic Inc. as an intern student.

Dr. Michael J. Bortner and Dr. William L. Harrison for their help and invaluable assistance during my internship at NanoSonic Inc..

NanoSonic Inc. and Alf Knobler Scholarship for their financial support. All employee at NanoSonic Inc. for their friendship and help with various tasks over the years.

Most importantly, my family for encouraging and inspiring me even while they are halfway around the world. I want to especially thank my loving husband for his understanding, patience, and encouragement, without which I would not have succeeded this far.

TABLE OF CONTENTS

LIST OF FIGURES

LIST OF TABLES

CHAPTER 1

INTRODUCTION AND LITERATURE REVIEW

1.1 Introduction

Inorganic semiconductors such as silicon, germainum and gallium arsenide have been widely used in the microelectronics industry for more than forty years [1]. Silicon dioxide insulators and metals such as aluminum and copper are the backbones of this technology. However, solution processable semiconductors and metals are fast replacing traditional inorganic materials due to their numerous advantages. Ease of device fabrication, large area applications, compatibility with light weight and mechanically flexible base materials, and control of electrical, optical and magnetic properties are among the most important advantages of solution processable materials. Solution processable materials are generally organic based materials. Therefore, the branch of electronics that deals with these materials is called organic or plastic electronics. One can also use the term "flexible electronics" to refer to the electronics technology using solution processable organic, inorganic and hybrid materials to build functional devices on mechanically flexible substrates.

[1] (a) E. J. M. Kendall , Transistors, Pergamon Press, New York, 1969, (b) J. T. Wallmark, Field-effect Transistors: Physics, Technology, and Applications, Prentice-Hall, Englewood Cliff (1966), (c) J. J. Liou, F. Schwierz, Solid State Electronics, Vol. 47, 1881-1895 (2003).

Organic electronics technology was born during the 1980's and developed enormously in recent years as a result of combinational studies in chemistry, physics and materials science. Worldwide universities, national laboratories, defense offices, and large companies such as Philips, IBM, Motorola, and Siemens are actively working in the organic electronics area. This technology has the potential to produce light emitting diodes, radio frequency identification tags and even integrated circuits cheaper and more efficient. Organic light emitting diodes and displays have taken their places in current markets [2,3]. It is expected that in the near future more organic electronic devices will be commercially available.

The main aim of this dissertation research has been to design, fabricate, and characterize basic electronic circuit elements on flexible substrates using solution processable materials. Various fabrication methods and different solution processable metals and semiconductors have been used to compare performance and efficiency. Therefore, this first chapter will review the research in flexible electronics. Also, the basic understanding of solution processable semiconductors and metals, flexible electronic device fabrication methods and application areas will be introduced.

The next section compares the characteristics of organic electronics with those of traditional inorganic electronics. This section also introduces the materials used in flexible electronics. The solution processable semiconductors and metals will then be discussed. Some fabrication techniques and application areas will be given in latter sections of this chapter.

1.2 Organic versus Inorganic Electronics

Building a silicon chip requires long and expensive fabrication steps including photolithography and high temperature and high vacuum evaporation steps. Solution processability of organic materials instead provides the direct patterning of active

[2] Universal Display Corporation (http://www.universaldisplay.com)
[3] World Wide Web sites of Philips (http://www.philips.com)

material. It is also possible to manufacture very large area products using "roll-to-roll" fabrication processes similar to the continuous printing press that revolutionized publishing. Moreover, organic materials are compatible with commercially available plastic substrates, which provide mechanical flexibility. Table 1.1 summarizes the most important characteristics of organic electronics that distinguish them from the traditional inorganic semiconductor technology.

Organic materials such as polymers, oligomers, and hybrid composites are promising candidates in aerospace, military and daily life to design flexible, low cost electronic circuits, which could be used to fabricate wearable electronics (also termed "sensitive skin"), smart sensors and full color displays on plastic.

Table 1.1:Characteristics of organic electronics versus silicon electronics [4]

Silicon Technology	**Organic Electronics**
Economic Differentiation	
High cost per unit area	Low cost per unit area
High capital in dedicated plant	Low capital flexible plant
Technological Differentiation	
Small area products	Large area products
Rigid substrates	Flexible substrate
Fragile	Robust

Organic semiconductors and metals, which are fast replacing conventional inorganic materials, have made tremendous advancements in various applications in electronics. The advantages of organic materials include the following:

[4] D. R. Gamota, P. Brazis, K. Kalyanasundaram. J. Zhang, Printed Organic and Molecular Electronics, Kluwer Academic Publishers, Boston (2004).

- Ease of fabrication techniques,
- Possibility of handling under ambient conditions,
- Relatively large scale and inexpensive production,
- Electronic tunability,
- Possibility of making composites and blends with other polymers and inorganic materials,
- Tunable mechanical and chemical characteristics (e.g. solubility, strain stress, crosslinking properties).

Hence, the organic materials are used in, or being developed for, almost all levels of electronics [5] (see Figure 1.1). This wide production range includes the fabrication of individual electronic components such as resistors, capacitors and transistors, and also includes the integration of these basic circuit elements into an active matrix display or into analog or digital circuits. Perhaps one of the most important electronic devices manufactured using conducting polymers is the transistor. Other uses for organic materials include photocells, chemical sensors, and pressure-sensitive materials [6].

[5] (a) W. R. Salaneck, D. T. Clark, E. J. Samuelsen, Science and Applications of Conducting Polymers, Proceedings of the Sixth Europhysics Industrial Workshop held in Lofthus, Norway (1990), (b) K. Yoshino, K. Tada, A. Fujii, E. M. Conwell, A. A. Zakhidov, IEEE Transactions on Electron Devices, Vol. 44, 1315-1324 (1997).

[6] (a) K. Tada, R. Hidayat, M. Hirohata, T. Kawai, S. B. Lee, L. U. Bakhadirov, A. A. Zakhidov, K. Yoshino, Synthetic Metals, Vol. 85, 1349-1350 (1997), (b) T. Someya, T. Sakuri, 2003 IEEE International Electron Devices Meeting (IEDM), December 8 -10 (2003), (c) B. Adhikari, S. Majumdar, Progress in Polymer Science, Vol. 24, 699–766 (2004).

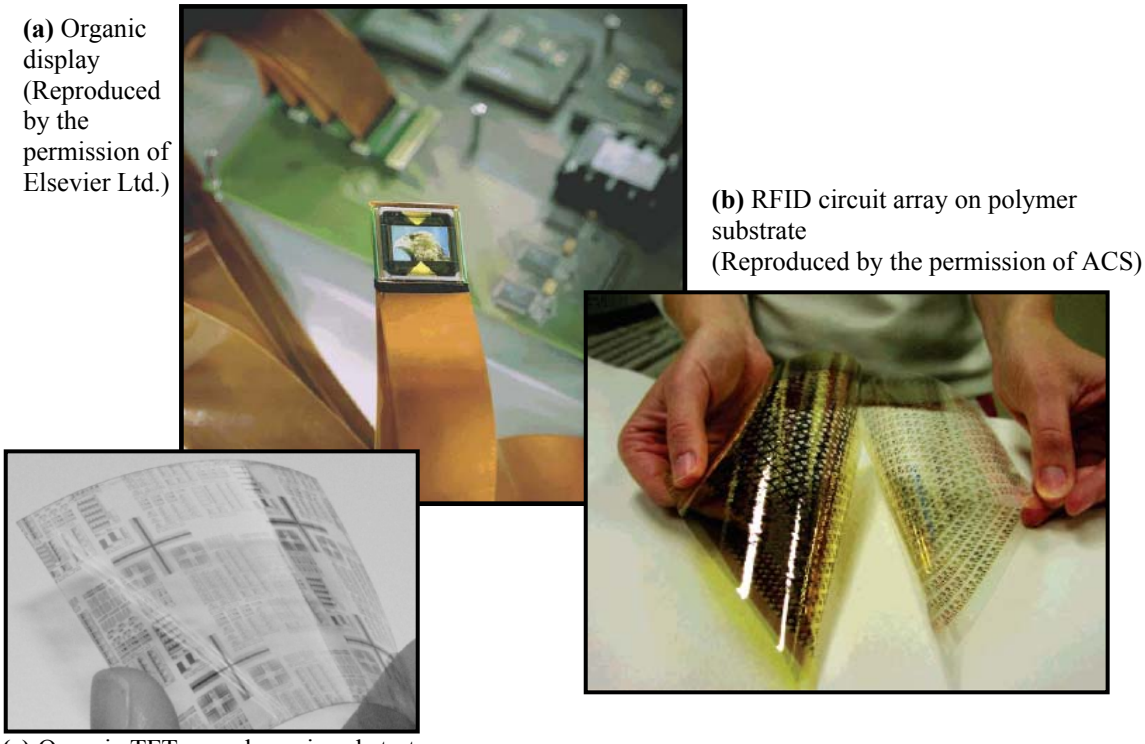

(a) Organic display (Reproduced by the permission of Elsevier Ltd.)

(b) RFID circuit array on polymer substrate (Reproduced by the permission of ACS)

(c) Organic TFT on polymeric substrate (Reproduced by the permission of © 2003 IEEE)

Figure 1.1: (a) Polymer light emitting diode produced by Philips [7] (b) Radio frequency identification (RFID) circuit array fabricated on polymeric substrate [8] (c) Pentacene thin film transistors and integrated circuits on flexible, transparent polyethylene naphthalate film [9]

Materials used in organic electronic technology can be divided into three main groups, which are i) organic dielectrics, ii) organic semiconductors, and iii) organic metals. Most of the polymers are electrically insulating. Therefore, they have been used in both organic and inorganic electronics as resists, encapsulants, and intermediate dielectrics. The high electrical resistivity and good mechanical properties of polymers made them useful as

[7] J. K. Borchardt, Materials Today, Vol. 7, 42-46 (2004)
[8] T. W. Kelley, P. F. Baude, C. Gerlach, D. E. Ender, D. Muyres, M. A. Haase, D. E. Vogel, and S. D. Theiss, Chemistry of Material, Vol. 16, 4413-4422 (2004)
[9] H. Klauk, M. Halik, U. Zschieschang, F. Eder, D. Rohde, G. Schmid, and C. Dehm, IEEE Transaction on Electron Devices, Vol. 52, 618-622 (2005)

passive insulators. Conjugated polymers and organic-inorganic hybrid materials are the well known two members of organic semiconductors. Metal nanoclusters, colloidal nanocrystals of metals and metal nanoparticles can be classified in the "organic metal" group. The following three sections will focus on the materials used in organic electronics.

1.3 Materials Used in Flexible Electronics

Since most of the materials used in flexible and/or organic electronics are polymeric materials, a very brief introduction to the polymer concept will be presented here. A polymeric solid is made of many repeating chemical units or molecules called monomers (see Figure 1.2). Within the backbone of the molecular chain there are strong covalent bonds. However, only weak bonding forces exist between these chains, due to secondary interchain interactions [10].

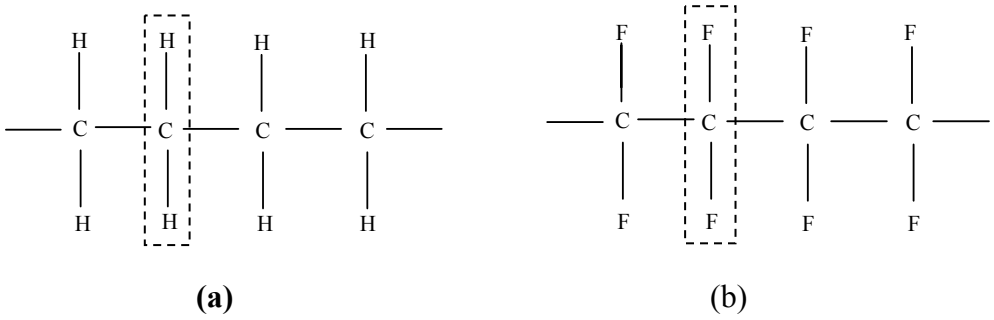

Figure 1.2: (a) Polyethylene (b) Polytetrafluoroethylene (Dashed squares show the repeated units)

Polymers can exhibit various mechanical, electrical and optical properties depending on the synthesis conditions and chemical properties of the backbone. For example, the Young's modulus of rubber can be varied between 10 kPa and 100 MPa. However, the Young's modulus of nylon fiber is 2 GPa and that for fiber of liquid-crystal polymer is

[10] D. I. Bower, An Introduction to Polymer Physics, Cambridge University Press, New York (2002).

350 GPa [11]. The electrical conductivity of insulating polymers is about 10^{-18} S/m whereas that of doped trans-polyacetylene is 10^{7} S/m [12]. Some polymers such as, poly(cis-1,4-isoprene) and poly(chloromethylstyrene) are sensitive to high-energy radiation. If the polymer is exposed to ultraviolet light, the chemical properties, such as solubility, of the polymer in the exposed area change. Photolithography, which is a very well known process in electronics, uses this principle [13].

In order to understand the electronic properties of polymers, it can be considered that every repeating unit is a separate molecule having molecular orbitals in a certain electronic state [14]. Therefore, the number of repeat units determines the electronic properties of the polymer. Some detailed information about the quantum theory of polymeric structures and basic theoretical models and approximations to determine the electronic properties of polymers can be found in Appendix A.

Controllable physical and chemical properties of polymers make them favorable in many areas including electronics. The next section discusses the use of electrically insulating polymeric materials used in flexible electronics. Semiconductor and metallic materials used in this area will be discussed in the following sections.

1.3.1 Insulating Polymers for Flexible Electronics

Polymers have been used in electronics as resists, encapsulants, insulators and intermediate dielectrics for more than forty years. The high electrical resistivity and good mechanical properties of polymers made them useful as a passive material meaning that these materials do not take any active role in the functioning device. In this section the polymeric solids used in flexible electronics as passive elements will be discussed briefly. There are numerous books, handbooks and publications concerning this area; therefore,

[11] G. H. Michler, F. J. Baltá-Colleja, Mechanical Properties of Polymers based on Nanostructure and Morphology, Taylor & Francis, Boca Raton (2005).
[12] H. S. Nalwa, Handbook of Organic Conductive Molecules and Polymers, Vol. 3, John Wiley & Sons, New York (1997).
[13] N. M. Albuquerque, Photolithography: a manual, Tamarind Institute (2002).
[14] J. Mort, G. Pfister, Electronic Properties of Polymers, John Wiley and Sons, New York (1982).

the aim of this section is not to give an extensive review of all potential polymers used in flexible electronics as passive components but instead, to give an overview of insulating polymers for flexible electronics.

1.3.1.1 Radiation sensitive polymers

Radiation-sensitive polymers play an important role in the semiconductor industry. These polymers undergo molecular rearrangement when irradiated and either degrade or crosslink following exposure. Such radiation-sensitive polymers can be used to stencil and transfer a two-dimensional circuit pattern to underlying layers. Using this idea, silicon substrates or printed circuit boards can be patterned to fabricate advanced logic and memory chips [15]. There are many commercially available radiation-sensitive polymers, some of which are summarized in Table 1.2 according to their optical sensitivity.

[15] C. P. Wong, Polymers for Electronic and Photonic Applications, Academic Press Inc., Harcout Brace Jovanovich Publishers, Boston (1993).

Table 1.2: Commercially available radiation-sensitive polymers for lithography

Name	Specifications	Properties/Current Limits
Riston® (DuPont) [16]	Dry Film	A "general purpose" dry film to for acid and alkaline etch up to 15 μm
SU-8 (Microchem Corp., Shell Chemicals etc.) [17]	Negative near-UV resist (400 nm)	For applications requiring high aspect ratios in very thick layers
PMMA [18] (Polymethylmethacrylate)	E-Beam positive resist	-Inexpensive polymer with T_g of 114 °C - Has moderate etch resistance and high resolution
Polysiloxanes [19]	E-beam negative resist	Dry process
Poly(hexafluorobutyl methacrylate) [19]	Positive X-ray resist	Sensitivity: 52 mJ/cm^2

1.3.1.2 Encapsulants

Encapsulation of high-power and large integrated circuit devices is another very important application area of polymers in electronics. The basic purpose of the encapsulation of integrated circuits is to enhance the life time of the device by protecting it from harsh environmental conditions such as moisture, radiation and mechanical impact. Every year the dimensions of semiconductor circuit devices are decreasing and

[16] http://www.dupont.com/pcm/riston/riston.html
[17] http://www.microchem.com/products/su_eight.htm
[18] D. S. Soane, Z. Martynenko, Polymers used in Microelectronics: Fundamentals and Applications, Elsevier, New York (1989).
[19] R. D. Miller and G. M. Wallraff, Advanced Materials for Optics and Electronics, Vol. 4, pp: 95-127, John Wiley, New York (2000).

consequently the number of the components per chip is increasing enormously. The number of components per chip has been increased over a million times during the last forty years and it is continuing to increase with new advances in molecular electronics [20]. This tremendous increase results in faster operation speed, higher power consumption and therefore more heat dissipation. Hence, encapsulation technology has become more challenging.

Encapsulation polymers should have high electrical resistance, good adhesion, resistance to thermal and mechanical shock as well as resistance to moisture and solvents. Both inorganic and organic materials can be used as encapsulants. Silicon dioxide, silicon nitride, diamond and silicon carbide are among the inorganic encapsulants [21]. Organic encapsulants can be divided into three groups; i) thermosetting polymers, ii) thermoplastics and iii) elastomers [22]. Since the pros and cons of organic encapsulants for flexible electronics have been studied extensively [23], only a few of the most widely used polymers will be discussed here.

Silicone compounds are one of the thermoset polymers most commonly used as encapsulants. The backbone of this polymer is based on alternating silicon and oxygen with organic groups attached to silicon atoms $[(R_2SiO)_n]$ [24]. The high average bond energy of the Si-O bond provides thermal stability. It is possible to control physical properties of silicone such as refractive index, dielectric constant and processability by changing the organic substitute. Another reason for the popularity of silicone compounds in electronics is that the intermolecular forces do not change significantly with temperature. Hence, the physical and dielectric properties of the polymer are also stable

[20] D. R. Gamota, P. Brazis, K. Kalyanasundaram, J. Zhang, Printed Organic and Molecular Electronics, Kluwer Academic Publishers, Boston (2004).
[21] M. S. Htoo, Microelectronic Polymers, Marcel Dekker Inc., New York (1989).
[22] E. R. Salmon, Encapsulation of Electronic Devices and Components, Marcel Dekker Inc., New York (1987).
[23] (a) L. F. Thompson, C. G. Willson, S. Tagawa, Polymers for Microelectronics: Resists and Dielectrics, American Chemical Society, Washington (1994), (b) D. T. Grubb, I. Mita, D. Y. Yoon, Materials Science of High Temperature Polymers for Microelectronics, Materials Research Society, Pittsburg (1991), (c) K. Gilleo, Polymer Thick Film, Van Nostrand Reinhold, New York (1996).
[24] M. T. Goosey, Plastics for Electronics, Elsevier Applied Science Publishers, London (1985).

[25]. Excellent moisture protection, high thermal stability and low dielectric constant of silicone compounds make them the backbone of conformal coatings for integrated circuits [26].

Polyimides, polyesters and alkyl resins are among other widely utilized polymeric materials as encapsulant thermosets [27]. Polystyrene, polyethylene and fluorocarbon polymers can be classified as thermoplastic organic encapsulants due to their capability of repeatedly softening when heated and hardening when cooled [28]. Polyurethanes, silicone rubbers and gels are favorable as flexible encapsulants due to their low modulus. Table 1.3 summarizes some physical properties of polymers commonly used as encapsulants.

[25] J. J. Licari, Plastic Coatings for Electronics, McGraw-Hill Book Company, New York (1970).
[26] C. P. Wong, Polymers for Electronic and Photonic Applications, Academic Press Inc., Harcout Brace Jovanovich Publishers, Boston (1993).
[27] H. Ito, S. Tagawa, K. Horie, Polymeric Materials for Microelectronic Applications: Science and Technology, American Chemical Society, Washington (1994).
[28] S. Fakirov, Handbook of Condensation Thermoplastic Elastomers, Weinheim: Wiley-VCH (2005).

Table 1.3: Some physical properties of selected organic encapsulants

	Solid Silicon	RTV Silicone	*Polyurethane	Polyester resin
Manufacturer	Rogers Corporation	Transene Company Inc.	Conap Inc.	Dupont
Commercial Name	Bisco®	Translastic ®	Conathane EN-2	Crastin® PBT
Electrical Properties	Dielectric Strength:400 V/mil	Dielectric Strength: 500 V/mil	Dielectric Strength: 645 V/mil	Dielectric Strength: 380-660 V/mil
	Dielectric Constant: 3.0-3.2	Dielectric Constant: 3.1-4.0	Dielectric Constant: 3.42	Dielectric Constant: 3.2
Thermal Conductivity (W/mK)	0.21-0.29	0.29-0.31	0.15	0.25
Mechanical Properties	Tensile Strength:5.3-7.6 MPa	Tensile Strength:2.6-5.9 MPa	Tensile Strength:5.5 MPa	Yield Stress: 58 MPa
	Elongation:250-450 %	Elongation:130-175 %		Tensile Modulus: 1600 MPa

* Source: M. J. Howard, Plastics for Electronics: desk-top data bank, The International Plastic Selector Inc., San Diego (1979).

1.3.1.3 Interconnect Dielectrics

Traditional inorganic insulators such as silicon dioxide and silicon nitride are limited by their mechanical properties. It is very difficult to form thick films of these inorganic materials without producing mechanical defects. Moreover, they are not mechanically flexible. Hence, extensive studies have been dedicated to the search for polymeric interconnect dielectrics [29].

Polyimides are very attractive in multilayering processing due to their ability to withstand high temperature, and their electrical and chemical resistance. Furthermore they have high mechanical strength, low dielectric constant and low dissipation factor [30]. Parylenes are another group of polymers used as interconnect dielectrics. They have low dielectric constant, low moisture absorption and high abrasion resistance [31]. The major drawback of parylenes is their poor temperature stability in air. Additionally, parylenes require special vacuum deposition processing to form thin films. Table 1.4 summarizes the physical and chemical properties of commonly used polymeric interconnect dielectrics and silicon dioxide for comparison. Process temperature and decomposition temperature for silicon dioxide refers to deposition temperature and melting point, respectively.

[29] (a) Y.S Liu, R.J. Wojnarowski, W.A. Hennessy, P.A. Piacente, J. Rowlette, M. Kadar-Kallen, J. Stack, Y. Liu, A. Peczalski, A. Nahata, J. Yardley, Electronic Components and Technology Conference, 999 – 1005 (1998), (b) J. I. Wright, R. Fillion, L. Meyer, D. Shaddock, Advanced Packaging Materials: Processes, Properties and Interfaces, 63 – 68 (2004), (c) T. M. Long and T. M. Swager, Journal of the American Chemical Society, Vol. 125, 14113-14119 (2003).
[30] H. R. Kricheldorf, Progress in Polyimide Chemistry, Springer, New York (1999).
[31] E. Reichmanis, C. K. Ober, S. A. MacDonald, T. Iwayanagi, T. Nishikubo, and Microelectronics Technology: Polymers for Advanced Imaging and Packaging, American Chemical Society, Washington (1995).

Table 1.4: Some physical properties of selected interconnect dielectrics

Properties [32]	SiO_2	Polyimide	Parylene	Polyphenyl Sulfide
Process Temperature (°C)	350-450	300-350	80	>315[b]
Decomposition Temperature (°C)	1710	450	125[a]	1000[c]
Dielectric Constant	3.5-4.0	3.2-3.8	2.65-3.15	3.0-4.4
Dissipation factor	0.001	0.01-0.02	0.0002-0.02	0.01-0.068
Thermal Conductivity (W/cm.C)	0.021	0.0017	0.36	0.8
Density (g/cm^3)	2.2	1.42	1.11-1.42	1.35-1.4

[a] Above this temperature air oxidation occurs, [b] Compression molding temperature, [c] 40% weight retention in nitrogen

1.3.1.4 Substrate Materials

Both mechanically rigid and flexible polymeric materials have been used in electronics as substrate materials on which to mount chips or other electrical components. Depending on the physical characteristics required by the application, such as operating temperature, frequency or mechanical strength, various types of organic materials including paper impregnated with phenolic resin, woven or non woven glass cloth, polyimide or polyester can be used as base material in flexible electronics [33]. Low cost, ease of manufacture and reparability are also among the parameters affecting the choice of material. In this section, a few polymeric materials that are used as substrate materials in flexible electronics will be briefly discussed.

Polyimide film (Kapton®) is one of the most commonly used materials in flexible electronics. Kapton® is synthesized by polymerizing an aromatic dianhydride and an

[32] (a) D. S. Soane, Z. Martynenko, Polymers in Microelectronics, Elsevier, New York (1989), (b) C. P. Wong, Polymers for Electronic and Photonic Applications, Academic Press, Boston (1993), (c) M. T. Goosey, Plastics for Electronics, Elsevier Applied Science Publishers, New York (1985).
[33] C. F. Coombs, Printed Circuits Handbook, McGraw-Hill, New York (1996).

aromatic diamine [34]. It has excellent thermal stability, solvent resistance and adhesion. Kapton® is being used to produce laminates with metal such as copper [35]. The major draw backs of polyimide are its high cost and difficult fabrication steps [36]. Phenolic resins are also used as base material in electronics. They exhibit high thermal and chemical resistivity. Phenolic resins have comparatively low cost and ease of processing[10]. The major disadvantages of phenolic resins are poor resistance to bases and oxidizers, and requirement for fillers during molding. Cyanate ester, epoxy/cyanate ester blends and Teflon® are among other substrate materials used in today's technology.

By increasing the population of the electrical devices integrated on a single chip the need for more densely packed systems has become crucial. Multilayering of electronic circuit boards and forming interconnections between the layers have solved this problem. Multiple layer boards (MLB) can be built using the polymers mentioned above. MLBs are fabricated by gluing or laminating each layer via hydraulic lamination, vacuum-assisted hydraulic lamination or autoclave processes [19]. The electrical connection between multiple layers can be obtained via plated through-holes drilled through the entire board.

Thus far the polymeric materials having passive roles in flexible electronics have been summarized. The following sections discuss polymeric or solution processable materials used in electronics as active elements.

1.3.2 Organic Semiconductors

Organic semiconductors can be divided into three main groups: i) conjugated polymers, (ii) short polymer chains or oligomers, and (iii) organic-inorganic hybrids. The possibility of transport charge (holes and electrons) due to the π-orbital overlap of neighboring molecules allows the conjugated polymers to emit light, conduct current and act as

[34] http://www.dupont.com
[35] http://www.rogerscorporation.com
[36] D. S. Soane, Z. Martynenko, Polymers in Microelectronics Fundamentals and Applications, Elsevier, New York, 1989.

semiconductors. The electrical conductivity of the conjugated polymers can be tuned by treating them with an oxidizing or a reducing agent, through a procedure called doping. In recognition of the important role of conjugated polymers in technology, Alan J. Heeger, Alan G. MacDiarmid and Hideki Shirakawa received the Nobel Prize in Chemistry in 2000 for their discovery of highly conductive polyacetylene.

Semiconducting properties of conducting polymers come from the delocalized π-electron bonding along the polymer chain. Molecular orbitals of the repeated units overlap in space and lift their degeneracy by forming a series of energy bands; π-bonding and π^*-antibonding orbitals form delocalized valance and conduction bands, respectively. The band gap for conducting polymers can be described as the energy gap between the highest occupied molecular orbital (HOMO), which is referred to as the valance band, and the lowest unoccupied molecular orbital (LUMO), which is referred to as the conduction band. As seen in Figure 1.3, the energy gap (E_g) decreases with an increase in the conjugation length which also corresponds to an increase in the number of energy levels [37]. The energy gap determines the electronic and electric properties of the conducting polymers. Hence, control of the HOMO-LUMO gap and specifically the design of low band gap polymers have gained importance in recent years.

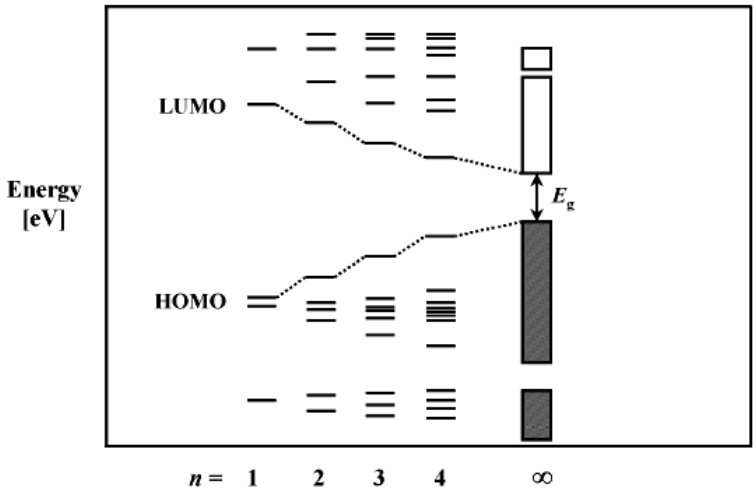

Figure 1.3: Band formation in conducting polymers with increasing conjugation length (Reproduced by the permission of RSC) [37]

[37] A. Ajayaghosh, Chemical Society Review, Vol. 32, 181-191 (2003).

There are different transport mechanisms for conducting polymers depending on the morphology and the doping level of the polymer. Generally, charge transport mechanisms are based on the motion of radical cations or anions, which are created by oxidation or reduction, along a polymer chain. More detailed information about the transport mechanisms for conducting polymers can be found in Appendix B.

As in inorganic semiconductors, it is possible to increase the electrical conductivity of the polymers dramatically by a doping process. For example, through doping it is possible to increase the conductivity of trans-polyacetylene up to ten orders of magnitude, approaching the conductivity of bulk copper (see Figure 1.4). Impurity or dopant atoms in the polymer backbone can be thought as interstitial defects that take up positions between the chains. Polymers can be either n- type doped, anionic rich, or p-type doped, cationic rich. There are three ways to accomplish the oxidation or reduction processes, which are through chemical, electrochemical and photo doping processes.

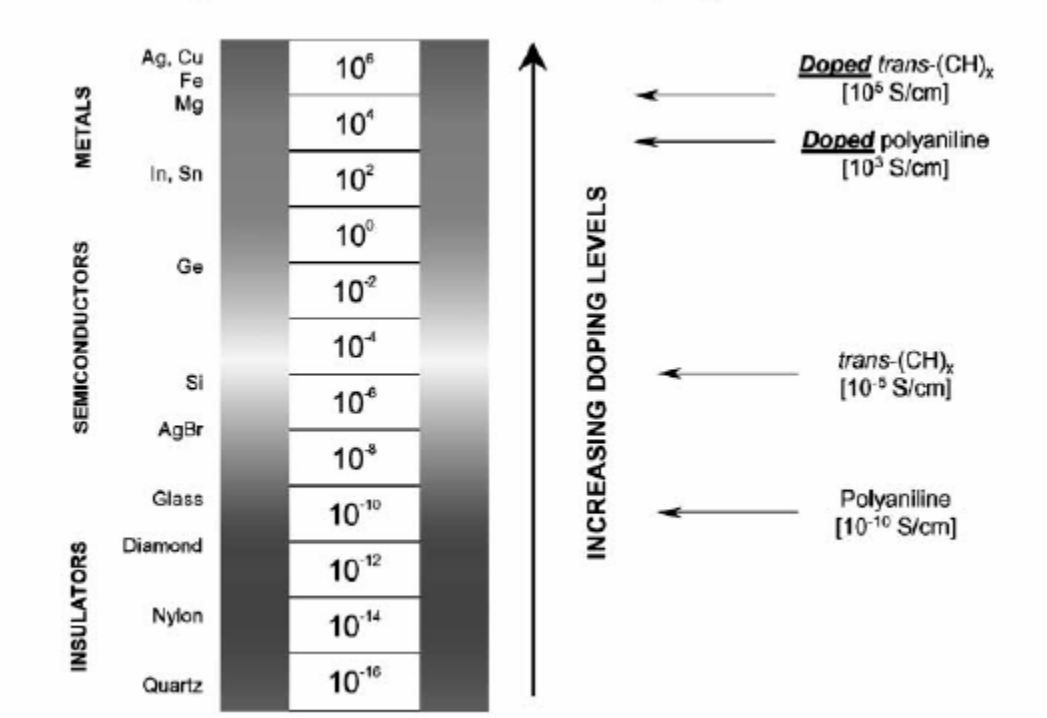

Figure 1.4: Conductivity of electronic polymers (Reproduced by the permission of Elsevier) [38]

[38] A. G. MacDiarmid, Synthetic Metals, Vol. 125, 11-22 (2002).

Most of the semiconductor polymers are p-type, such as polyethylene dioxythiophene (PEDOT) doped with polystyrene sulphonate (PSS) and polyaniline emaraldine base. There have been attempts to manufacture n-channel organic transistors [39, 40]. C_{60}-based, tetracarboxylic dianhyride (NTCDA), carbon nanotubes, and copper hexadecafluorophthalocyanine ($F_{16}CuPc$) are among the n-channel organic transistor active materials. The major problem with the n-type organic materials is their high sensitivity to atmospheric conditions. For example, it is reported that the resistivity of C_{60}-based thin film increases by 4 or 5 orders of magnitude upon exposure to air [47].

The major drawback of conjugated polymers is their low mobility compared to that of inorganic semiconductors (see Table 1.5). However, with new advances in chemistry and materials science, highly ordered organic semiconductors with mobility as high as that of amorphous silicon have been synthesized.

Small organic molecules (or oligomers), such as phthalocyanines, and oligothiophenes have higher mobility than conjugated polymers [41]. Recently solution processable or vacuum deposited pentacene has gained attention due to its high performance and potential for use in the synthesis of organic thin film transistors [42].

[39] H. E. Katz, Journal of Matreilas Chemistry, Vol. 7, 369-376 (1997).
[40] L. Torsi, Microelectronics Reliability, Vol. 40, 779-782 (2000).
[41] G. Horowitz, Advanced Materials, Vol. 10, 365-377 (1998).
[42] H. Klauk, D. J. Gundlach, J. A. Nichols, and T. N. Jackson, IEEE Transactions on Electron Devices, Vol. 46, 1258-1263 (1999).

Table 1.5: Mobility and on-off ratio of field effect transistor having different configurations

Active Semiconductor Material	*Field Effect Mobility ($cm^2/V.s$)*	*On-off Ratio*	*Reference*
Polythienylenevinylene	0.001	10^3	[43]
Bis(1,2,5-thiadiazolo)-p-quinobis(1,3-dithiole)	0.044	10^3	[44]
Poly(3-hexylthiophene)	0.01	10^3	[45]
Poly(hexylthiopene)	0.05	10^6	[46]
C_{60}	0.08	10^6	[47]
Pentacene	1.7	10^8	[48]
Pentacene	0.5	10^7	[49]
Single-Wall Carbon Nanotube	10	10^5	[50]

Another promising family of semiconductor materials for flexible electronics is organic-inorganic hybrids. These materials integrate the desirable characteristics of both inorganic and organic materials into one molecular composite [51]. Recently David B. Mitzi at the IBM T. J. Watson Research Center reported organic-inorganic hybrids under the title of "Solution-processed inorganic semiconductors" [52]. In his study, layered organic-inorganic perovskite structures are proposed as solution processable

[43] G. H. Gelinck, T. C. T. Geuns, D. M. De Leeuw, Applied Phyiscs Letters, Vol.77 1487-1489 (2000).
[44] J. Xue, S. R. Forest, Applied Physics Letters, Vol. 79, 3714-3716 (2001).
[45] Z. Bao, A. Dodabalapur, A. Lovinger, Applied Physics Letters, Vol. 69, 4108-4110 (1996).
[46] H. Sirringhaus, N. Tessler, R. H. Friend, Science, Vol. 280, 1741-1744 (1998).
[47] R. C. Haddon, A. S. Perel, R. C. Morris, T. T. M. Palstra, A. F. Hebard, R. M. Fleming, Applied Physics Letters, Vol. 67, 121-123 (1995).
[48] D. J. Gundlach, H. Klauk, C. D. Sheraw, C. Kuo, J. Huang, T. N. Jackson, Electron Devices Meeting, 111-114 (1999).
[49] H. Klauk, D. J. Gundlach, T. N. Jackson, IEEE Electron Device Letters, Vol. 20, 289-291 (1999).
[50] E. S. Snow, J. P. Noval, P. M. Campbell, D. Park, Applied Pyhsics Letters, Vol. 82, 2145-2147 (2003).
[51] J. E. Mark, C. Y-C Lee, Hybrid Organic-Inorganic Composites, American Chemical Society, Washington, 1995.
[52] D. N. Mitzi, Journal of Materials Chemistry, Vol. 14, 2355-2365, 2004.

semiconductors. Generally perovskite structures are constructed in three-dimensional AMX_3 structures where A is a small organic cation, M is metal and X is halide [53]. Such a perovskite structure can be layered between organic moieties (see Figure 1.5). In this geometry the covalently-bonded inorganic lattice provides high mobility and the organic layer between these layers provides mechanical flexibility and solution processability.

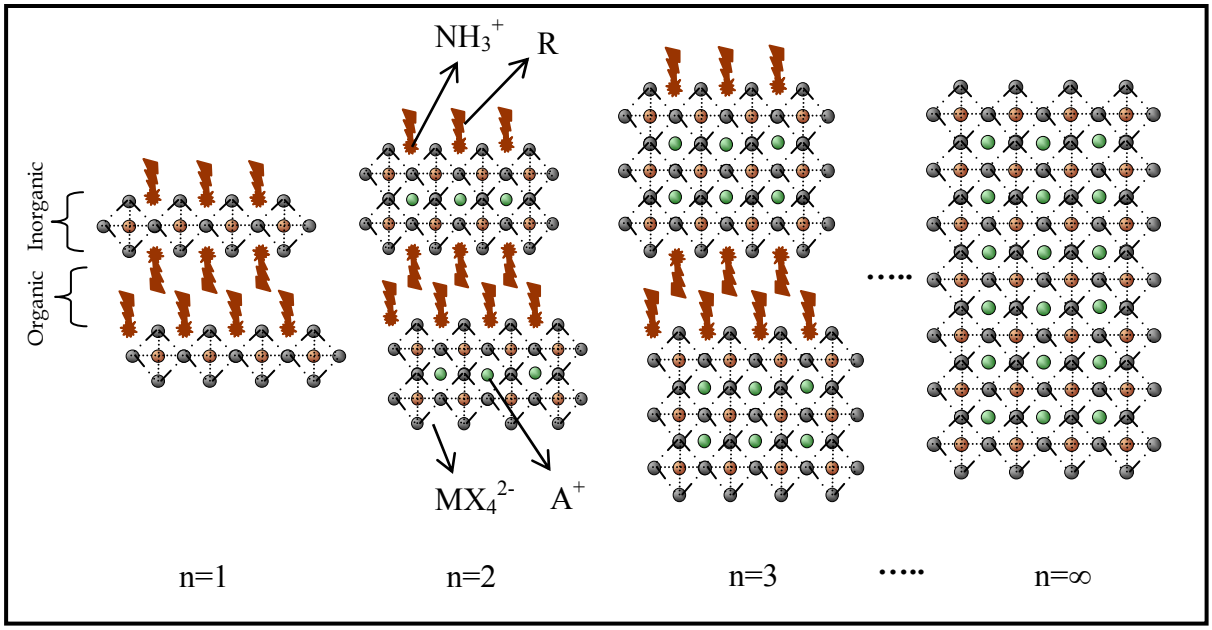

Figure 1.5: Schematic representation of layered organic-inorganic perovskites

As seen in Figure 1.5 the organic moieties lying between the inorganic perovskite layers may consist of monoammonium (NH_3). The hydrogen of monoammonium bonds to the halogens in the inorganic layers and therefore makes it possible to build multiple layers. The general structure of this hybrid can be written as $(R\text{-}NH_3)_2A_{n-1}M_nX_{3n+1}$ where R is an organic group such as an alkyl chain or a single-ring aromatic group. Increasing the number of perovskite layers (i.e. increasing n) changes the physical properties of the hybrids. For example a semiconductor-metal transition was reported for $(R\text{-}NH_3)_2(CH_3NH_3)_{n-1}Sn_nI_{3n+1}$ by Mitzi et al. [54]. More specifically for n<3; perovskite

[53] D. B. Mitzi, K. Chondrousdis, C. R. Kagan, IBM Journal of Reaserch and Development, Vol. 45, 29-44, 2001.
[54] D.B. Mitzi, C. A. Felid, W.T. A. Harrison, A. M. Guloy, Letters to Nature, Vol. 369, 467-469, 1994.

structures exhibit semiconducting behavior and for n>3 they exhibit metallic behavior. The major drawback of Sn containing perovskite hybrids is their atmosphere sensitivity. These perovskite hybrids easily oxidize in air. Solution processable chalcogenides such as $SnSe_2$ and SnS_2 semiconductors were also reported by the same group [53]. Table 1.6 summarizes advantages and disadvantages of some perovskite hybrids and chalcogenides.

Table 1.6: Advantages and disadvantages of some selected perovskite hybrids and chalcogenides

Chemical Formula	*Properties and Advantages*	*Disadvantages*	*Reference*
$(PEA^*)2SnI_4$	Rapid crystallization process, easy implementation (physical mixing)	High sensitivity to air	[55]
$(C_6H_5C_2H_4NH_3)_2SnI_4$	Relatively high mobility (~0.6 $cm^2/V.s$)	High sensitivity to air	[56]
CdSe	Mechanical flexibility, relatively high mobility (~1 $cm^2/V.s$)	Need for tight control on particle size	[57]
$SnS_{2-x}Se_x$	Continuous crystalline semiconducting tin chalcogenide films	Toxicity of solvent (hydrazine)	[58]

*PEA: phenethylammonium

[55] Z. Xu, D. B. Mitzi, Chemistry of Materials, Vol. 15, 3632-3637 (2003)
[56] C. R. Kagan, D. B. Mitzi, C. D. Dimitrakopoulos, Science, Vol. 286, 945-947 (1999)
[57] B. A. Ridley, B. Nivi, J. M. Jacobson, Science, Vol. 286, 746-749 (1999)
[58] D. B. Mitzi, L. L. Kosbar, C. E. Murray, M. Copel, A. Afzali, Letters to Nature, Vol. 428, 299-303 (2004)

Inorganic semiconductor nanowires, nanotubes, and nanorods are another promising active material group in electronics [59]. They are also promising candidates in photonics and catalysis [60]. Basically, inorganic nanowires and nanotubes can be grown in two different ways: i) vapor phase growth and ii) solution based growth [61]. Vapor phase deposition methods include vapor-liquid-solid (VLS) growth, physical methods such as laser or thermal evaporation, as well as chemical methods such as chemical vapor deposition [62]. Solution based growth, also called chemical methods, have been gaining attention due to their potential for large scale production and comparatively low fabrication costs [63]. Porous materials can be used as physical templates to grow the nanowires from solution form. These physical templates provide good control of both morphology and dimension of the grown nanowires [64]. Nanowiskers of group III-V and II-VI semiconductors such as gallium arsenide, indium phosphate and cadmium sulfide can be synthesized using solid-liquid-solid process [65]. In this process a metal with low melting point is used as a catalyst. Nanowires can be grown on catalyst particles by the decomposition of organometallic compounds of desired material.

Using the methods mentioned above, elemental semiconductor nanowires such as silicon, germanium, indium and selenium [66] and compounds of those, and metallic nanowires

---

[59] (a) Y. Wu, H. Yan, M. Huang, B. Messer, J. H. Song, P. Yang, Chemistry A European Journal, Vol. 8, 1260-1268 (2002), (b) Z. L. Wang, Materials Today, Vol. 7, 26-33 (2004), (c) J. Hu, M. Ouyang, P. Yang, C. M. Lieber, Nature, Vol. 399, 48-51 (1999).

[60](a) J. Wang, M. S. Gudiksen, X. Duan, Y. Cui, C. M. Lieber, Science, Vol. 293, 1455-1457 (2001), (b) X. Duan, Y. Huang, R. Agarwal, and C. M. Lieber, Nature, Vol. 421, 241-245 (2003), (c) J. L. Mohanan, I. U. Arachchige, S. L. Brock, Science, Vol. 307, 397-400 (2005).

[61] A. M. Rao, Nanotubes and Related Materials, Materials Research Society, Pennsylvania (2000)
Y. Hao, G. Meng, C. Ye, L. Zhang, Crystal Growth and Design, Vol. 5, 1617-1621 (2005)
P-C. Chang, Z. Fan, D. Wang, W-Y. Tseng, W-A. Chiou, J. Hong, J. G. Lu, Chemistry of Materials, Vol. 16, 5133-5137 (2004)

[62] Z. L. Wang, Y. Liu, Z. Zhang, Handbook of Nanophase and Nanostructured Materials: Material Systems and Applications (I), Kluwer Academic/ Plenum Publishers New York (2003)

[63] B. Cheng, J. M. Russell, W. Shi, L. Zhang, and E. T. Samulski, Journal of the American Chemical Society, Vol. 126, 5972-5973 (2004).

[64] D. J. Peña, J. K. N. Mbindyo, A. J. Carado, T. E. Mallouk, C. D. Keating, B. Razavi, and T. S. Mayer, Journal of Physical Chemistry B, Vol. 106, 7458-7462 (2002).

[65] C.N.R. Rao, F.L. Deepak, G. Gundiah, A. Govindaraj, Progress in Solid State Chemistry, Vol. 31 5–147, (2003).

[66] (a) J. M. Redwing, K-K. Lew, T. E. Bogart, L. Pan, E. C. Dickey, A.H. Carim, Y. Wang, M. A. Cabassi and T. S. Mayer, Proceedings of SPIE, Vol. 5361, 52-59 (2004), (b) H-Y. Tuan, D. C. Lee, T. Hanrath, B. A. Korgel, Chemistry of Materials, Vol. 17, 5705-5711 (2005).

such as silver and gold nanowires, can be synthesized [67]. Among these nanomaterials carbon nanotubes (CNTs) occupy an important place due to their unique properties [68]. CNTs can display both metallic and semiconducting electrical conductivity depending on the synthesis conditions [69]. Metallic CNTs can be used as interconnects in micro and nanoelectronics [70]. Semiconducting CNTs exhibit mobilities as high as 100,000 $cm^2/V.s$ at room temperature [71]. This extraordinary mobility opens the possibility of a new era in microelectroncis. CNTs are also very promising candidates in optics [72]. The major current drawback of CNTs is relatively poor control of their electrical and physical properties during synthesis [73].

In order to integrate the nanowires and nanotubes into functional devices various patterning methods have been used including electric field assisted assembly, fluid directed assembly, and Langmuir-Blodgett techniques [74]. Nanowires and nanotubes can be suspended in a limited number of solvents including ethanol [75]. Therefore, it is possible to hierarchically assemble them onto plastic substrates. Huang et al. used a PDMS mold as a fluidic channel to pass a suspension containing indium phosphate nanowires and to align nanowires on silicon [75]. Hanon et al. [76] and Saran et al.[77] used

---

[67] (a) C.W. Lai, J.Y. Dai, X.Y. Zhang, H.L.W. Chan, Y.M. Xu, Q. Li, H.C. Ong, Journal of Crystal Growth, Vol. 282, 383–388 (2005), (b) Y. Liu, Y. Chu, L. Yang, D. Han, Z. Lu, Materials Research Bulletin, Vol. 40, 1796–1801 (2005).

[68] D. Tománek and R. J. Enbody, Science and Application of Nanotubes, Kluwer Academic, New York (2000)

[69] (a) Y. Li, D Mann, M. Rolandi, W. Kim, A. Ural, S. Huang, A. Javey, J. Cao, D. Wang, E. Yenilmez, Q. Wang, J. F. Gibbons, Y. Nisher, H. Dai, Nano Letters, Vol. 4, 317-321 (2004), (b) R. Krupke, F. Hennrich, H. V. Löhneysen, M. M. Kappes, Science, Vol. 301, 344-347 (2003).

[70] (a) T. Furukawa, M. C. Hakey, D. V. Horak, C. W. Koburger, M. E. Masters, P. H. Mitchell, S. Polonsky, United States Patent Application 20050189655 (2005), (b) A. Raychowdhury, K. Roy, IEEE-NANO 2004, Fourth IEEE Conference on Nanotechnology, 553-555 (2004).

[71] T. Du1rkop, S. A. Getty, E. Cobas, and M. S. Fuhrer, Nano Letters, Vol. 4, 35-39 (2004)

[72] (a) D. E. Milkie, C. Staii, S. Paulson, E. Hindman, A. T. Johnson, and J. M. Kikkawa, Nano Letters, Vol. 5, 1135-1138 (2005), (b) Xiaohui Qiu, Marcus Freitag, Vasili Perebeinos, and Phaedon Avouris, Nano Letters, Vol. 5, 749-752 (2005)

[73] M. S. Dresselhaus, G. Dresselhaus, P. Avouris, Carbon Nanotubes: synthesis, structures, properties, and applications, Springer, New York, 2001.

[74] X. Duan, C. Niu1, V. Sahi, J. Chen, J. W. Parce, S. Empedocles, and J. L. Goldman, Nature, Vol. 425, 274-278 (2003)

S. Fan, M. G. Chapline, N. R. Franklin, T. W. Tombler, A. M. Cassell, and H. Dai, Science, Vol. 283, 512-514 (1999)

D. Whang, S. Jin, Y. Wu, and C. M. Lieber, Nano Letters, Vol. 3, 1255-1259 (2003)

[75] Y. Huang, X. Duan, Q. Wei, and C. M. Lieber, Science, Vol. 291, 630-633 (2001)

[76] J. B. Hannon, A. Afzali, Ch. Klinke, and Ph. Avouris, Langmuir, Vol. 21, 8569-8571 (2005)

microcontact printing and line patterning methods respectively to selectively deposit carbon nanotubes. The details of these fabrication methods are discussed in section 1.4.

In this section promising semiconducting materials candidates for the manufacture of active components in flexible electronics are discussed. The next section will briefly summarize the solution processable metals, which are the last group of materials presented in this review.

1.3.3 Solution Processable Metals

Vacuum evaporation has been the most commonly used method in electronics to deposit metal. Over the last decade advances in nanotechnology and science have made it possible to synthesize and modify metal nanoparticles which are soluble in typical organic solvents such as toluene, xylene and even water [78]. Such solution processability of metal nanoparticles facilitates simple and cost affective manufacturing technologies instead of time-consuming and expensive conventional methods. Organic and/or flexible electronics fabrication methods will be discussed in the next section. The purpose of this chapter is to give a very brief summary of solution processable metals and make the reader familiar of with some of the recent advances in this area.

The solution processable metals can be classified into two main groups namely i) encapsulated or chemically modified metal nanoparticles and ii) organometallic compounds. In order to prepare stable suspensions or solutions of metal nanoparticles, organic groups are attached around metallic nanoparticles or nanoclusters. Many research groups are currently working on the preparation of noble metal nanoparticles and nanoclusters due to their potential application in electronics as electrode materials, and

---

[77] N. Saran, K. Parikh, D-S Suh, E. Munoz, H. Kolla, and S. K. Manohar, Journal of the American Chemical Society, Vol. 126, 4462-4463 (2004)

[78] (a) R. W. J. Scott, O. M. Wilson, and R. M. Crooks, Journal of Physical Chemistry B, Vol. 109, 692-704 (2005), (b) C. Hayashi, J. Vacuum Sci. Technol. A, Vol. 5, 1375–1384 (1987), (b) M. Tsuji, M. Hashimoto, Y. Nishizawa, M. Kubokawa, and T. Tsuji, Chemistry A European Journal, Vol. 11, 440 – 452, (2005).

also in biology and catalysis [79]. There are both physical and chemical routes to synthesize metal nanoparticles and nanoclusters. Laser ablation, metal-vapor and solvated metal atom dispersion techniques are among the well known physical methods [80]. Chemical routes are the preferred methods due to their simplicity. Noble metal nanoclusters such as palladium, platinum and gold can be synthesized by reducing the salt form of the required metal with alcohol, triorganoborate or 3- Methylbutanol [81]. The full details of the synthesis methods will not be discussed in this section. Instead, physical and chemical properties of some noble metal nanoparticles and their application areas will be briefly summarized here.

1.3.3.1 Gold Nanoparticles

Gold nanoparticles or gold colloids are known as the most stable metal nanoparticles. The most commonly used synthesis process of gold nanoparticles involves the reduction of gold (III) derivatives such as $HAuCl_4$ salt in the presence of thiols [82]. Strong gold sulfur bonding makes the thiols excellent stabilizers. Thiol coated gold nanoparticles can be isolated and dissolved in nonpolar solvents. Depending on the chain length of the thiol group the physical and chemical properties of gold nanoparticles change [83]. Table 1.7 summarizes the various stabilizers, reductants, solvents, and particle sizes of gold nanoparticles reported by various research groups.

Selective spatial deposition of gold nanoparticles to fabricate functional devices is another challenging topic. Photolithography, micro contact printing, self assembly or

---

[79] J. Bourdon, Growth and Properties of Metal Clusters: Applications to Catalysis and The Photographic Process, Elsevier, New York (1980)
[80] (a) J. A. Young, K. T. Lynch, A. J. Walsh, A. A. Ruth, Proceedings of SPIE, Vol. 5824, 138-148 (2005), (b) M. Lal, M. Plummer, N. J. Richmond, and W. Smith, Journal of Physical Chemistry B, Vol. 108, 6052-6061 (2004).
[81] N. Toshima, Y. Shiraishi, T. Teranishi, M. Miyake, T. Tominaga, H. Watanabe, W. Brijoux, H. Bönnemann, G. Schmid, Applied Organometallic Chemistry, Vol. 15, 178-196 (2001)
[82] M. Brust, M. Walker, D. Bethell, D. J. Schiffrin, R. Whyman, Journal of the Chemical Society, Chemical Communications, Vol. 7, 801 - 802 (1994)
[83] (a) M. M. Maye, W. Zheng, F. L. Leibowitz, N. K. Ly, and C-J. Zhong, Langmuir, Vol. 16, 490-497 (2000), (b) S. Huang, G. Tsutsui, H. Sakaue, S. Shingubara, and T. Takahagi, Journal of Vacuum Science & Technology, B: Microelectronics and Nanometer Structures, Vol. 19, 115-120 (2001).

inkjet printing can be used to organize and pattern gold colloids on different substrates including plastics. Tanaka et al. patterned gold nanoparticles, which were prepared by the aqueous reduction of $HAuCl_4$ by sodium citrate at reflux, on silicone substrates [84]. They first built ultra thin poly(N-dodecyl acrylamide-co-4-vinyl pyridine)s layers on silicone substrates using the Langmuir-Blodgett (LB) technique and then patterned this thin polymer layer using photolithography. Finally, they attached the gold on to the patterned polymer thin film layers by immersing the substrates into aqueous gold nanoparticle solution. Recently Fresco et al. reported a method for the patternwise placement of gold nanoparticles with nanometer resolution [85]. They selectively spatially transformed the thiocarbonate moieties into thiols by applying voltage via an AFM tip. Then they deposited the gold nanoparticles on to this thiol-patterned surface. Huang et al. used an inkjet printing method to selectively deposit thiol encapsulated gold nanoparticles on plastic substrates [86]. Numerous other patterning techniques can be found in the literature [87].

Table 1.7: Survey of gold nanoparticles

Starting Material	***Reductant***	***Stabilizer***	***Solvent***	***Particle Size (nm)***	***Reference***
$AuCl_3$[i]	Alkalide	THF[ii]	THF	6-11	[88]
$HAuCl_4$[iii]	$NaBH_4$[iv]	thiolated b-cyclodextrins	water	2-3	[89]
$HAuCl_4$	$NaBH_4$	dodecylamine or oleylamine	toluene	2.5-7	[90]
$HAuCl_4$	$NaBH_4$	Lysine	water	5.8-7.2	[91]
$HAuCl_4$	formamide	poly(vinylpyrrolidone)	formamide	27-37	[92]

[i]$AuCl_3$: Gold(III) Chloride, [ii] THF: Tetrahydrofuran, [iii]HAuCl4: Hydrogen tetrachloroaurate(III) [iv] Sodium Borohydrate

[84] H. Tanaka, M. Mitsuishi, and T. Miyashita, Langmuir, Vol. 19, 3103-3105 (2003)
[85] Z. M. Fresco and J. M. J. Frěchet, Journal of the American Chemical Society, Vol. 127, 8302-8303 (2005)
[86] D. Huang, F. Liao, S. Molesa, D. Redinger,and V. Subramanian, Journal of The Electrochemical Society, Vol. 150, G412-G417 (2003)
[87] (a)V. Santhanam and R. P. Andres, Nano Letters, Vol. 4, 41-44 (2004), (b) J. Xu, J. Drelich, and E. M. Nadgorny, Langmuir, Vol. 20, 1021-1025 (2004)
[88] K-L Tsai and J. L. Dye, Chemistry of Materials, Vol. 5, 640-546 (1993)
[89] L. Sun, R. M. Crooksa and V. Chechik, Chemical Communications, 359-361 (2001)
[90] D. V. Leff, L. Brandt, and J. R. Heath, Langmuir, Vol. 12, 4723-4730 (1996)
[91] P. R. Selvakannan, S. Mandal, S. Phadtare, R. Pasricha, and M. Sastry, Langmuir, Vol. 19, 3545-3549 (2003)
[92] M. Y. Han,C. H. Quek, W. Huang, C. H. Chew, and L. M. Gan, Chemistry of Materials, Vol. 11, 1144-1147 (1999)

1.3.3.2 Silver Nanoparticles

Silver nanoparticles are another promising nanomaterial used in many different areas such as catalysis, optics, and surface-enhanced Raman scattering [93]. Many synthesis methods of silver nanoparticles have been reported in the literature including the chemical reduction method, electrochemical method, laser ablation method and photochemical method [94]. Among these methods, the chemical reduction method is most commonly used due to its simplicity. Typically, it includes the reduction of silver nitrite or silver acetate salt in the presence of stabilizers. Table 1.8 summarizes some reductants and stabilizers used in silver nanoparticle synthesis. Depending on the stabilizer and the synthesis conditions the shape of the silver nanoparticles can be controlled. Sun et al. reported single crystal silver nanocubes which were stabilized by poly (vinyl pyrrolidone) [95]. Chimentão et al. synthesized silver nanowires and nanopolyhedra using the polyol process [96]. Silver nanoparticles containing free standing polymer films have been gaining attention due to their ability to combine mechanical stability with desired electrical and optical properties [97].

[93] (a) S. Nie and S. R. Emory, Science, Vol. 275, 1102-1106 (1997), (b) D. Yu, X. Sun, J. Bian, Z. Tong, Y. Qian, Physica E, Vol. 23, 50-55 (2004), (c) H. Wang, X. Qiao, J. Chen, X. Wang, S. Ding, Materials Chemistry and Physics, Vol. 94, 449–453 (2005).
[94] (a) L. Rodríguez-Sánchez, M. C. Blanco, and M. A. López-Quintela, Journal of Physical Chemistry B, Vol. 104, 9683-9688 (2000), (b) H. H. Huang, X. P. Ni, G. L. Loy, C. H. Chew, K. L. Tan, F. C. Loh, J. F. Deng, and G. Q. Xu, Langmuir, Vol. 12, 909-912 (1996), (c) F. Mafunè, J. Kohno, Y. Takeda, T. Kondow, H. Sawabe, Journal of Physical Chemistry B, Vol. 104, 8333-8337 (2000).
[95] Y. Sun and Y. Xia, Science, Vol. 298, 2176-2179 (2002)
[96] R.J. Chimentão, I. Kirm, F. Medina, X. Rodríguez,Y. Cesteros, P. Salagre, J.E. Sueiras, J.L.G. Fierro, Applied Surface Science, Vol. 252, 793-800 (2005)
[97] (a) S. Porel, S. Singh, S. S. Harsha, D. Narayana Rao, and T. P. Radhakrishnan, Chemistry of Materials, Vol. 17, 9-12 (2005), (b) Z. Liu, X. Wang, H. Wu, C. Li, Journal of Colloid and Interface Science, Vol. 287, 604-611 (2005).

Table 1.8: Survey of silver nanoparticles

Starting Material	*Reductant*	*Stabilizer*	*Particle Size (nm)*	*Reference*
Silver Perchlorate	Sodium Borohydride	Dodecanethiol	2-7.5	[98]
Silver Sulfate	Hydrazine monohydrate	Aniline	125	[99]
Silver Nitrate	Ethanol	Polyvinylpyrrolidone	3-25	[100]

1.3.3.3 Platinum, Palladium Nanoparticles and Others

Platinum and palladium nanoparticles can be synthesized by chemically reducing the proper salt or organometallic compound [101]. Platinum and palladium nanoparticles have particular importance as catalysts due to their ability to reduce carbon dioxide [102] and their electrocatalytic performance for fuel cell reactions [103]. Platinum and palladium nanoparticles are also excellent catalysts for hydrogenation [104].

Early transition metal-colloids such as organosols of titanium, vanadium, and zirconium are very promising materials in both power technology and catalysis [105]. Bönnemann and Brijoux reported an ether soluble titanium nanoparticles $[Ti(0)\cdot 0.5\ THF]_x$[106]. This nanomaterial can be used as an activator for heterogeneous hydrogenation catalysts.

[98] J. R. Heath, C. M. Knobler, and D. V. Leff, Journal of Physical Chemistry, Vol. 101, 189-197 (1997)
[99] Y. Tan, Y. Li, and D. Zhu, Journal of Colloid and Interface Science, Vol. 258, 244–251 (2003)
[100] S. Ayyappan, R. Srinivasa Gopalan, G. N. Subbanna, C. N. R. Rao, Journal of Materials Research, Vol. 12, 398-401 (1997)
[101] (a) B. Veisz and Z. Király, Langmuir, Vol. 19, 4817-4824 (2003), (b) J. Huang, C. He, X. Liu, Y. Xiao, K. Y. Mya, and J. Chai, Langmuir, Vol. 20, 5145-5148 (2004)
[102] M. G. Crestani, I. Puente-Lee, L. Rendo´n-Vazquez , P. Santiago, F. d. Rio, D. Morales-Morales, J. J. García, Letters to the Editor / Carbon, Vol. 43, 2618–2641 (2005)
[103] J. Ding, K-Y Chana, J. Rena, F-S Xiao, Electrochimica Acta, Vol. 50, 3131–3141 (2005)
[104] S. Mandal, D. Roy, R. V. Chaudhari, and M. Sastry, Chemistry of Materials, Vol. 16, 3714-3724 (2004)
[105] (a) J. W. Long, B. Dunn, D. R. Rolison, and H. S. White, Chemical Reviews, Vol. 104, 4463-4492 (2004), (b) C. P. Nicholas, H. Ahn, and T. J. Marks, Journal of the American Chemical Society, Vol. 125, 4325-4331 (2003).
[106] H. Bönnemann and W. Brijoux, NanoStructured Materials, Vol. 5, 135-140 (1995)

Bogdavonić et al. also used ether soluble titanium nanoparticles to dope sodium alanate. This material has high hydrogen storage capability which is especially important in hydrogen fuel cell technology [107]. Monodisperse bimetallic composite nanocrystals such as silver/cobalt nanocrystals are another group of solution processable metallic materials which have wide applications in ferromagnetic technology [108].

Solution processable passive and active materials used in current technology have been summarized. The following section will concentrate on the possible manufacturing methods which can be used to integrate solution processable materials into functional devices.

1.4 Organic Electronic Device Fabrication Methods

One of the most important advantages of conducting polymers is the variety of device fabrication methods that may be used to form them into useful devices. It is possible to use traditional vacuum and lithography methods to fabricate organic electronic devices [109,110,111]. However, traditional methods include expensive production steps such as chemical or physical vapor deposition and plasma etching, which generally require high temperature and high vacuum. Figure 1.6 shows the temperature-pressure ranges for various material process techniques [112]. As seen in this Figure, solution-based preparation methods are characterized by room temperature and atmospheric pressure. Therefore solution-based processes are potentially environmentally friendly and inexpensive. In recent years, new fabrication techniques, which build on the advantage of solution processability of organic semiconductors, have been introduced. In this section, solution-based fabrication of organic electronic devices will be explained.

---

[107] B. Bogdavonić, M. Felderhoff, S. Kaskel, A. Pommerin, K. Schlichte, and F. Schüth, Advanced Materials, Vol. 15, 1012-1015 (2003)
[108] (a) N. S. Sobal, M. Hilgendorff, H. Mo1hwald, and Michael Giersig, Nano Letters, Vol. 2, 621-624 (2002), (b) S. Rudenkiy, M. Frerichs, F. Voigts, W. Maus-Friedrichs, V. Kempter, R. Brinkmann, N. Matoussevitch, W. Brijoux, H. Bönnemann, N. Palina, H. Modrow, Applied Organometallic Chemistry, Vol. 18, 553-560 (2004)
[109] K. Kudo, M. Iizuka, S. Kuniyoshi, K. Tanaka, Thin Solid Films, Vol. 393, 362-367 (2001)
[110] T. Dobbertin, E. Becker, T. Benstem, G. Ginev, D. Heithecker, H.-H. Johannes, D. Metzdorf, H. Neuner, R. Parashkov, W. Kowalsky, Thin Solid Films, Vol. 442, 132-139 (2003)
[111] J-H. Sung, S-J. Kim, K-H. Lee, Journal of Power Sources, vol. 124, 343-350 (2003)
[112] M. Yoshimura, W. Suchanek, K-S. Han, Journal of Materials Chemistry, Vol. 9, 77-82 (1999).

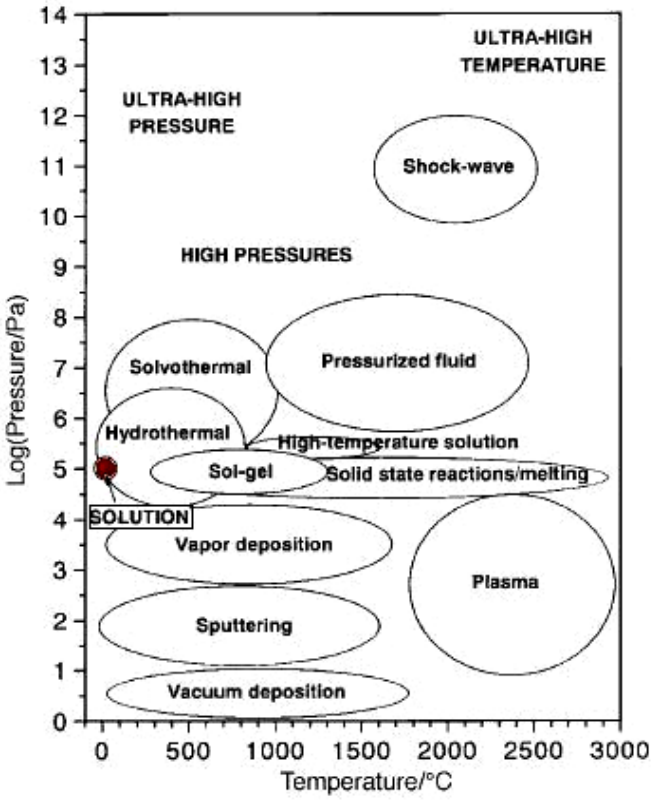

Figure 1.6: Schematic pressure-temperature ranges for various materials processing techniques (Reproduced by the permission of RSC)

1.4.1 Inkjet Printing

Inkjet printing techniques, have been gaining attention recently because of their unique features, such as simplicity of fabrication, compatibility with different substrates, feasibility of non-contact and no-mask patterning, low temperature processing and low cost [113, 114]. Inkjet printing is a familiar method used in nearly every office and household to transfer computer data to paper or transparencies. The same technology with a simple modification can be used to pattern solution processable polymers or nanoparticle inks on various substrates including glass, semiconductor materials, overhead transparencies and even paper.

[113] G. G. Rozenberg, E. Bresler, S. P. Speakman, C. Jeynes, J. H. G. Steinke, Apllied Physics Letters, Vol. 81, 5249-5251 (2002).
[114] Z. Bao, J. A. Rogers, H. E. Katz, Journal of Materials Chemistry, Vol. 9, 1895-1904 (1999).

Generally inkjet printers can be divided into two groups; continuous and drop-on-demand. In continuous jet printers the ink is pumped through a nozzle and the formed liquid jet is deflected by electrostatic plates to the paper or to a reservoir for recirculation. Today most inkjet printers are based on the drop formation process, which is called drop-on-demand (DOD). The drop-on-demand method provides smaller drops and higher placement accuracy compared to those possible using the continuous inkjet printers. In this method the pulse that creates ink drop can be generated either thermally or piezoelectrically. As seen in Figure 1.7, in a thermal inkjet printer a heated plate causes a vapor bubble, which pushes the ink out through the nozzle. The total ejection time is a few microseconds and the temperature of the plate can rise by about 300 °C during the ejection.

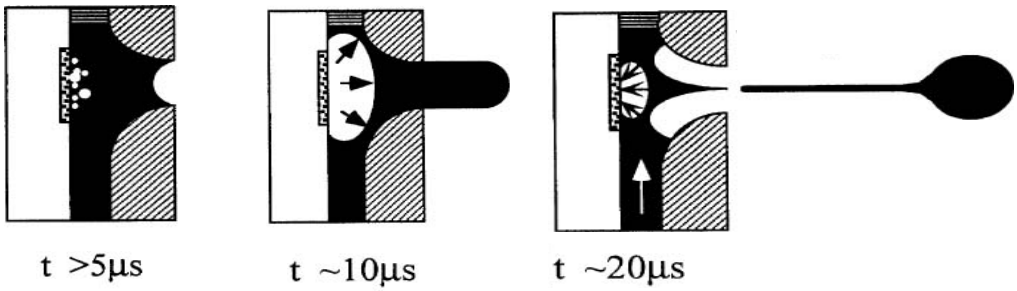

Figure 1.7: Drop formation by a thermal inkjet printer (Reprinted with permission of IS&T: The Society for Imaging Science and Technology sole copyright owners of *The Journal of Imaging Science and Technology*) [115]

Piezoceramic tubes, rods, or plates can be used in piezoelectric inkjet printers. Figure 1.8 (a) shows a schematic of a shear mode piezoelectric printhead. In this type of printhead, an electric field applied to a piezoceramic actuator element causes shear action deformation and due to this deformation ink is ejected through the nozzle [116]. The printhead design shown in Figure 1.8 (b) is called the bend-mode design. In this design, ink rejection is caused by the piezoceramic plates bonded to the diaphragm to form an array of bilaminar electromechanical transducers. The printheads in Tetronix's Phaser

[115] H. P. Le, Journal of Imaging Science and Technology, Vol. 42, 49-62 (1998).
[116] K. Yoshimura, M. Kishimoto, T. Suemune, OKI Technical Review, Vol. 64, 41-44 (1998).

300 and 350 and Epson's Color Stylus 400, 600, and 800 inkjet printers are of the bend-mode piezoceramic type. More detailed information about the inkjet printer technology can be found in H. P. Le's article [115].

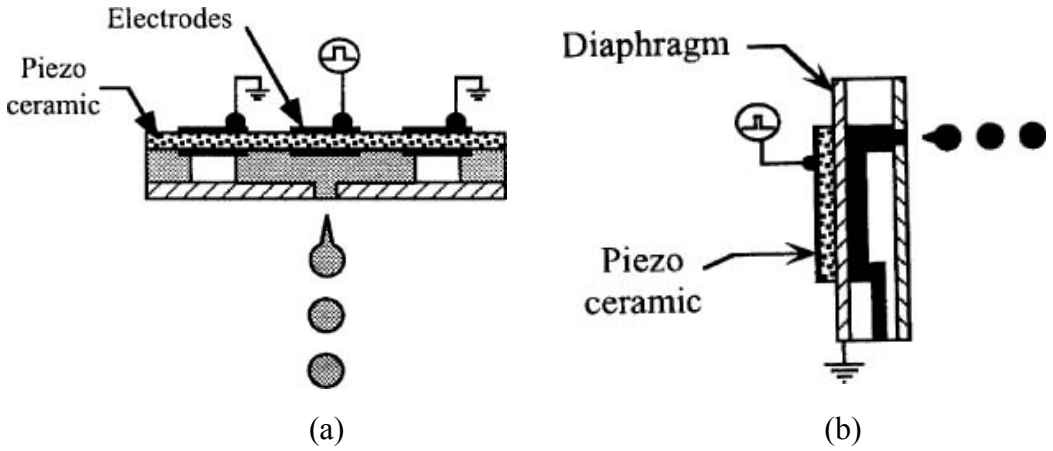

Figure 1.8: Design of a (a) shear mode (b) bend mode piezoelectric ink-jet printhead (Reprinted with permission of IS&T: The Society for Imaging Science and Technology sole copyright owners of *The Journal of Imaging Science and Technology*) [115]

1.4.2 Screen Printing

Screen printing is a simple and environmentally friendly printing process for depositing ceramic and polymer "inks" [117]. In general, screen printing is used to manufacture conductive interconnections between electronic components on circuit boards. This method involves moving a squeegee blade across a screen mesh. The squeegee blade pushes ink through a screen mesh, which is patterned by means of a stencil, to produce open areas which result in a conductive material pattern on the circuit board [118]. This method is compatible with high viscosity materials including conductive inks, dielectric pastes, UV curable materials and various adhesives. Bao et al. [119] fabricated organic FETs using screen printing technology. They used a screen mask made of a stainless steel fabric with 400 mesh count/in to deposit an insulating polymer layer (polyimide) and a

[117] C. R. M. Grovenor, *Microelectronic Materials*, Institute of Physics Publishing, Bristol, 1992.
[118] K. Gilleo, *Polymer Tick Film*, Van Nostrand Reinhold, New York, 1996.
[119] Z. Bao, Y. Feng, A. Dodabalapur, V. R. Raju, A. J. Lovinger, Chemistry of Materials, Vol. 9, 1299-1301 (1997).

source-drain electrode (conductive ink 479SS from Acheson Co.). Knobloch et al. [120] also manufactured organic FETs by screen printing a semiconductor active layer of poly(3-alkythiophene). Screen printed inductors [121], biosensors [122, 123], solar cells [124, 125], gas sensors [126, 127], and strain sensors [128] have been reported.

1.4.3 Line Patterning

Among the printing methods, line patterning, introduced by MacDiarmid and coworkers [129, 130], is the simplest and the cheapest method. This method includes; (i) the design of a negative image of the required pattern using computer aided design software, (ii) deposition of conductive polymer on substrate, and (iii) removing the printed mask by sonicating the substrate in toluene for ~10s. Resistors, R-C filters, field effect transistors (see Figure 1.9), and RF identification tags can be fabricated by using this line patterning method.

Figure 1.9: Structure of line patterned field effect transistor (Reproduced by the permission of Elsevier) [38]

120 A. Knobloch, A. Bernds, W. Clemens, First International IEEE Conference on Polymers and Adhesives in Microelectronics and Photonics, 84-90 (2001).
121 J. Y. Park, L. K. Lagorce, M. G. Allen, IEEE Transactions on Magnetics, Vol. 33, 3322-3324 (1997).
122 M. Albareda-Sirvent, A. Merkoçi, S. Alegret, Sensors and Actuators B, Vol. 69, 153-163 (2000).
123 N. G. Patel, S. Meier, K. Cammann, G.-C. Chemnitius, Sensors and Actuators B, Vol. 75, 101-110 (2001).
124 J. Szlufcik, F. Duerinckx, J. Horzel, E. V. Kerschaver, H. Dekkers, S. De Wolf, P. Choulat, C. Allebe, J. Nijs, Solar Energy Materials and Solar Cells, Vol. 74, 155-163 (2002).
125 T. Aramoto, F. Adurodija, Y. Nishiyama, T. Arita,A. Hanafusa, K. Omura, A. Morita, Solar Energy Materials and Solar Cells, Vol. 75, 211-217 (2003).
126 D. Vincenzi, M. A. Butturi, V. Guidi, M. C. Carotta, G. Martinelli, V. Guarnieri, S. Brida, B. Margesin, F. Giacomozzi, M. Zen, G. U. Pignatel, A. A. Vasiliev, A. V. Pisliakov, Sensors and Actuators B, Vol. 77, 95-99 (2001).
127 B. Riviere, J.-P. Viricelle, C. Pijolat, Sensors and Actuators B, Vol. 93, 531-537 (2003).
128 K. I. Arshak, D. McDonagh, M. A. Durcan, Sensors and Actuators A, Vol. 79, 102-114 (2000).
129 D. Hohnholz, A. G. MacDiarmid, Sythetic Metals Vol. 121, 1327-1328 (2001).
130 A. G. MacDiarmid, Current Applied Physics, Vol. 1, 269-279 (2001).

MacDiarmid et al. fabricated field effect transistors on overhead transparency substrates using PEDOT/PSS as the active material and UV curable epoxy as the insulating material between the source-drain and gate electrodes. When a positive voltage is applied to the gate electrode, electrons will be induced into the channel at the interface between the insulator and PEDOT/PSS layer due to a capacitance effect. The induced electrons will recombine with the holes in the channel. As a result of this recombination, the drain current decreases [131].

1.4.4 Self Assembly

As emphasized in previous sections, traditional lithography is based on very large scale integration (VLSI) and is fast approaching its limits. Recently, molecular electronics have gained attention since the use of single or small groups of molecules in device-based structures made it possible to prepare ~10^{23} devices in a single beaker using routine chemical synthesis [132]. Fundamental units for electronic components such as wires, switches, memory, and gain elements are among the molecular electronic devices that have been formed [133, 134, 135, 136].

Self assembly is a process of a self-organization of molecules upon dipping a substrate into a solution of molecules. After removing the substrate from the solution and rinsing, a monolayer of molecules will stay on the surface as a result of minimization of the energy in a stable state. By self assembly both two and three-dimensional arrays and networks of molecules, nanowires or nanotubes can be obtained [137]. Self assembled monolayers can be held together by electrostatic forces. This type of self assembly is called electrostatic

---

[131] J. Lu, N. J. Pinto, A. G. MacDiarmid, Journal of Applied Physics, Vol. 92, 6033-6038 (2002).
[132] J. M. Tour, *Molecular Electronics Commercial Insights, Chemistry, Devices, Architecture and Programming*, World Scientific, New Jersey, 2003.
[133] J. M. Tour, Accounts of Chemical Research, Vol. 33, 791-804 (2000).
[134] Book Reviews, Journal of American Chemical Society, Vol. 123, 12745-12748 (2001).
[135] P. A. Derosa, S. Guda, J. M. Seminario, Journal of American Chemical Society, Vol. 125, 14240-14241 (2003).
[136] S. Paul, C. Pearson, A. Molloy, M. A. Cousins, M. Green, S. Kolliopoulou, P. Dimitrakis, P. Normand, D. Tsoukalas, M. C. Petty, Nano Letters, Vol. 3, 533-536 (2003).
[137] W. A. Goddard III, D. W. Brenner, S. E. Lyshevski, G. J. Iafrate, *Handbook of Nanoscience , Engineering, and Technology*, CRC Press, Boca Raton, 2002.

self assembly (ESA) and relies on the formation of alternating simple polyelectrolyte monolayers. Figure 1.10 describes the ESA process. In this process, a pre cleaned and functionalized substrate first is dipped into a solution containing polyanionic complexes that are attracted to the cationic surface. The alternating anionic-cationic-anionic process results in a multilayer material [138]. Organic photovoltaic devices [139], gas and pH sensors [140, 141] can be fabricated by this ESA technique.

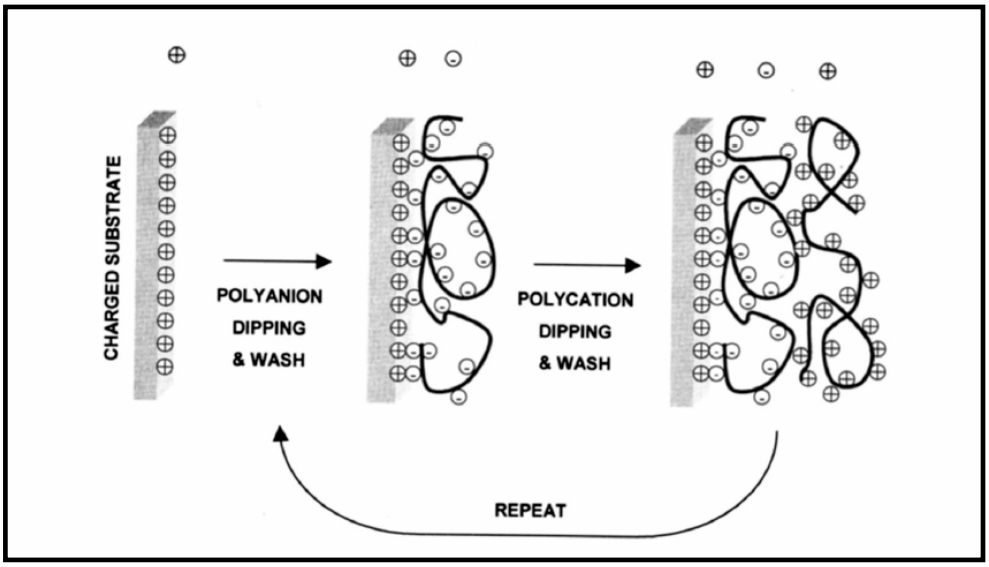

Figure 1.10: ESA Schematic for buildup of multilayer assemblies by consecutive adsorption of anionic and cationic polyelectrolytes from aqueous solutions (Reproduced by the permission of © 2003 IEEE) [140]

Practical devices and systems are comprised of more than one type of functional nanoparticle. Therefore, patterning techniques must be developed to integrate the self-assembled monolayers (SAMs) into a device or systems at a micro or nano meter level. There are various ways to pattern SAMs including micro contact printing (see Section

[138] Y. Liu, A. Wang, R. O. Claus, Applied Physics Letters, Vol. 71, 2265-2267 (1997).
[139] M. F. Durstock, B. Taylor, R. J. Spry, L. Chiang, S. Reulbach, K. Heitfeld, J. W. Baur, Synthetic Metals, Vol. 116, 373-377 (2001).
[140] F. J. Arregui, I. R. Matias, R. O. Claus, IEEE Sensors Journal, Vol. 3, 56-61 (2003).
[141] F. J. Arregui, I. Latasa, I. R. Matias, R. O. Claus, Sensors, Proceedings of IEEE, Vol.1, 107-110 (2003).

1.4.5), dip-pen nanolithography [142, 143, 144], selective removal of particular adsorbates [145, 146], destruction with energetic beams, deliberate removal with scanning probe microscopes moving in a determined rastering pattern and the application of force or delivery of low energy beams [147, 148, 149]. Micro contact printing, which is the most commonly used SAMs patterning method, will be explained in the next section.

1.4.5 Micro Contact Printing

Micro contact printing (μCP), which is a flexible, non-photolithographic method, was introduced by Whitesides and coworkers [150]. A structured, elastomeric stamp is used in this method to transfer an "ink" to the surface of a substrate by contact. After transferring the stamp's pattern onto the substrate, different self assembled monolayers can be formed on the stamped or unstamped regions. Figure 1.11 describes the production of a SAM of hexadecanethiolate on a silicon substrate using the μCP technique [151]. In this study, Whitesides et al., first fabricated the elastomeric stamp by casting poly(dimethylsiloxane) (PDMS) on a pre-patterned silicon substrate. Next, they applied hexadecanethiol solution on the PDMS stamp and contacted with it the gold coated silicon substrate. After transferring the SAM of hexadecanethiol by contact of the PDMS stamp either selective etching or deposition of appropriately charged materials is achieved.

Micro contact printing has been used extensively for the direct deposition of SAMs of thiols and silanes [152, 153, 154]. Recently, this technique has been extended to also stamp

---

[142] B. W. Maynor, Y. Li, J. Liu, Langmuir, Vol. 17, 2575-2578 (2001).
[143] H. Zhang, S-W. Chung, C. A. Mirkin, Nano Letters, Vol. 3, 43-45 (2003).
[144] S. K. Kwak, G. S. Lee, D. J. Ahn, J. W. Choi, Materials Science and Engineering, Vol. 24, 151-155 (2004).
[145] T. Cui, F. Hua, Y. Lvov, Sensors and Actuators A, Vol. 114, 501-504 (2004).
[146] S. Y. Oh, I. S. Oh, J-W Choi, Materials Science and Engineering C, Vol. 24, 307-309 (2004).
[147] S. Hong, C. A. Mirkin, Science, Vol. 288, 1808-1811 (2000).
[148] J. Zhao and K. Uosaki, Nano Letters, Vol. 2, 137-140 (2002).
[149] R. Maoz, S. R. Cohen, J. Sagiv, Advanced Materials, Vol. 11, 55-61 (1999).
[150] A. Kumar, G. M. Whitesides, Applied Physics Letters, Vol. 63, 2002-2004 (1993).
[151] Y. Xia, X-M. Zhao, G. M. Whitesides, Microelectronic Engineering, Vol. 32, 255-268 (1996).
[152] C. Marzolin, A. Terfort, J. Tien, G. M. Whitesides, Thin Solid Films, Vol. 315, 9-12 (1998).
[153] H. S. Shin, H. J. Yang, Y. M. Jung, S. B. Kim, Vibrational Spectroscopy, Vol. 29, 79-82 (2002).
[154] M. Geissler, H. Schmid, B. Michel, E. Delamarche, Microelectronic Engineering, Vol. 67-68, 326-332 (2003).

proteins [155], co-polymers in combination with proteins [156], organic semiconductors [157, 158] and metal nanoparticles [159].

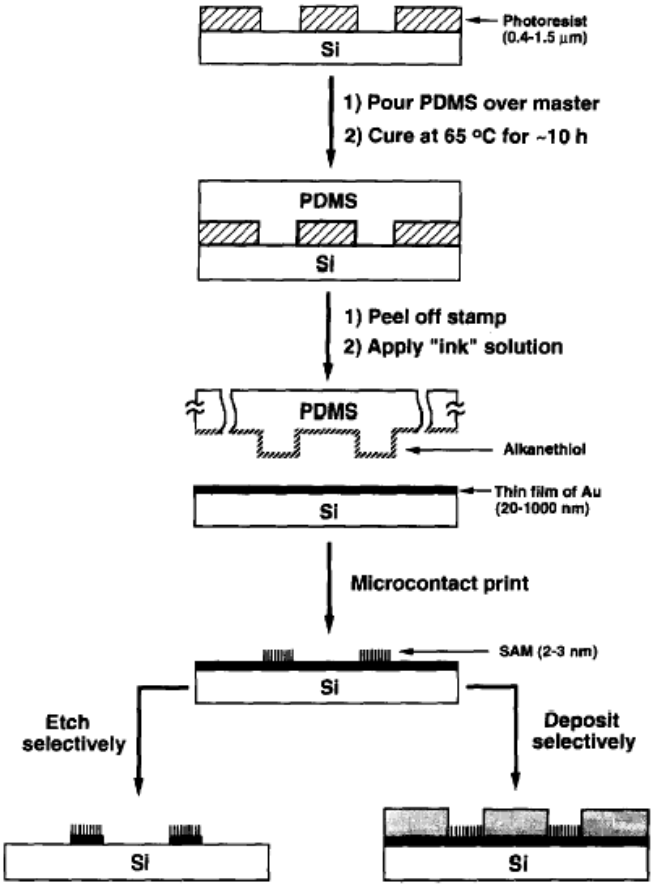

Figure 1.11: Schematic diagram of μCP of SAM of hexadecanethiolate on silicon substrate (Reproduced by the permission of Elsevier) [151]

1.5 Applications

The aforementioned organic or solution processable materials are being used at almost all levels of electronics and their application areas are increasing because of their ease of

[155] N. Sgarbi, D. Pisignano, F. Di Benedetto, G. Gigli, R. Cingolani, R. Rinaldi, Biomaterials, Vol. 25, 1349-1353 (2004).
[156] G. Csucs, R. Michel, J. W. Lussi, M. Textor, G. Danuser, Biomaterials, Vol. 24, 1713-1720 (2003).
[157] X. Wang, M. Östblom, T. Johansson, O. Inganäs, Thin Solid Films, Vol. 449, 125-132 (2004).
[158] F. Guan, M. Chen, W. Yang, R. Zhang, S. Yang, Q. Xue, Applied Surface Science, Vol. 230, 131-137 (2004).
[159] W. K. Ng, L. Wu, P. M. Moran, Applied Physics Letters, Vol. 81, 3097-3099 (2002).

fabrication, light weight and low cost of those materials. Some possible applications have already been discussed briefly. Here, more detailed information will be provided. The major focus of this section is inkjet printable materials and their applications, while, sensors, actuators, photovoltaic devices and smart structures and composites will also be discussed.

Inkjet printing is one of the most frequently used techniques to deposit and pattern solution processable insulators, semiconductors and metals. The most crucial parameter of the inkjet printing process is the ink. Ink chemistry and formulation not only affects the resolution of the inkjetted patterns but also affects the drop ejection characteristics. Generally, the viscosity of the ink should be lower than 20 cP [160]. If the viscosity of the ink is too high, ink droplets are not ejected through the nozzle due to high viscously dissipated kinetic energy. Because of this, polymer inks should be sufficiently dilute, consisting of about 1-2 weight percent solids. Surface tension is another important parameter. Typically it should be about 30 mN/m [161]. If the surface tension is too low, ink will not be stable on the printhead surface. On the other hand, if it is too high, ink cannot be jetted properly. Numerical models of droplet formation as a function of ink properties have been studied extensively [162, 163, 164]. Resolution of printed patterns depends on the jetting conditions, nozzle dimensions and ink properties. Clarke et al. [165] and Holman et al. [166] researched spreading of liquid ink droplets on a porous substrate. Speakman et al.[167] investigated single solid inkjet printed polythiophene dot features ranging from 42-175 μm. They observed "Gaussian-like" dots, which have a maximum thickness at the center and "Doughnut-like" dots, which have a maximum thickness at the edge. Speakman et al. concluded that the shape of the inkjet printed dots depends on ink

[160] M. M. Mohebi, J. R. G. Evans, Journal of Combinational Chemistry, Vol. 4, 267-274 (2002).
[161] P. Calvert, Chemistry of Materials, Vol. 13, 3299-3305 (2001).
[162] D-Y. Shin, P. Grassia, B. Derby, International Journal of Mechanical Sciences, Vol. 46 181-199 (2004).
[163] T. M. Liou, K. C. Shih, S. W. Chau, S. C. Chen, International Communications in Heat and Mass Transfer, Vol. 29, 1109-1118 (2002).
[164] H. C. Lee, IBM Journal of Research and Development, Vol. 18, 364-369 (1974).
[165] A. Clarke, T. D. Blake, K. Carruthers, A. Woodward, langmuir, Vol. 18, 2980-2984 (2002).
[166] R. K. Holman, M. J. Cima, S. A. Uhland, E. Sachs, Journal of Colloid and Interface Science, Vol. 249, 432-440 (2002).
[167] S. P. Speakman, G. G. Rozanberg, K. J. Clay, W. I. Milne, A. Ille, I. A. Gardner, E. Bresler, J. H. G. Steinke, Organic Electronics Vol. 2 65-73 (2001).

formulation, printhead droplet firing parameters, drop impact, and solidification properties.

In recent years, there has been an intense interest in organic light emitting diodes (OLEDs) fabricated by inkjet printing [168]. Hebner et al. [168(c)] used a Cannon PJ-1080A color inkjet printer having a 65 μm nozzle diameter to fabricate organic light emitting diodes on flexible polyester. They mixed the hole-transport polymer polyvinylcabazol (PVK) and light emitting dyes coumarin 6 (C6), coumarin 47 (C47), and nile red and then deposited than by inkjet printing. Kobayashi et al. [168 (d)] developed a system for patterning electroluminescent layers on thin film transistor substrates using inkjet technology. They deposited poly(para-phenylene vinylene) (PPV) as a green or a red emitter by inkjet printing and polyethylene dioxythiophene (PEDOT) doped with polystyrene sulphonate (PSS) to fabricate thin film transistors. Kobayashi et al. succeeded in displaying a multicolor image using the thin film transistor- light emitting polymer displays formed using this method. Duineveld et al. also used the same conducting polymers to fabricate OLEDs [168 (e)]. They printed polymers using single nozzle inkjet printheads on pre-patterned substrates. They first built barriers using photolithography to prevent the spreading of the polymer on the surface. Using this method, Duineveld et al. fabricated 64x96 full color passive matrix displays with 300 micron diameter pixels. Yang et al. and Chang et al. have also reported electroluminescent devices manufactured by hybrid inkjet printing.

Wang et al. [169] also used the inkjet printing method to fabricate organic thin film transistors (OTFTs). They first made a hydrophobic surface-energy barrier on the glass substrate by a direct write process based on laser patterning. Then they inkjet printed

[168] (a) S-C. Chang, J. Bharathan, Y. Yang, R. Helgeson, F. Wudl, M. B. Ramey, J. R. Reynolds, Applied Physics Letters, Vol. 73, 2561-2563 (1998), (b) Y. Yang, S-C. Chang, J. Bharathan, J. Liu, Journal of Materials Science: Materials in Electronics, Vol. 11, 89-96 (2000), (c) T. R. Hebner, C. C. Wu., D. Marcy, M. H. Lu, J. C. Sturm, Applied Physics Letters, Vol. 72, 519-521 (1998), (d) H. Kobayashi, S. Kanbe, S. Seki, H. Kigchi, M, Kimura, I. Yudasaka, S. Miyashita, T. Shimoda, C. R. Towns, J. H. Burroughes, R. H. Friend, Synthetic Metals, Vol. 111-112, 125-128 (2000), (e) P. C. Duineveld, M. M. de Kok, M. Buechel A. H. Sempel, K. A. H. Mutsaer, P. van de Weijer, I. G. J. Camps, T. J. M. van den Biggelaar, J-E. J. M. Rubingh, E. I. Haskal, Proceedings of SPIE, Vol. 4464, 59-67 (2002).

[169] J. Z. Wang, Z. H. Zheng, H. W. Li, W. T. S. Huck, H. Sirringhaus, Nature Materials, Vol. 3, 171-176 (2004).

PEDOT/PSS as the source and drain electrodes. Predefined surface energy patterns control the flow and spreading of jetted droplets on the substance. Hence, Wang et al. succeeded in making very-well defined channels with standard lengths of 5 μm and 10 μm. Regarding the diameter of inkjet printhead nozzle size, which is approximately 50 μm, Burns et al.'s method is very promising to reduce the size of inkjet printed devices. In this study, semiconductor, poly(dioctyl-fluorene-co-bithiophene) (F8T2), layers are also produced by inkjet printing technology. Finally, they built dielectrics and gate electrodes on top of this structure.

Another design of OTFT was reported by Kawase et al. [170]. Similarly, they used PEDOT/PSS as an electrode material, F8T2 as the semiconductor material, and poly(vinyl phenol) (PVP) as the dielectric material. They made a via-hole connection between the bottom and top electrodes by inkjet printing the solvent of the dielectric polymer (PVP) (see Figure 1.12). Using an inkjet etching technique Kawase et al. fabricated depletion-load, enhancement-load and resistor-load inverters based on all-polymer TFTs. Chen et al. has fabricated RC filters on transparencies using inkjet printing technology [171]. They used PEDOT/PSS and polyaniline as active semiconductor materials and poly(4-vinylphenol) as insulating material.

One of the most promising organic materials for OFETs is pentacene, due to its higher mobility, better on-off ratio, and improved environmental stability compared to other organic semiconductors. Generally, lithographically subtractive processing and vacuum-based deposition techniques are used to fabricate flexible electronic devices, because of the severe insolubility of pentacene [172, 173]. However, recently, Afzali et al.[174] has

[170] T. Kawase, H. Sirringhaus, R. H. Friend, T. Shimoda, Advanced Materials, Vol. 13, 1601-1605 (2001).
[171] B. Chen, T. Cui, Y. Liu, K. Varahramyan, Solid-State Electronics, Vol. 47, 841-847 (2003).
[172] H. Klauk, D. J. Gundlach, J. A. Nichols, T. N. Jackson, IEEE Transactions on Electron Devices, Vol. 46, 1258-1263 (1999).
[173] U. Zschieschang, H. Klauk, M. Halik, G. Schmid, W. Radlik, W. Weber, Polymers and Adhesives in Microelectronics and Photonics, 2002. POLYTRONIC 2002. 2nd International IEEE Conference, 191-195 (2002).
[174] A. Afali, C. D. Dimitrakopoulos, T. L. Breen, Journal of American Chemical Society, Vol. 124, 8812-8813 (2002).

reported synthesis of soluble pentacene precursors. Subramanian et al. [175] fabricated inkjetted pentacene TFTs having mobility of 0.02 cm^2/Vs and on-off ratio of 10^5.

Inkjet printing technology has also been used to deposit photoresist lines having spacing of 10 μm [176]. Inkjet printable UV-curable resins and optical thermoplastics have been used to fabricate polymer micro-optical elements [177, 178].

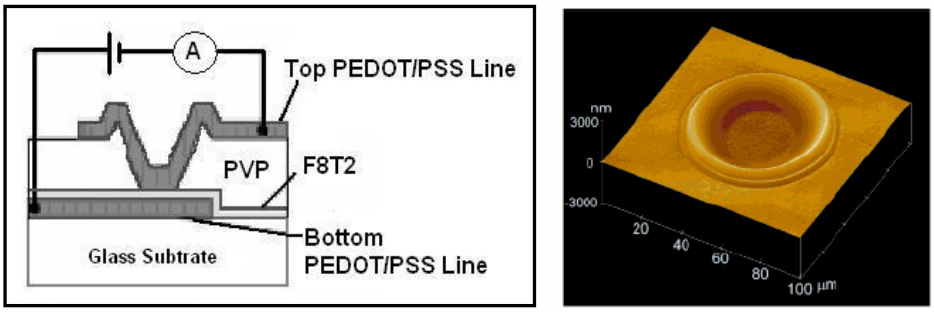

(a) **(b)**

Figure 1.12: (a) Schematic diagram of via-hole connected OTFT (b) AFM image of via-hole connected OTFT (Reproduced by the permission of WILEY-VCH) [170].

Inkjet printing of ceramics has been developed by different groups [184-187]. In 1998, Slade and Evans prepared ink based on zirconia and they used a Hewlett Packard Deskjet 500 having 60-nozzles with 50 μm diameter [179]. In 1999, Mott and Evans developed zirconia/alumina ink and used an IBM 3852-2 color-jet printer to fabricate a continuous functionally graded alumina-zirconia composite thin films [180]. Another group at the University of London also worked on zirconia ink for drop-on-demand inkjet printers

[175] S. K. Volkman, S. Molesa, B. Mattis, P. C. Chang, V. Subramanian, Materials Research Society Proceedings, Vol. 769, H11.7.1/L12.7.1-H11.7.6/L12.7.6 (2003).
[176] G. Percin, T. S. Lundgren, B. T. Khuri-Yakub, Applied Physics Letters, Vol. 73, 2375-2377 (1998).
[177] Y. Ishii, S. Koike, Y. Arai, Y. Ando, Japanese Journal of Applied Physics Letters, Vol. 39, 1490-1493 (2000).
[178] W. R. Cox, T. Chen, D. J. Hayes, Optics & Photonics News, Vol. 12, 32-35 (2001).
[179] C. E. Slade, J. R. G. Evans, Journal of Materials Science Letters, Vol. 17, 1669-1671 (1998).
[180] M. Mott, J. R. G. Evans, Materails Science and Engineering, Vol. A271, 344-352 (1999).

[181]. A ceramic ink for multilayer printing using submicron titania powder was formulated by P. Blazdell [182].

There is an interest in nanoparticle inks for inkjet printing technology, especially nanoparticle magnetic and metallic inks [183-192]. Printable metallic nanoparticle inks are favorable due to the need for low cost interconnection and electrodes for electronic devices. Inkjet printed silver [184], copper [185], diamond [186], and gold [187] nanoparticles have been reported. Solder droplet printing or solder paste printing is another method to deposit metals [188]. This technology is similar to conventional printing technology, through the solder paste printing technique is performed at temperatures higher than 200 °C.

Besides the field effect transistors and light emitting diodes solution processable materials can be used to build radio frequency identification tags (RFID), sensors, and actuators. Electronic textile, electronic papers and very large area displays are among the other promising application areas. The demand to fabricate flexible or wearable electronic devices is increasing every year and these products have started to find a place in the market. Table 1.9 summarizes the some commercially available products made of solution processable materials offering mechanical flexibility and low weight.

[181] X. Zhao, J. R. G. Evans, M. J. Edirisinghe, J. H. Song, Ceramics International, Vol. 29, 887-892 (2003).
[182] P. Blazdell, Journal of Materials Processing Technology, Vol. 137, 49-54 (2003).
[183] S. Sen, M. Manciu, F. S. Manciu, Applied Physics Letters, Vol. 75, 1479-1481 (1999).
[184] S. Magdassi, A. Bassa, Y. Vinetsky, A. Kamysshny, Chemistry of Materials, Vol. 15, 2208-2217 (2003).
[185] C. M. Hong, S. Wagner, IEEE Electron Device Letters, Vol. 21, 384-386 (2000).
[186] N. A. Fox, M. J. Youh, J. W. Steeds, W. N. Wang, Journal of Applied Physics, Vol. 87, 8187-8191 (2000).
[187] D. Huang, F. Liao, S. Molesa, D. Redinger, V. Subramanian, Journal of Electrochemical Society, Vol. 150, G412-G417 (2003).
[188] (a) Q. Liu, M. Orme, Journal of Materials Processing Technology, Vol. 115, 271-283 (2001), (b) S. Haferl, D. Poulikakos, International Journal of Heat Mass Transfer, Vol. 46, 353-550 (2003), (c) MicroFab Technologies, Inc. (www.microfab.com).

Table 1.9: Commercially available flexible electronics products

Application	Notes	Company Name	Reference
Flexible electronic paper display	-Display thickness: 300 µm - As flexible as construction paper	E Ink and LG.Phillips LCD	http://www.devlib.org/news
High Resolution Flexible Displays	-Display Thickness: 1.25 mm -Display Weight: 35 g	E Ink	http://www.eink.com
Flexible Microprocessor	-Active material: polysilicon -Microprocessor is composed of 32,000 transistors, operates at between 3.5 and 7.0 volts, and weighs 140 mg.	Epson	J. Boyd, Technology Newsline No 13, 2005
Printed RFID	-Types of printed substrates: paper, PET or polyester (heat-stabilized, print-treated) -Minimum antenna pad size is -0.006 square inches -Minimum trace (line) thickness 0.15mm (.006 inch) -Minimum space between traces (lines) 0.15mm (.006 inch)	Graphic Solutions International LLC	http://www.graphicsolutionsinc.com
Wearable electronics	-Snow gloves and jackets incorporate a wireless remote control for Apple's iPod MP3 players.	O'Neill	http://www.gizmag.com

1.6 OUTLINE OF DISSERTATION

The aim of this dissertation research is to investigate low cost methods to manufacture flexible electronic devices, and also to fabricate and characterize basic electronic devices. In this dissertation six chapters, including the above literature review are presented.

Inkjet printing of solution processable metals and the experimental fabrication of electrodes on flexible substrates will be described in Chapter 2. Conductive ink development and the electrical characterization of inkjet printed devices are the primary focus areas of this chapter.

Alternative metallization techniques of flexible materials will be discussed in Chapter 3. The design, preparation, and characterization of mechanically and thermally stable, electrically tunable organic semiconductor composite films, which can be used as electrodes, semiconductor substrates, and active materials in various electronic device applications, will be described in Chapter 4.

The line patterning method and its use to experimentally synthesize field effect transistors, and resistors will be discussed in Chapter 5. This chapter will also include the electrical characterization of inkjet printed solution processable semiconductors on flexible substrates.

Conclusions and a discussion of possible future work with organic flexible materials and the fabrication of organic electronic devices will be given in Chapter 6.

CHAPTER 2

Inkjet Printing of Solution Processable Metals: Ink Formulations and Characterizations

2.1 Introduction

The use of inkjet technology for the direct deposition of metals and various other materials not only reduces the cost but also eliminates the time-consuming production steps. Inkjet printers can transfer a required pattern on various substrates, including plastics in just seconds with high resolution. The major challenge in inkjet technology is the ink formulation and properties. Ink must contain the appropriate precursors and have certain viscosity and surface tension depending on the application and type of inkjet printer.

Solution processable metal-organic (MO) complexes and nanoparticles can be used as the ink for direct write applications. Various ink formulations for copper direct write have been reported previously [189,190]. Schulz [191] et al used Cu(I)-vinyltrimethylsilane and copper nanoparticles to direct write ~5 μm thick lines with ~3 Ω/□ sheet resistivity on polyimide substrate. However, extra care must be taken while working with copper ink since it oxidizes easily. Moreover, generally high deposition temperatures (~350-400 °C)

[189] H. K. Shin, K. M. Chi, M. J. Hampden-Smith, T. T. Kodas, J. D. Farr, M. Paffett, Chemistry of Materials, Vol. 4, 788 (1992)
[190] J. Rickerby, J. H. G. Steinke, Chemical Reviews, Vol. 102, 1525 (2002)
[191] D. L. Schulz, C. J. Curtis, D. S. Ginley, Electrocchemical and Solid-State Letters, Vol. 4, C58-C61 (2001)

are needed to convert the copper ink into the elemental metal form. Silver based inks are more promising due to their better environmental stability. Different researchers have tried to develop silver based ink formulations for solar cell applications [192,193]. Recently, a low curing temperature silver ink has been reported [194]. They prepared the ink by dissolving a synthesized silver carboxylate into an organic solvent. The following section describes an environmentally friendly and easy way to fabricate silver conductors on both glass and mechanically flexible polyimide substrates.

Monolayer protected metal nanoclusters (MPMCs) are another promising candidate of solution processable metals. Organic ligands or polymers can stabilize the metal nanoclusters and make them soluble into common nonpolar solvents [195,196]. Therefore, it is possible to use solution based manufacturing processes such as inkjet printing, microcontact printing and micropipette deposition to fabricate functional devices. In section 2.3, inkjet printing of gold nanoclusters onto flexible substrates will be discussed in detail.

2.2 Inkjet-printed Silver Conductors using Metal-organic Ink

In this study, silver MO complex (1,5-cyclooctadiene)(hexafluoroacetyl-acetonato)silver(I) (Ag(hfa)COD) was purchased from Aldrich and used as received. Toluene and butanol (Aldrich) were chosen as the solvents. Three different deposition techniques were used, which are micro-pipetting, micro pen deposition and inkjet printing. Effects of the deposition and post annealing temperatures on conductivity were examined. To measure the resistance of MO ink, 20 weight percent of Ag(hfa)COD was dispersed in toluene and deposited on a glass slide via a micropipette and a home made micro-pen. For inkjet printing of silver MO ink, toluene was replaced with butanol. In

[192] K. F. Teng, R. W. Vest, IEEE Electron Device Letters Vol. 9, 591 (1988)
[193] T. Rivkin, C. Curtis, A. Miedaner, J. Perkins, J. Allegan, D. Ginley, Photovoltaic Specialists Conference, Conference Record of the Twenty-Ninth IEEE, 1326 (2002)
[194] A. L. Dearden, P. J. Smith, D-Y Shin, N. Reis, B. Derby, P. O'Brien, Macromolecular Rapid Communications Vol. 26, 315 (2005)
[195] N. Toshima, Y. Shiraishi, T. Teranishi, M. Miyake, T. Tominaga, H. Watanabe, W. Brijoux, H. Bönneman, G. Schmid, Applied Organometallic Chemistry, Vol 15, 178 (2001)
[196] O. Tzhayik, P. Sawant, S. Efrima, E. Kovalev, J. T. Klug, Langmuir, Vol. 18, 3364 (2002)

this study, a Spectra printing system assembled on the Aerotech XYZ table was used to direct write both the silver MO ink.

2.2.1 Micro-pipetted Silver MO Ink

A saturated solution of Ag(hfa)COD in toluene filtered by 0.45 μm syringe filter and deposited on the glass slides. Prior to deposition glass slides were cleaned by sonication in isopropyl alcohol for 5 min and masked using polyimide tape to obtain a fine geometry. The silver MO ink was deposited on the substrate at room temperature in air. Samples were then annealed at 200 °C for 5 minutes to convert the deposited precursor to metallic silver. A rapid transition of the film color from dark yellow to white, accompanied by the sublimation of the organic component, was observed. The bulk resistivity of micro-pipetted films was 4.8×10^{-4} Ω.cm. A slight decrease in bulk resistivity was observed for the samples pre-heated to 200°C.

It was observed that micro-pipette deposition was useful to test the resistivity of the ink. However, it is very difficult to produce a fine patterns on the surface and, therefore, to calculate the resistivity. The next section describes a more effective way to test the ink before preparing large batches for inkjet printing.

2.2.2 Micro-pen Deposition of Silver MO ink

A home made micro-pen was used to try different ink formulations before printing on the inkjet printer. A pin ball pen tip with 1 mm resolution was attached to a glass tube using epoxy (see Figure 2.1). Like micro-pipetting, very little amount of ink, usually 0.3-0.5 ml, is enough to make conductive patterns. On the other hand, micro-pen deposition provides better line resolution compare to micro-pipetting.

18 weight percent Ag(hfa)COD was suspended in toluene and deposited on glass slides. The resolution of lines deposited at room temperature was poor. Therefore, experiments

were performed at 60±5 °C. After transferring the ink, the samples were annealed at 200 °C for 20 min. The sheet resistivity of the silver lines was 0.42 (Ω/□).

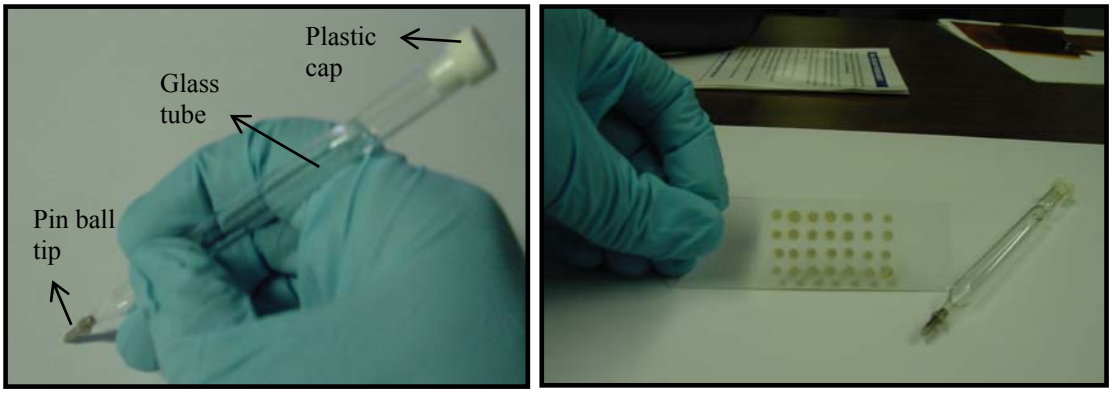

Figure 2.1: Picture of home made micro-pen (left), silver dot matrix on glass slide deposited via micro-pen (right)

Both micro pipetting and micro-pen depositions of silver MO ink showed very promising results. Therefore, a more sophisticated way to direct write this silver ink onto various substrates was studied. The next section describes the inkjet printing of silver MO ink.

2.2.3 Inkjet Printing of Silver MO ink

For inkjet printing, toluene was replaced with butanol, since the high evaporation rate of toluene causes clogging of the printhead. The physical properties of toluene, butanol and the ink requirements for the Spectra inkjet printhead can be seen in Table 2.1. The low viscosity of butanol provides an advantage by facilitating addition of polymeric modifiers to not only increase viscosity, but also increases adhesion between the rapid prototyped plies and the insulating substrate, if desired.

Table 2.1: Some physical properties of butanol and toluene at 20 ^{o}C and ink requirements for Spectra printhead.

	Butanol	Toluene	Spectra Ink Requirement
Viscosity (cP)	2.98	0.59	8-20
Surface Tension (dynes/cm)	25	28	28-32
Evaporation Rate (BuAc=1)	0.46	2.24	-

Silver MO ink was printed on pre-heated glass slides using the Spectra piezoelectric inkjet printer. Substrates were heated on a hot plate at 215 °C for a few minutes before printing. Lines were printed at various widths changing from 52 μm to 156 μm. The length of the lines was kept constant, which is 0.5 inch (see Figure 2.2). A resolution of 2117 dpi was used. In order to increase the ink loading on the surface multiple passes were performed, which caused wider lines on the surface. Following printing, the substrates were heated in air at 215 ^{o}C for 5 minutes.

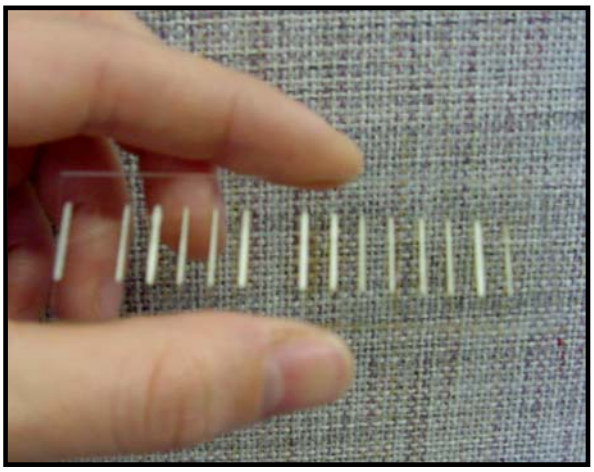

Figure 2.2: Inkjet printed silver lines on glass slide

Single pass silver lines were not conductive. Hence, multiple-layer lines were printed. The sheet resistivity decreased two orders of magnitude when the number of passes increased from 3 to 7. The sheet resistivity for the lines printed from 7 passes was 0.3 Ω/☐ (see Figure 2.3). Scotch tape pulling tests confirmed the good adhesion of silver thin film to the glass slide.

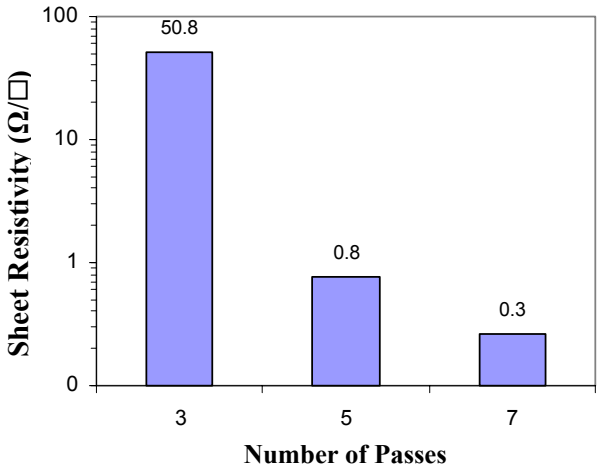

Figure 2.3: Sheet resistivity versus number of passes plot of inkjet printed ~1 mm wide silver lines.

The effect of the printing temperature on conductivity was also examined. A temperature sensor controlled hot plate was placed under the printhead to keep the substrate at a constant temperature. Prior to printing, glass slides were cleaned by sonicating in isopropyl alcohol for 5 min. Resolutions of 1058 and 2117 dpi were used and multiple passes were performed. Lines were printed on substrates at 50, 100 and 150 °C. As seen in Table 2.2, the lines printed at 50 °C were not conductive as printed. However, lines printed at 100 °C and 150 °C were conductive (see Figure 2.4). The resistivity of lines printed at 100 °C and 150 °C were 0.3 and 0.13 Ω/☐ respectively. After annealing at 300 °C for 20min in air, these values decreased to 0.15 and 0.12 Ω/☐. Also other lines printed at 50 °C became conductive. The lines printed at 150 °C spread too much on the surface due to the vigorous evaporation of the solvent. Therefore, it was difficult to make multiple passes more than 3 with a well defined geometry.

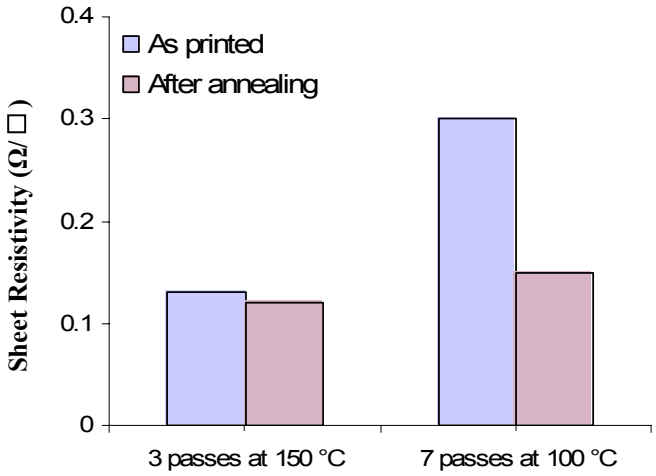

Figure 2.4: Sheet resistivity of silver lines printed different temperatures.

Silver MO ink was also inkjet printed on polyimide (Kapton) substrate that enabled us to combine electrical conductivity with mechanical flexibility (see Figure 2.5). Similar resistivity data were observed. Single pass lines were not conductive. Before annealing, the lines printed at 50 °C were not electrically conductive from 5 and 7 passes. However the lines printed at 100 and 150 °C were conductive without annealing. The resistivity of the samples decreased with annealing at 300 °C in air for 20 min. The sheet resistivity of silver lines on Kapton before and after annealing process and the printing conditions can be seen in Table 2.3.

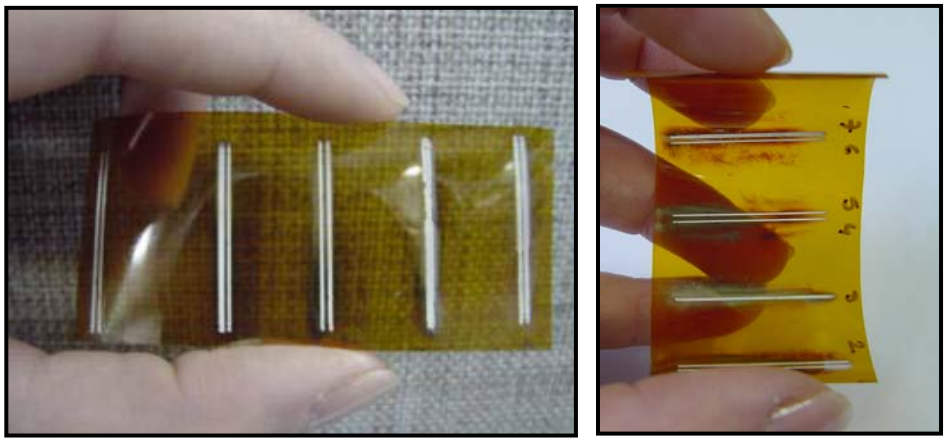

Figure 2.5: Inkjet printed silver lines on Kapton

Table 2.2: Sheet resistivity of silver lines inkjet printed on glass slide (a) before annealing (b) post annealed at 300 °C for 20 min

Number of Passes	Printing Temp (°C)	Resolution (dpi)	ρ (Ω/□)
5	50±5	1058	-
7	50±5	1058	-
7	50±5	2117	-
7	100±5	2117	0.30
3	150±5	2117	0.13

(a)

Number of Passes	Printing Temp (°C)	Resolution (dpi)	ρ (Ω/□)
5	50±5	1058	8.69
7	50±5	1058	0.76
7	50±5	2117	0.77
7	100±5	2117	0.15
3	150±5	2117	0.12

(b)

Table 2.3: Sheet resistivity and printing conditions of silver lines inkjet printed on Kapton (a) as printed, (b) post annealed at 300 °C for 20 min

Number of Passes	Printing Temp (°C)	Resolution (dpi)	ρ (Ω/□)
7	50±5	2117	-
5	100±5	2117	0.40
7	100±5	2117	0.35
2	150±5	2117	1.61
3	150±5	2117	1.21

(a)

Number of Passes	Printing Temp (°C)	Resolution (dpi)	ρ (Ω/□)
7	50±5	2117	0.52
5	100±5	2117	0.27
7	100±5	2117	0.26
2	150±5	2117	1.08
3	150±5	2117	0.82

(b)

As seen in Figure 2.6 the best resolution was obtained for the lines printed at 100 °C. The 50 °C substrate temperature was not enough to evaporate the solvent of silver MO ink leaving behind the conductive pattern. At 150 °C butanol spread too much on the polyimide substrate due to rapid evaporation resulting in distortion of pattern. A printing temperature of 100 °C, which is very close to boiling point of butanol (116-117 °C), resulted in the best resolution.

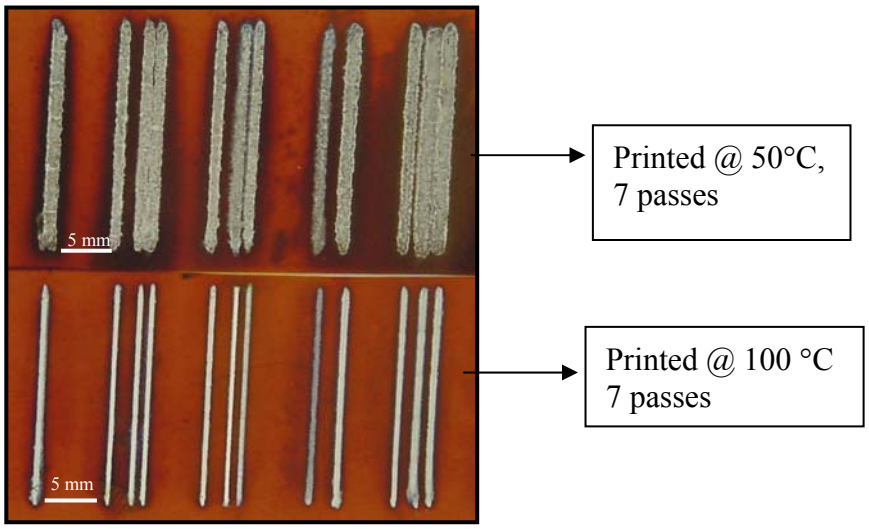

Figure 2.6: Resolution of inkjet printed silver lines printed at two different temperatures on Kapton

The effect of the silver nanoparticle on the resistivity of inkjet printed line was also investigated. For this purpose, 0.19 g silver nanopowder and 1.42 g Ag(hfa)COD were blended together and dispersed in 7 mL butanol. After filtering the suspension via 0.45 μm syringe filter silver lines printed on both glass and Kapton at different temperatures. Samples were annealed at 300 °C for 20 min in air. It is observed that sheet resistivity decreased ~75% for the lines printed on Kapton at 150 °C. This decrease was ~50 % for the line printed on Kapton at 100 °C (see Figure 2.7). Higher silver nanopowder fraction may results smaller sheet resistivity. However, one should keep in mind that silver

nanoparticles have a tendency to agglomerate and higher amounts increase the possibility of agglomeration.

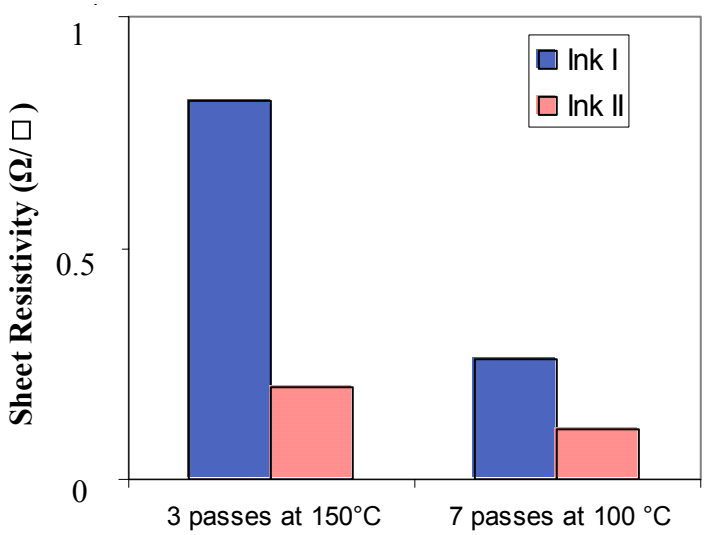

Figure 2.7: Sheet resistivity of silver lines printed on Kapton at two different temperatures using two different ink formulations. (Ink I contains 1.42 g Ag(hfa)COD in 7 mL butanol, Ink II contains 1.42 g Ag(hfa)COD and 0.19 g silver nanopowder in 7 mL butanol)

Successful inkjet printing of silver MO ink has been demonstrated in this section. The electrical conductivity high enough to fabricate electrode for electronic applications was combined with the mechanical flexibility of substrate material. The next section describes the inkjet printing of conducting nanoclusters on mechanically flexible substrates.

2.3 Inkjet Printing of Conducting Nanoclusters

As discussed in Chapter 1 encapsulated metal nanoclusters are favorable due to their solution processability. This section is focusing on the processing of encapsulated gold nanoclusters for generating solution processable metal nanoclusters. Investigation of the physical properties, such as viscosity and surface tension of inkjet printable gold ink, and

electrical conductivity and spatial resolution of printed gold lines are discussed in the following section.

The gold nanoclusters were prepared using the procedure reported by R. W. Murray's research group in University of North Carolina [197]. Basically synthesis of these nanoclusters is performed by transferring a gold salt hydrate from the aqueous to the organic phase, followed by encapsulation of the resulting nanoclusters and finalized by reduction of these gold nanoclusters. The inkjet printable conductive ink was prepared by re-dispersing encapsulated gold nanoclusters were in appropriate solvents. Prepared conductive ink was jetted via Spectra Inkjet System. The following section describes the conductive ink properties and electrical characterization of inkjet printed gold lines.

2.3.1 Results and Discussion

The physical properties of the inkjet printable gold ink and therefore the electrical properties of printed thin films can be controlled by the nanoparticle size. It has been shown in the literature that the resulting nanoparticle size can be controlled [198]. Size of the gold nanoclusters is very important for inkjet printing process in two aspects. First, due to the small size of printer nozzle the conductive ink should contain very small particles, generally less than 1 micrometer. Second, the sizes of gold nanoclusters affect the melting temperature. Smaller sized nanoclusters tend to melt at lower temperatures. As seen in Figure 2.8 the particle size of gold nanoclusters synthesized in our laboratory was ranging between 1-10 nm. This particle size is sufficiently small to facilitate inkjet printing.

[197] M. J. Hostetler, J. E. Wingate, C.-J. Zhong, J. E. Harris, R. W. Vchet, M. R. Clark, J. D. Longdono, S. J. Green, J. J. Stokes, G. D. Wignall, G. L. Glish, M. D. Porter, N. D. Evans, and R. W. Murray, Langmuir, Vol. 14, 17-30 (1998)
[198] D. V. Leff, P. C. Ohara, J. R. Heath, W. M. Gelbart, Journal of Physical Chemistry **99**, 7036 (1995)

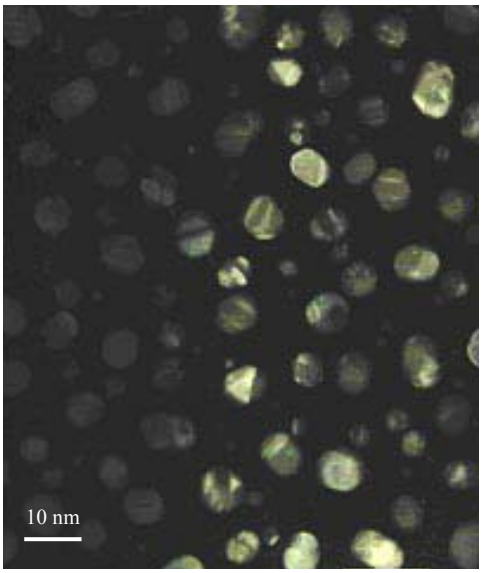

Figure 2.8: TEM image of inkjet printable gold ink

Inkjet printed gold thin film from encapsulated gold nanoclusters become conductive upon annealing at 140-200°C for anywhere from 2 minutes to 2 hours. Both chemistry of ink and annealing temperature affects the coalescence time of the gold ink. The relation between the coalescence time and the temperature of gold nanoclusters was studied by recording the resistivity data of inkjet printed gold lines which were placed in a temperature controlled oven. It was observed that ~15 and ~30 minute of annealing at 200 and 180 ˚C respectively was enough to convert the printed line into metallic form. This temperature range was well below the melting point of bulk gold (1064 ˚C) and compatible with lots of commercially available plastic substrates.

Table 2.4 compares the physical properties of gold ink and Epson's Durabrite® ink, which is used as "control ink". The similarity in physical properties of these two ink suggests that gold ink could be feasibly used in Epson printer for rapid print prototyping of conductive plies.

Table 2.4: Room temperature viscosity and surface tension of NanoSonic's conductive ink compared to Epson Durabrite® ink

	Printable Gold Ink	Spectra Ink Requirement	Epson Durabrite® ink
Viscosity (cP)	0.7-1.0	8-20	2.4-4.8
Surface Tension (dynes/cm)	29.5	28-32	31

Micropipette deposition of gold ink onto glass microscope slides at room temperature showed that the encapsulated gold nanoparticle ink was feasible for inkjet printing (Figure 2.9). The conductivity of gold thin film on glass slide was 1 Ω/□ via a two point measurement after annealing at 200˚C.

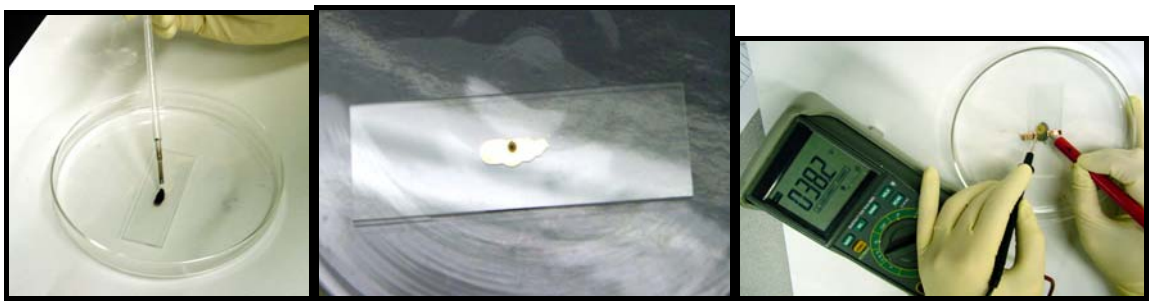

Figure 2.9: Micropipetting, annealing, and conductivity measurements of deposited gold nanocluster based inks on glass

Next, the gold nanocluster ink was inkjet printed on various substrates. Line-width and resolution of printed lines were 0.5 mm and 1058 dpi. The spatial resolution can be improved by changing the ink formulation (viscosity, surface tension), surface preparation of substrates, and printhead control systems.

Several substrate materials such as DuPont Melinex® PET polyester film, polyurethane, and polyvinylidenefluoride (PVDF) were investigated. The gold inks were printed on Melinex® film from single, double, and triple passes. During the printing process the substrate was kept at room temperature. Gold printed Melinex® film substrates were annealed at 200°C for 90 seconds in the oven. The annealing time was minimized to prevent degradation of the Melinex® film. Resistance measurements were performed at room temperature by Hewlett Packard 34401A multimeter (see Figure 2.10).

Figure 2.10: Inkjet printed gold lines on DuPont Melinex® PET polyester film

Table 2.5 summarizes the conductivity values of the single pass inkjet printed gold line using 1058.3 dpi. The maximum conductivity on Melinex® film was approximately $8x10^2$ S/cm. The thickness and sheet resistivity of the same sample were 2 μm and 5 Ω/□ respectively. The gold lines printed from double and triple passes were not electrically conductive, probably due to incomplete coalescence. As mentioned previously longer annealing times are not suitable for plastic substrates.

Table 2.5: Dimensions and electrical conductivities of gold lines (Printing Conditions: 1058.3 Dpi, 1 pass)

Sample Number	Resistance (Ω)	Length (cm)	Width (cm)	Thickness (cm)	Sheet Resistivity (Ω/□)	Bulk Resistivity (Ω.cm)	Conductivity (S/cm)
1	142	1.27	6.35×10^{-2}	2.54×10^{-4}	7.10	1.80×10^{-3}	554.51
2	72.6	1.27	1.27×10^{-1}	5.08×10^{-4}	7.26	3.69×10^{-3}	271.14
3	94.3	1.21	6.35×10^{-2}	2.54×10^{-4}	4.96	1.26×10^{-3}	793.25
4	111	1.21	1.27×10^{-1}	2.54×10^{-4}	11.68	2.97×10^{-3}	336.95
5	66	1.21	1.27×10^{-1}	2.54×10^{-4}	6.95	1.76×10^{-3}	566.69

In order to test the electrical conductivity of bent samples a simple experiment was performed by wrapping gold printed Melinex® film around a curved substrate, for a radius of curvature of approximately 0.5". It was observed that the conductive pathways were not disrupted during elastic deformation, as indicated by the curved and flat resistivity measurements in Figure 2.11. Moreover, it is worth to note that the curved substrate had approximately the same resistivity as the flat substrate. The bent lines appeared to have reasonable adhesion, supported by the lack of delamination.

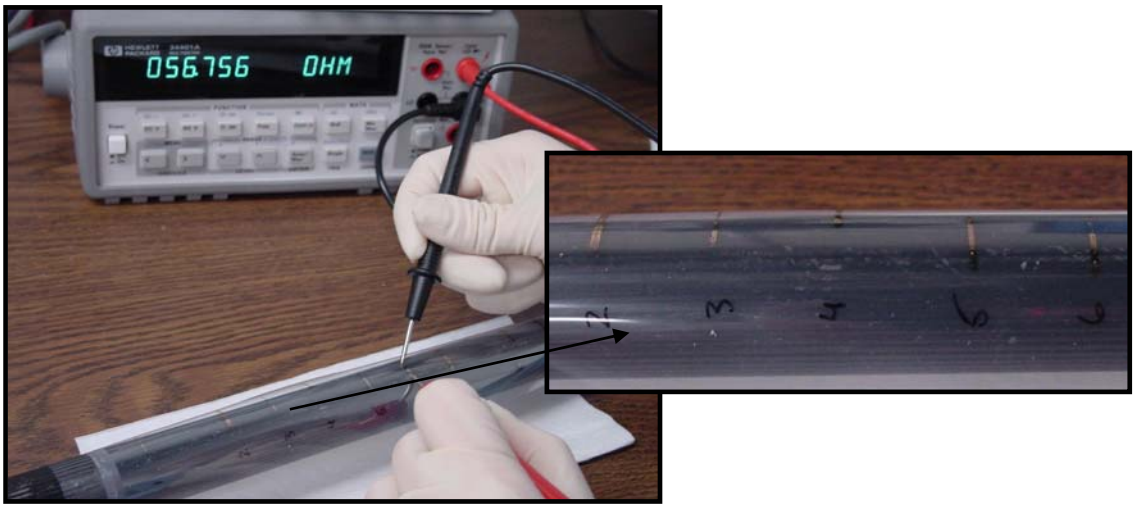

Figure 2.11: Conductivity measurement of inkjet printed gold lines on bent PET films.

Polyurethane and poly(vinylidene fluoride) were also used as substrate materials. Low resistivities were again obtained during the conductivity measurements on the poly(urethane) samples, as low as approximately 2 Ω/□ via two point measurements. However, the PVDF samples were not conductive. The primary reason for this could be the very quickly deformation of the PVDF substrate during annealing process.

2.4 Conclusions

Inkjet printing method is one of the key technologies to transfer the solution processable metals, semiconductors and insulators using computer aided tools. This technique eliminates the need for high temperature and high pressure fabrication steps. Using inkjet printing method it is possible to fabricate both passive and active electronic elements onto various substrates including traditional semiconductors, plastics and even paper.

The ink formulation and the surface properties of the substrates are the two crucial phenomena for inkjet printing process. As mentioned, ink must contain certain active materials and also should have specific viscosity and surface tension. In our laboratory both silver and gold inks were synthesized and inkjet printed on various substrates. The sheet resistivities as low as 0.1 and 5 Ω/□ for silver and gold inks were obtained respectively. Both ink formulations are compatible with lots of commercially available plastics such as PET, polyimide and polyurethane films. The silver and gold thin films are highly adhesive and patterns readily pass the Scotch-tape tests.

So far, the possible metal ink formulations, physical and chemical properties of ink, inkjet printing conditions and thin film formation on flexible substrates have been discussed. Although the inkjet printing method has aforementioned advantages over traditional metallization techniques, it is a challenge to make high resolution complex patterns using this technology. The next chapter describes an alternative method for metallization of the flexible substrates. By describing various methods, it is aimed to find the most cost effective and facile process to fabricate flexible electronics.

CHAPTER 3

Alternative Methods for Metallization of Flexible Substrates

3.1 Introduction

Metallization of the dielectrics such as polymers is extremely important in the fabrication of microelectronic devices. In previous chapter, pros and cons of inkjet printing of gold and silver on flexible materials have been discussed. In this chapter, we will focus on alternative selective metal deposition techniques of flexible materials. Also some basic electrical characteristics of patterned metal thin films will be discussed in this chapter.

Electroless plating is a widely used process in electronics to fabricate thin metal films on dielectric materials including plastics. Basically, this process involves the chemical reduction of metal compounds in a solution of a proper reducing agent [199]. Electroless nickel, copper and gold plating are among the well known metallization processes [200]. In order to integrate electrolessly deposited metals into functional devices it is crucial to pattern those metals onto surface. Traditional photolithography method is the most commonly used technique for this purpose [201]. Recently, new patterning methods such

[199] J. Mcdermott, Electroless Plating and Coating of Metals, Noyes Data Corporation, New Jersey (1972).
[200] (a) G. O. Mallory, Electroless Plating: Fundamentals and Applications, William Andrew Publishing/Noyes, New York (1990), (b) R. Jagannathan, M. Krishnan, IBM Journal of Research and Development, Vol. 37, 117-123 (1993).
[201] (a) K. Akamatsu, A. Kimura, H. Matsubara, S. Ikeda, and H. Nawafune, Langmuir, Vol. 21, 8099-8102 (2005), (b) M. Topper, Th. Stolle, H. Reichl, Advanced Packaging Materials: Processes, Properties and Interfaces, Proceedings. International Symposium on 14-17 March 1999 Page(s):202 - 208

as microcontact printing, dip-pen lithography and inkjet printing have been reported to make selective electroless metal deposition [202]. In these techniques, first the catalyst material is deposited in a desired pattern and then the metal is deposited using electroless method. Since the metal thin film grows only on the catalyst material, a complex pattern can be observed. All these techniques require specific tools. Therefore, fabrication cost increases. Here we are proposing a cost effective and simple way to selectively metallize flexible substrates. Essentially, this method is combination of electroless deposition and line patterning method.

The Line patterning method was introduced by MacDiarmid et al. [203]. This method includes three steps; (i) the design of the negative image of the required pattern by using a computer aided design software, (ii) deposition of the water soluble active material on the substrate, (iii) removing the printed mask by sonicating the substrate in toluene or acetone for ~10s. Figure 3.1 summarizes the corresponding experimental procedure.

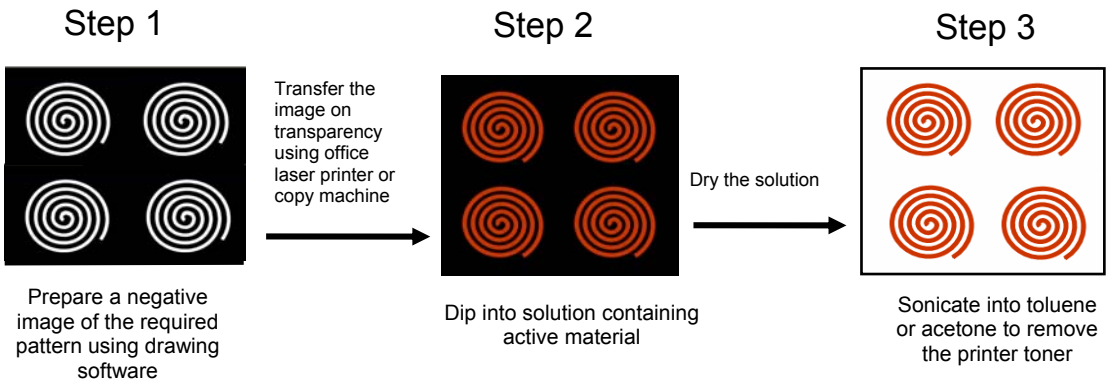

Figure 3.1: Experimental procedure to transfer the water based active material on the transparency via line patterning technique

[202] (a) T. B. Carmichael, S. J. Vella, A. Afazali, Langmuir, Vol. 20, 5593-5598 (2004), (b) K. Cheng, M-H Yang, W. W. W. Chui, C-Y Huang, J. Chang, T-F Ying, Y. Yang, Macromolecular Rapid Communications, Vol. 26, 247-264 (2005), (c) L. A. Porter, H. C. Choi, J. M. Schmeltzer, A. E. Ribbe, L. C. C. Elliot, J. M. Buriak, Nano Letters, Vol. 2, 1369-1372 (2002).
[203] D. Hohnholz, A. G. MacDiarmid, Synthetic Metals Vol. 121, 1327-1328 (2001).

MacDiarmid et al. used line patterning method to make polymer field effect transistors and simple push–button switches on paper and transparency films [204]. Okuzaki et al. [205] also fabricated field effect transistors using line patterning method. They used poly-3-4-ethyleneoxythiophene/poly-4-sytrensulfonate (PEDOT/PSS) as active material and poly (4-vinyl phenol) (PVP) as gate insulator. MacDiarmid et al. extended the line patterning method to fabricate metal electrode on paper and transparency [206]. Recently, Argun et al. used the same method to build gold electrodes for electrochromic devices [207].

We modified and improved their method to fabricate complex metal patterns on plastic substrates. Selectively silver, gold and copper deposition on flexible substrates using line-patterning method will be discussed in the following sections. Also a novel method to pattern copper on plastics will be discussed in Section 3.3.

3.2 Line-Patterning of Silver

Line patterning is the simplest and the most cost effective method among the printing techniques. It allows one to selectively deposit the water based materials onto flexible substrates including plastics and even paper. Due to its hydrophobic nature, printer toner repels the water based solution of active material. Therefore, the active material can be deposited on the unprinted areas. Based on this concept, we selectively deposited silver on to a polyimide substrate.

As mentioned in Chapter 1, polyimide is one of the most promising candidates in microelectronics as an insulating low-k dielectric for on-chip interconnects due to its good thermal properties and high chemical resistance [208]. The surface of the polyimide films can be modified using bases such as sodium hydroxide (NaOH) and potassium

[204] A. G. MacDiarmid, Synthetic Metals, Vol. 125, 11-22 (2002).
[205] H. Okuzaki, M. Ishihara, S. Ashizawa, Synthetic Metals, Vol. 137, 947-948 (2003).
[206] N.J. Pinto and A.G. MacDiarmid, Proceeding of the National Conference On Undergraduate Research (NCUR), 1-5 (2002).
[207] (a) A. A. Argun, P-H Aubert, B. C. Thompson, I. Schwendeman, C. L. Gaupp, J. Hwang, N. J. Pinto, D. B. Tanner, A. G. MacDiarmid, and J. R. Reynolds, Chemistry of Materials, Vol. 16, 4401-4412 (2004), (b) A. A. Argun and J. R. Reynolds, Journal of Materials Chemistry, Vol. 15, 1793-1800 (2005).
[208] K.L. Mittal, Polyimides: synthesis, characterization and applications, Plenum, New York (1984).

hydroxide (KOH) to open the imide rings and to form amides and carboxylate salts [209]. In this study, polyimide film was treated by KOH to open the imide rings on the surface and to convert it into potassium polyamate. Therefore, it is possible to exchange the potassium ions with silver ions by depositing the silver nitrate ($AgNO_3$) on the surface. Silver nitrate is highly soluble in water and can be easily reduced to the metallic silver form by thermal annealing.

The schematic presentation of processing steps employed in this work can be seen in Figure 3.2. The production of silver thin film on polyimide involves five steps: (1) surface modification of the polyimide film in 2M KOH at 50 ˚C for 5 min, (2) printing a black ink pattern "negative" on the substrate, (3) deposition of 0.2 M silver nitrate ($AgNO_3$) via pipette, (4) removal of the mask (if necessary), (5) thermally induced reduction of $AgNO_3$ into metallic silver.

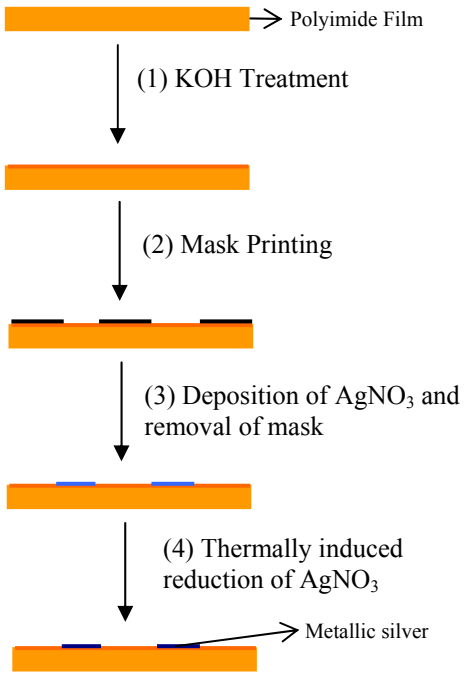

Figure 3.2: Schematic diagram of formation silver on modified polyimide film via line patterning method

[209] K-W Lee and A. Viehbeck, IBM Journal of Research and Development, Vol. 38, 457-474 (1994).

After $AgNO_3$ deposition, the substrates were annealed at 330 ˚C for 30 min. This process reduced the surface bounded silver ions into metallic form. Figure 3.3 shows the line patterned silver spirals and lines on Kapton ® Type HN polyimide film. It was observed that the silver thin films are electrically conductive and highly adhesive. Silver patterns readily pass the Scotch-tape tests.

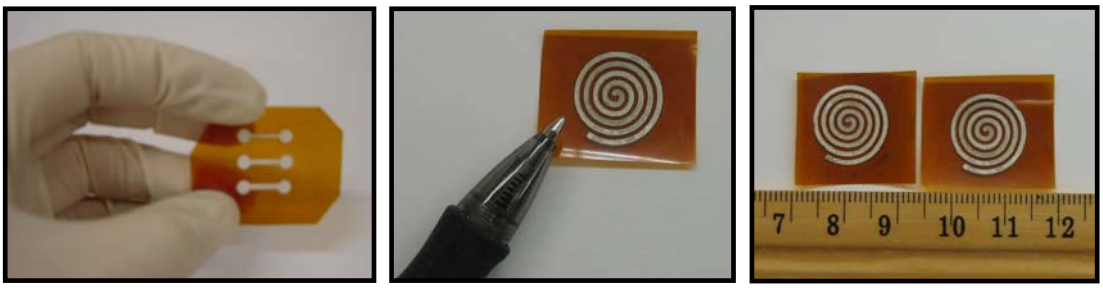

Figure 3.3: Pictures of line patterned silver on Kapton® Type HN polyimide film (end to end resistance of spirals is ~50 Ω)

As seen in Table 3.1 the resistivity of line patterned silver is ~$2x10^{-5}$ Ω.cm. For comparison resistivity of bulk silver is ~$2x10^{-6}$ Ω.cm. This low resistivity or high conductivity of line patterned silver with combination of mechanical flexibility of base material would make them very desirable for electronics. Longer annealing time or higher silver nitrate concentrations may help to increase the conductivity.

Table 3.1: Dimensions and electrical conductivities of line patterned 1 µm thick silver lines on polyimide

Length (cm)	Width (cm)	Resistivity (Ωcm)	Conductivity (S/cm)
0.7	0.07	$1.9x10^{-5}$	$5.3x10^{4}$
0.8	0.10	$2.0x10^{-5}$	$5.0x10^{4}$
0.7	0.13	$2.6x10^{-5}$	$3.9x10^{4}$

Dependence of the current density on applied voltage has been investigated using a Precision Programmable DC Power Supply and Agilent 34401 Multimeter. The applied voltage was increased stepwise until the microstrip burn-out. Figure 3.4 shows the increase in current density with voltage up to burn-out point. The power dissipation at burn-out point is 2.16 W for 0.8 x 0.1 cm silver microstrip with ~1 μm thickness.

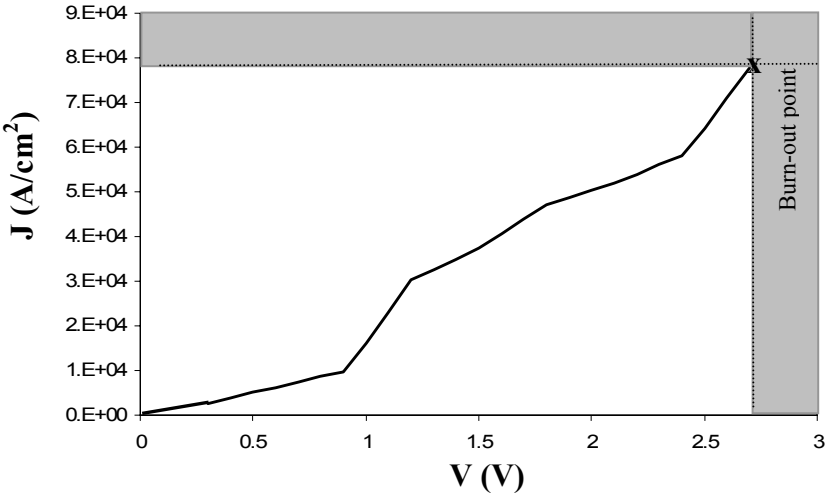

Figure 3.4: Current density versus voltage graph for line patterned silver on Kapton® Type HN polyimide film

3.3 Line-Patterning of Gold

In this section two different deposition techniques of gold on flexible substrates have been discussed. These methods will be called "Method 1" and "Method 2" for simplicity. In Method 1, McDiarmid et al.'s procedure was followed to pattern gold thin films on Xerox 3R3028 transparency film [207]. First, the negative pattern of required pattern printed on substrates. Then these substrates were immersed into tin and palladium baths successively. The substrates were then placed in to a nickel bath which is the catalyzer for electroless gold deposition. Before placing substrates into the gold bath, printer toner was removed by washing with acetone. The bath formulations and conditions are summarized in Table 3.2.

Table 3.2: Bath compositions for electroless gold deposition

	Chemical	*Concentration*	*Condition*
Tin Bath	Tin Chloride	0.1 g/L	-Room temperature -2 min immersion
	Hydrochloric acid (12 M)	0.1 ml/L	
Palladium Bath	Palladium Chloride	0.1 g/L	-Room temperature -2 min immersion
	Hydrochloric acid (12 M)	0.1 ml/L	
Nickel Bath	Nickel(II) sulfate heptahydrate	29g/L	-60 °C -until obtain a homogenous layer on the substrate
	Sodium hypophosphite monohydrate	17g/L	
	Sodium succinate	15 g/L	
	Succinic acid	0.36 g/L	
Gold Bath Solution A	Gold (I) sodium thiosulfate	25.2 g/L	-Mix equal amount of solution A and B -Room Temperature -until obtain a homogenous layer on the substrate
Gold Bath Solution B	Ascorbic acid sodium salt	19.8 g/L	
	Anhydrous citric acid	15.2 g/L	
	Potassium hydroxide	11.2 g/L	

The line patterned gold on transparency film can be seen in Figure 3.5. The conductivity of 0.4 cm wide and 2 cm long microstrip is about 1.9×10^4 S/cm which is very close to conductivity of bulk gold.

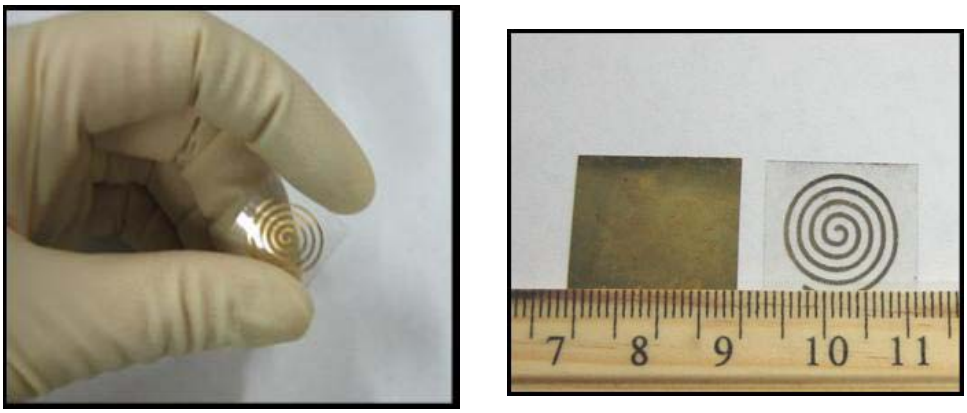

Figure 3.5: Pictures of line patterned gold on Xerox 3R3028 transparency film

In Method 2, the line patterned silver was used as the catalyst for electroless gold deposition. First, silver was selectively deposited on polyimide film as described in the previous section. Then, the substrate was directly immersed into the gold bath (see Table 3.2). This method not only provides deposition of gold on thermally, mechanically and chemically stable substrates but also eliminates the need for numerous chemicals. Moreover, more homogenous and thicker metal layers were obtained on the substrates using this technique. A very similar conductivity value, $1.5x10^4$ S/cm, was obtained with this deposition method compare to the first approach. The microstrips prepared by Method 2 showed higher power dissipation and lower current density compare to Method 1. Figure 3.6 shows current density dependency on applied voltage and power dissipation at burn-out point for two different methods.

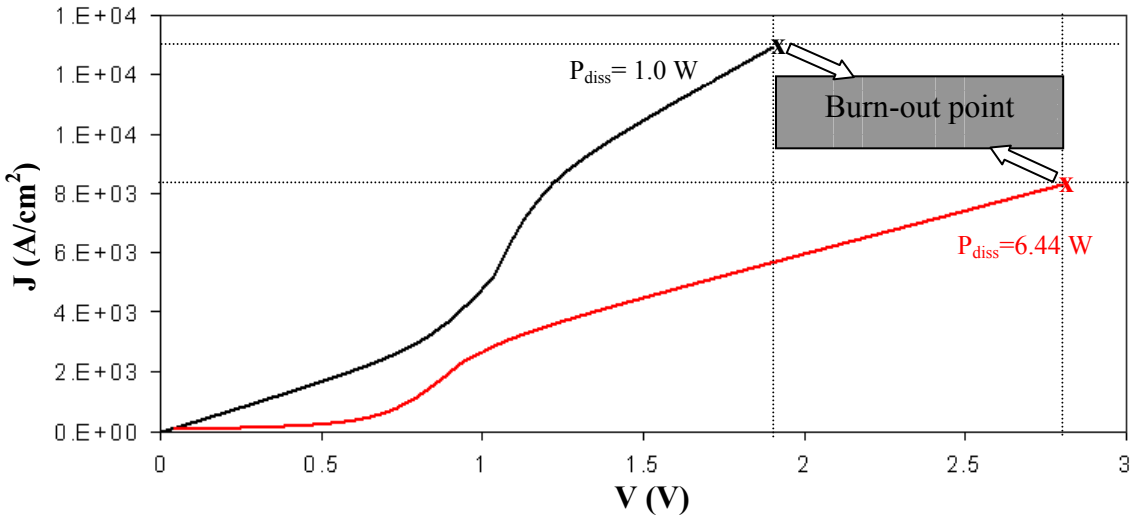

Figure 3.6: Current density versus voltage graph for line patterned gold on Xerox 3R3028 transparency film (black) and on Kapton® Type HN polyimide film (red).

3.4 Line Patterning of Copper

So far, the selective silver and gold patterning on flexible substrates has been discussed. Here a similar methodology will be applied to pattern copper. Two different low cost and low-tech selective patterning methods for copper will be introduced in this section. The first method is the line patterning method. As described earlier line-patterning method can be used to selectively activate the flexible substrates prior to electroless deposition of metal. The second method used in this dissertation is the printer masking method.

Electroless copper deposition is a well known process in microelectronics [210]. Selectively plated copper can be used as interconnect in printed circuit board, passive components in radio frequency (RF) and micro-electro-mechanical system (MEMS) technologies [211]. Therefore, finding a simple and cost effective way to selective copper deposition has been interest of many research groups [212]. However, all of these patterning methods require specific tools and multiple step manufacturing procedures.

A similar method with line patterning of silver and gold was used here to selectively deposit the copper on polyester (PET) and polyether imide (PEI). First, the surface of the substrate was cleaned by sonicating in isopropyl alcohol for 5 min. Then, corona treatment (~5 min/cm^2) was used to increase the hydrophilicity of the surface. Without corona treatment substrate failed to hold sensitizer and therefore catalizer solutions. Hence, copper did not grow homogenously on the surface (see Figure 3.7).

[210] C. F. Coombs, Printed Circuit Handbook, McGraw-Hill, New York (1996)
[211] (a) Y. Li, Z. Li, Y. Hao, G. Yan, W. Wu, X. Han, Solid-State and Integrated Circuits Technology, Proceedings, Vol. 3, 1900 - 1903 (2004), (b) M. Topper, T. Stolle, H. Reichl, Advanced Packaging Materials: Processes, Properties and Interfaces, Proceedings, Vol. 14-17, 202 – 208 (1999)
[212] (a) K. Akamatsu, S. Ikeda, H. Nawafune, and H. Yanagimoto, Journal of the American Chemical Society, Vol. 126, 10822-10823 (2004), (b) K. Akamatsu, A. Kimura, H. Matsubara, S. Ikeda, and H. Nawafune, Langmuir, Vol.21, 8099-8102 (2005), (c) C. D. Schaper, Nano Letters, Vol. 3, 1305-1309 (2003)

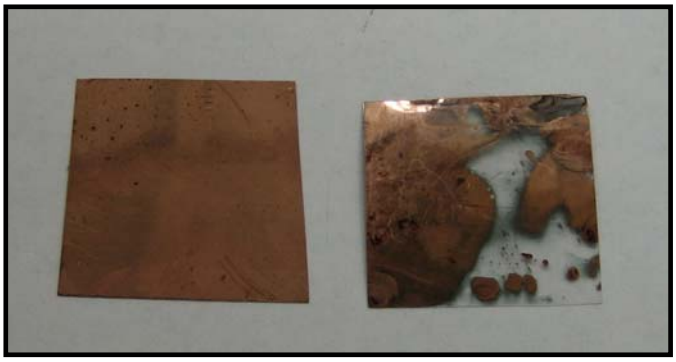

Figure 3.7: Effect of the corona treatment on electroless copper deposition (left: corona treated sample, right: without surface modification

A homogenous copper layer on a flexible surface was obtained using corona treated substrates. After corona treatment, the substrates were immersed into tin and palladium solutions successively for 5 minutes each. Then, the samples were dried in a forced air oven at 60 °C and the negative patterns were printed on the substrate using office laser printer. Finally, the substrates were immersed into copper sulfide bath for 5 minutes. The bath formulations can be seen in Table 3.3. Yu et al.'s [213] bath formulation has been modified in this study. We reduced the molarity of hydrochloric acid in both tin and palladium baths approximately three times. Higher pH bath formulations are preferable especially for plating plastic substrates. As seen in Figure 3.8, the line patterning method worked successfully with the copper.

[213] W.-X. Yu, L. Hong, B.-H. Chen, and T.-M. Koc, Journal of Materials Chemistry, Vol. 13, 818–824 (2003)

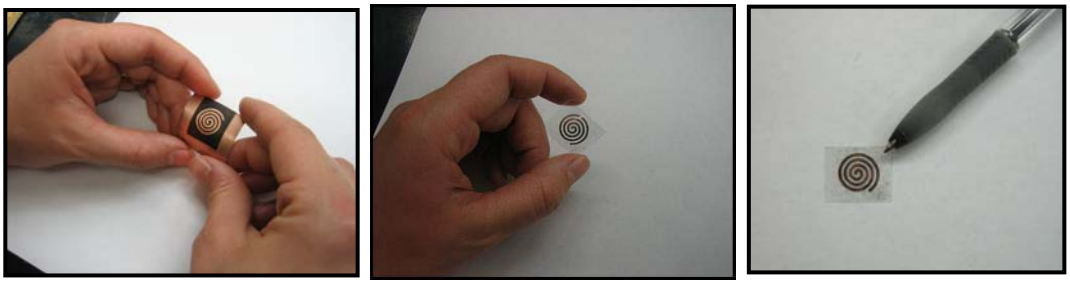

Figure 3.8: Line patterned copper spirals on PET before (left picture) and after (middle and right picture) removing printer toner.

Table 3.3: The composition of tin, palladium and electroless copper solutions

	Chemical	***Concentration***	***Conditions***
Tin Bath	Tin Chloride	10 g/L	-Room Temperature - 5 min immersion
	Hydrochloric acid	1.6 M	
Palladium Bath	Palladium Chloride	0.37 g/L	-Room Temperature - 5 min immersion
	Hydrochloric acid	0.5 M	
Copper Bath	Copper Sulfide	10 g/L	-Room Temperature - 5 min immersion for PET film and 3 min immersion for PEI film
	Potassium Sodium Tartrate	50 g/L	
	Sodium Carbonate	10 g/L	
	Sodium Hydroxide	10 g/L	
	Formaldehyde	50 mL/L	

PEI is also used as the flexible base material in this study. The PEI film, which is also called ULTEM, offers high performance across a broad range of demanding applications. It is used in flexible circuit technology because of the thermoplastic self-sealing properties of the films. Mobile phones, lap-top computers, bar code labels, flexible heaters, stiffeners, insulative tapes, motor insulation, speaker cones, and wire wrapping are among the potential application areas of Ultem films [214].

[214] (a) X. Li, K. Holappa, and K.Nelson, Oceans 2000 MTS/IEEE Conference and Exhibition Vol. 3, 2161 - 2168 (2000), (b) J.S. Kim, K.W. Paik, S.H. Oh, H.S. Seo, Multichip Modules and High Density Packaging, 7th International Conference on 15-17 April, 449 – 453 (1998), (c) S. Carroccioa, C. Puglisia, G. Montaudob, Polymer Degradation and Stability, Vol. 80, 459–476 (2003).

The same electroless copper formulation given in Table 3.3 was used to plate PEI films. Like PET films, it was observed that adhesion of copper on PEI was very pure without making any surface. Plasma treatment is one of the most commonly used methods to modify the surface of PEI films before electroless deposition [215]. Hence, we modified PEI substrates before electroless copper deposition via oxygen plasma for 5 minutes at 0.5 torr and 50W. The electrical conductivity of copper deposited on PET and PEI is $2x10^4$ and $1x10^4$ S/cm respectively. The current density versus voltage plot and power dissipation at burn-out point can be seen in Figure 3.9.

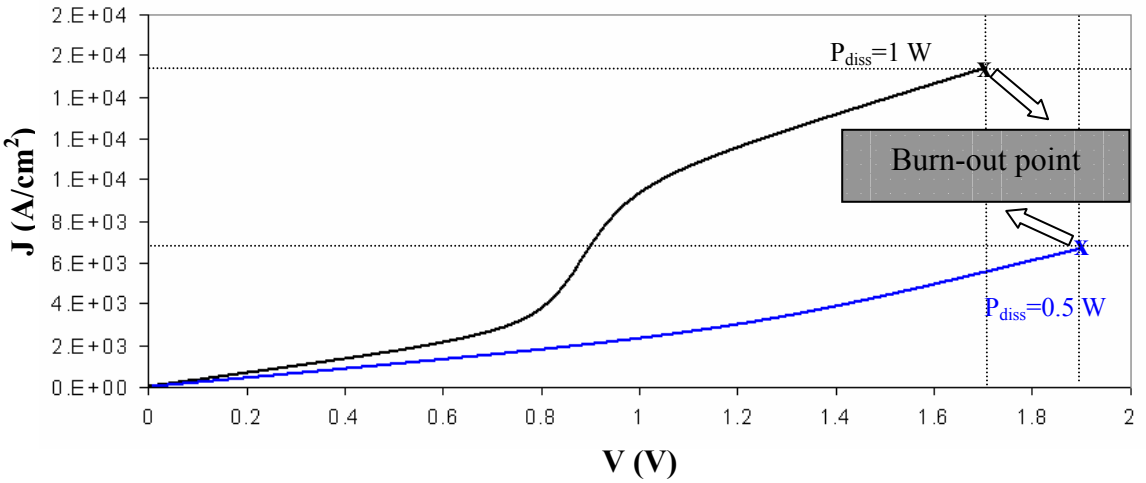

Figure 3.9: Current density versus voltage graph for copper on PET film (black) and on PEI film (blue)

Unlike silver and gold deposition, selective copper plating takes place at room temperature. Hence, this method is applicable to very large scale manufacturing processes such as roll-to-roll process. The major drawback of line patterning of copper is the penetration of active material through the printed mask during plating. Therefore, copper may grow unintentionally under the printed mask. This problem can be minimized by printing multiple layered masks or increasing the resolution of the printer.

[215] (a) T. Itabashi, M. Suzuki, R. Watanabe, Y. Okoshi, H. Suzuki, H. Akahoshi, Electronic Manufacturing Technology Symposium, 1995, Proceedings of 1995 Japan International, 18th IEEE/CPMT International 4-6 Dec., 318 – 322 (1995), (b) S. Kim, K-J. Lee, and Y. Seo, Langmuir, Vol. 18, 6185-6192 (2002).

Here we are proposing another cost effective and simple way to selectively metallize flexible substrates. Our method offers elegantly simple, extremely cost effective way to pattern copper on plastics. Experimental method includes; i) electroless copper deposition on flexible substrate, ii) image transfer on copper coated plastic substrates via laser printer, iii) etching unwanted copper using a proper etchant solution (iv) removing the printer toner with acetone washing. Figure 3.10 summarizes this experimental process. Using this experimental methodology it is aimed to minimize the unintentional copper growth under mask and also to have a better resolution control.

A similar bath formulation described in Table 3.3, is used here with one difference. Isopropyl alcohol was added into both the tin and palladium bath to increase the wetability of the plastic substrates. Hence, the need for any surface treatment prior to metallization process was eliminated.

A Brother HL-2070N laser printer was used to transfer the pattern on copper coated substrate. It has features of printing up to 20 ppm and up to 2400x600-dpi resolution. Printer toner acts as a resists against ferric chloride solution, which is the well known etchant for copper. Using this method copper lines with resolution as small as 100 micron were printed on PET and PEI substrates. This resolution is the best among our other patterned metals via line patterning and inkjet printing methods.

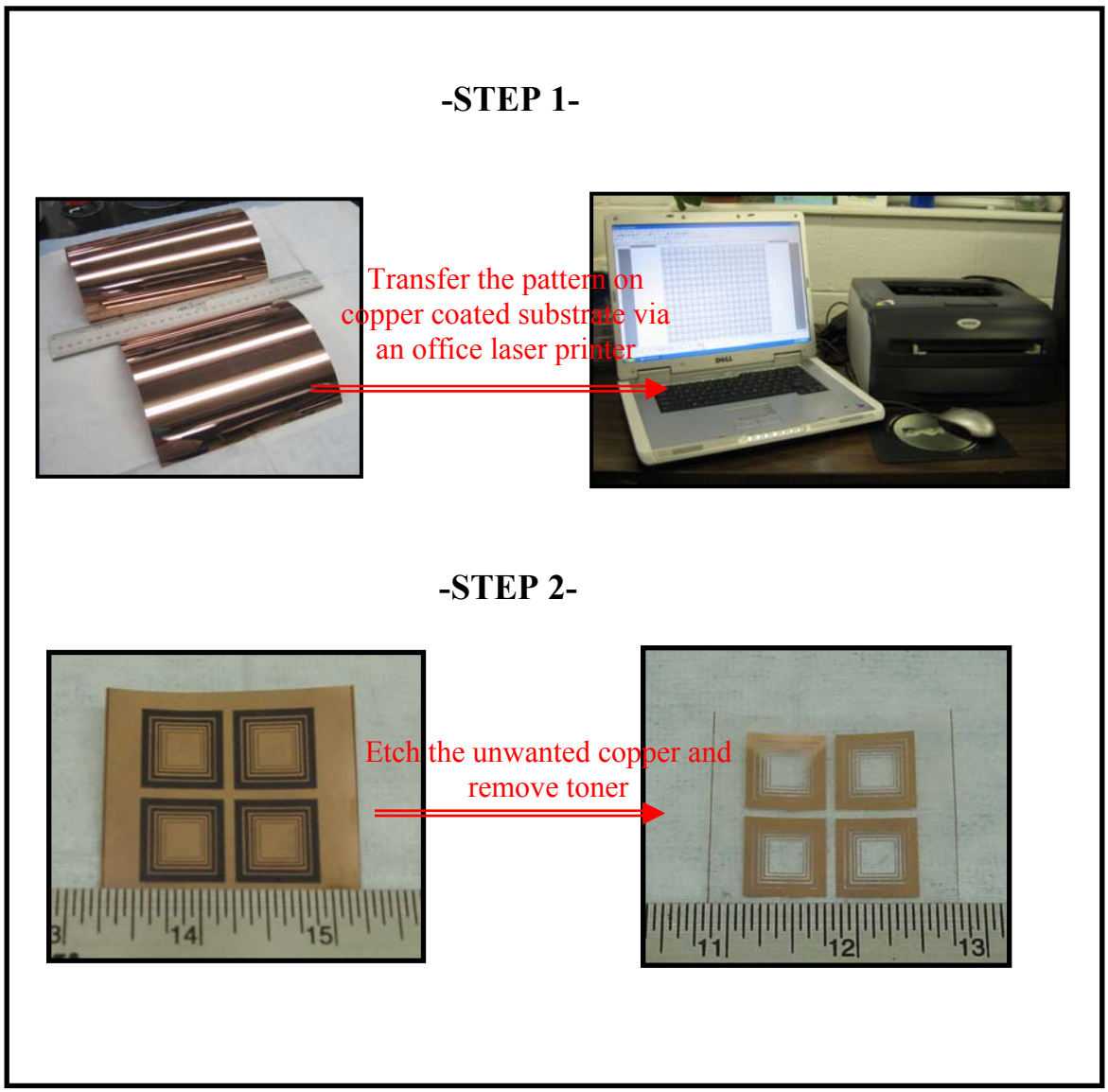

Figure 3.10: Summary of overall experimental process

Figure 3.11 shows the optical microscope pictures of patterned copper on PET film before and after etching process. The pin holes on the printer toner may result uneven copper thin film after etching process. This problem can be solved by printing multiple layers or by correcting them using a sharpie. The final resolution and surface properties of printed copper are amenable to numerous electrical applications.

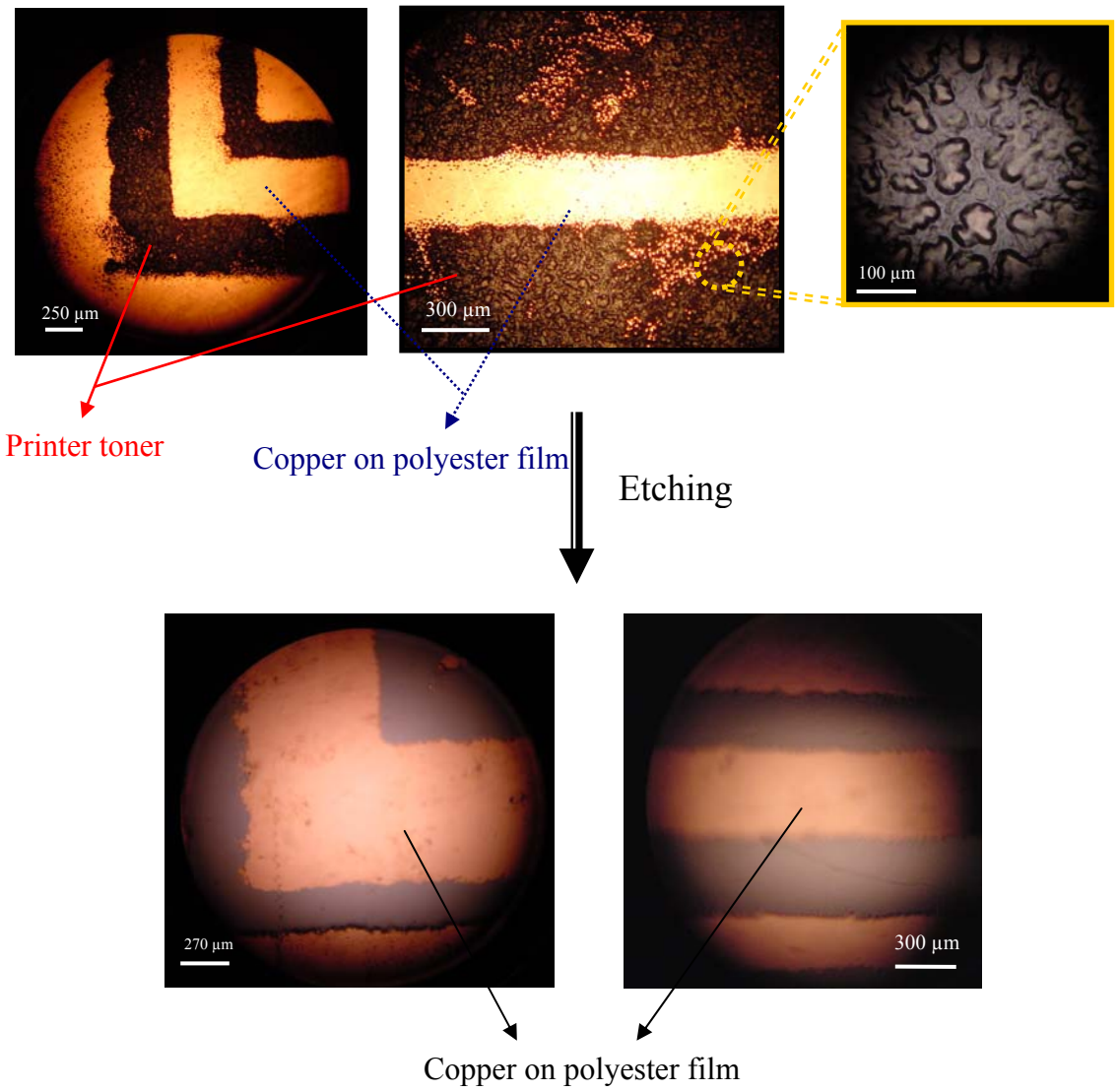

Figure 3.11: Optical microscope pictures of patterned copper on PET film before and after etching process

The electrical conductivity and power dissipation at the burn-out point of copper patterned via laser printer on both PET and PEI are very similar to that of line patterned copper on PET and PEI.

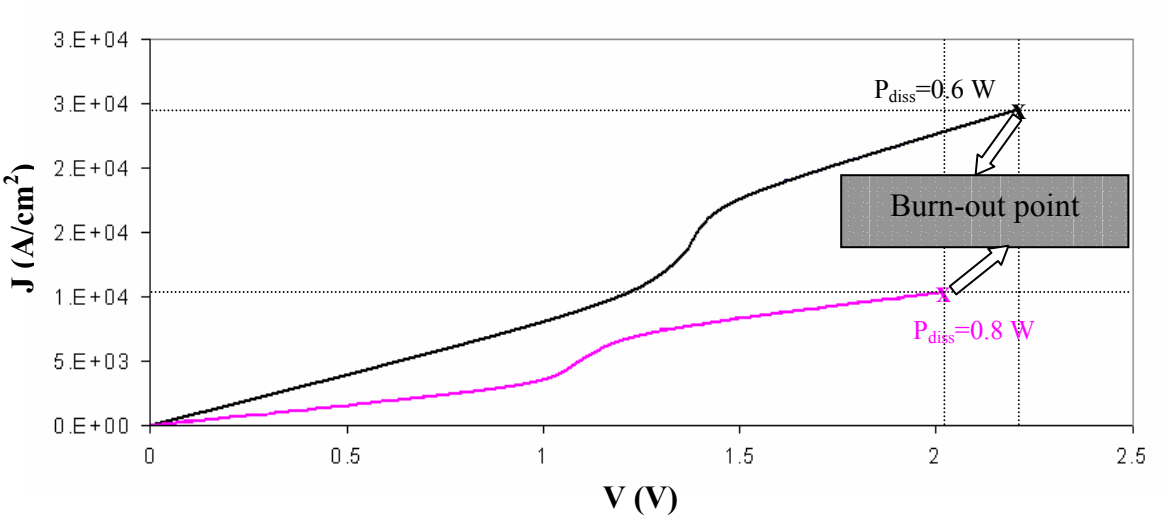

Figure 3.12: Current density versus voltage graph for copper patterned via laser printer on PET film (black) and on PEI film (pink)

Printer masking method can be used to manufacture electrodes for electronics and optics application requiring the mechanical flexibility. It is also possible to fabricate complex patterns on flexible substrates using this method. Figure 3.13 shows the flexible circuit boards fabricated in our laboratory using printer masking method.

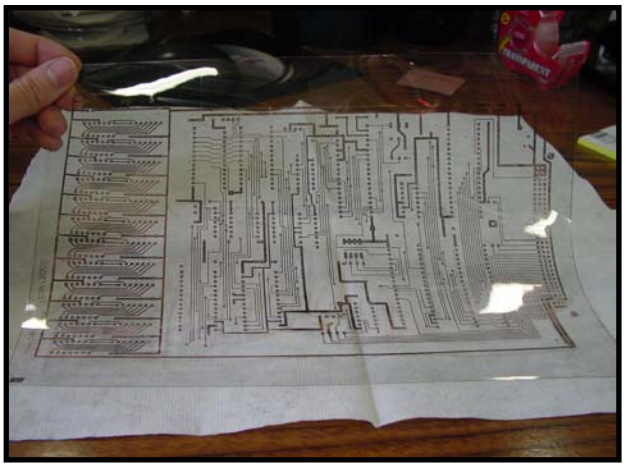

Figure 3.13: Flexible circuit boards manufactured using laser printing method.

3.5 Conclusions and Future Work

Patterning metals on flexible substrates with a controllable resolution is very important in order to build functional devices in electronics. The complexity of the fabrication techniques results in high cost, which is the major draw back of the current technology. Therefore there have been tremendous research efforts to find low-tech and cost effective ways to selectively deposit metals on mechanically flexible substrates. Here we proposed elegantly simple, very cost effective and reproducible methods to pattern silver, gold and copper on plastic substrates such as polyester, overhead transparency, polyimide and polyether imide. Table 3.4 summarizes some properties of patterned silver, gold and copper. Using these methods it is possible to build complex patterns on flexible substrates with electrical conductivity which is close to conductivity of bulk metals. Moreover, the proposed patterning techniques are compatible with mass production techniques. It is possible to make multiple layered devices using solution based metals, insulators and semiconductors via proposed patterning techniques.

Table 3.4: Summary of some properties of patterned metals on flexible substrates

Metal	***Substrate***	***Conductivity (S/cm)***	***Current Density[i] (A/cm^2)***	***Power Dissipation[i] (W)***
Silver	Polyimide	$5x10^4$	$8x10^4$	2.2
Gold (M1[ii])	Transparency film	$2x10^4$	$1 x10^4$	1.0
Gold (M2[iii])	Polyimide	$2x10^4$	$1x10^4$	6.4
Copper (M1)	Polyester film	$2 x10^4$	$2 x10^4$	1.1
Copper (M1)	Polyether imide film	$1x10^4$	$1x10^4$	0.5
Copper (M2)	Polyester film	$2 x10^4$	$2 x10^4$	0.6
Copper (M2)	Polyether imide film	$1 x10^4$	$1 x10^4$	0.8

[i] At burn-out point, [ii] Method 1, [iii] Method 2

CHAPTER 4

Electrically Conductive, Thermoxidatively Stable, Ductile Composites from Polyaniline/Sulfonated Poly(arylene ether sulfone)

Taken From:

N. D. Sankir, J. B. Mecham, W. L. Harrison, R. O. Claus, "Electrically Conductive Polyaniline-Sulfonated Poly(arylene ether sulfone) Composites", *Applied Physics Letters*, Vol**.** 87, 241910 (2005).

N. D. Sankir, J. B. Mecham, R. M. Goff, W. L. Harrison, R. O. Claus, *Smart Materials and Structures*, "Electrically Conductive Polyaniline-Sulfonated Poly(arylene ether sulfone) Composites", submitted, 2005.

4.1 Introduction

In Chapter 2 and 3 the selective metal thin film deposition on mechanically flexible substrates using inkjet printing, line patterning and mask printing methods have been discussed. In this chapter the solution processable semiconductor materials and their composites with insulating polymer matrices have been investigated. The next two sections explain the motives of this study, material selections and composite film preparation method. This chapter also includes: (1) investigation of room temperature DC conductivity, (2) effects of relative humidity and temperature on DC conductivity, (3) effect of temperature on DC conductivity of composite films, (4) fabrication and

investigation of metal/composite film junction, and (5) the influence of PANI loading on the thermal and mechanical properties, morphology and water absorption of the composite films.

For more than a decade, electrically conductive polymer blends and composite films have gained attention due to their tunable electrical properties, low weight, low cost, low fabrication temperatures and good mechanical strength and environmental stabilities [1-8]. These unique characteristics of conductive organic films make them favorable for electronics applications, especially in wearable electronics for both consumer and military applications [216,217]. The electrical conductivity of composite films can be arranged according to desired application over a wide range by changing the doping level and/or weight fraction of conductive filler. Films having lower conductivity have found use in antistatic and packaging material applications [218], while electrically conductive composite films with higher conductivity have been reported as electromagnetic shielding [219], and active materials in electronics [220, 221]. Membranes for gas separation of high selectivity [222], biosensors [223, 224] and humidity sensors [225] are among the other promising applications of organic composite films.

Various insulating polymers such as polyester [226], polyethylene [227], polyvinyl alcohol [228] and poly-methyl methacrylate [229, 230] have been reported as insulating matrices to

---

[216] V. J. Lumelsky, S. Shur, S. Wagner, IEEE Sensors Journal, Vol. 1, 41-51 (2001).

[217] W. E. Howard, O. F. Prache, IBM Journal of Research and Development, Vol. 45, 115-127 (2001).

[218] J. Anand, S. Palaniappan, D. N. Sathyanarayana, Progress in Polymer Science, Vol. 23, 993-1018 (1998).

[219] S. K. Dhawan, N. Singh, D. Rodrigues, Science and Technology of Advanced Materails, Vol. 4, 105-113 (2003).

[220] P. Somani, A. B. Mandale, S. Radhakrishnan, Acta Materialia, Vol. 48, 2859-2871 (2000).

[221] P. C. Ramamurthy, A. M. Malshe, W. R. Harrell, R. V. Gregory, K. McGuire, A. M. Rao, Solid-State Electronics, Vol. 48, 2019-2024 (2004).

[222] D. Xie, Y. Jiang, W. Pan, D. Li, Z. Wu, Y. Li, Sensors and Actuators B, Vol.81, 158-164 (2002).

[223] M. M. Castillo-Ortega, D. E. Rodriguez, J. C. Encinas, M. Plascencia, F. A. Méndez-Velarde, R. Olayo, Sensors and Actuators B, Vol. 85, 19-25 (2002).

[224] H. Xue, Z. Shen, Y. Li, Synthetic Metals, Vol. 124, 345-359 (2001).

[225] S. Jain, S. Chakane, A. B. Samui, V. N. Krishnamurthy, S. V. Bhoraskar, Sensors and Actuators B, Vol. 96, 124-219 (2003).

[226] C.Y. Yang, M. Reghu, A. J. Heeger, Y. Cao, Synthetic Metals, Vol. 79, 27-32 (1996).

[227] M. Chipara, D. Hui, P. V.Notingher, M. D. Chipara, K. T. Lau, J. Sankar, D. Panaitescu, Composites:Part B, Vol. 34, 637-645 (2003).

mechanically support polyaniline in conductive composite film applications. More interestingly, ionically conductive polymers have been used as the host polymers for polyaniline [231], which provides mixed ionic and electronic conduction. These composites are promising materials which have been used in batteries, sensors and electrochromic displays. Nafion®, which has a Teflon-like (Dupont) backbone and sulfonated side chains of ether-linked flurocarbons with good thermal and oxidative stability, is utilized in mixed ionically and electronically conductive polymer composites [232]. However, the high cost of Nafion limits its application in this area. In this study, we introduce a simple chemical route to fabricate electrically conductive, environmentally and mechanically stable freestanding films using poly(arylene ether sulfone) copolymers with 35 mole percent sulfonation (BPS-35) as an ionically conductive, supportive matrix and polyaniline emaraldine base (PANI) as electronically conductive polymeric filler.

4.2 Experimental

4.2.1 Materials

Emaraldine base polyaniline (MW ~65,000) was purchased from Aldrich and used as received. N-Methyl-2-pyrrolidinone (NMP), concentrated sulfuric and hydrochloric acids were obtained from Fisher Scientific. Sulfonated polyarylene ether sulfone (BPS) was generously provided by Prof. J. E. McGrath's research group in the Department of Chemistry at the Virginia Polytechnic Institute and State University.

Among various conducting polymers, PANI is a promising candidate for practical applications due to its environmentally stability, solution processability, reversible control of electrical properties, and commercial availability. Organic solvents such as N-Methyl pyrrolidone (NMP) and dimethyl formamide (DMF) can be used to process PANI

---

[228] Z. Zhang, M. Wan, Synthetic Metal, Vol. 128, 83-89 (2002).
[229] B. Wessling, P. K. Kahol, A. Raghunathan, B. J. McCormick, Synthetic Metals, Vol. 119, 197-198 (2001).
[230] S. Angappane, N. R. Kini, T. S. Natarajan, G. Rangarajan, B. Wessling, Thin Solid Films, Vol. 417, 202-205 (2002).
[231] X-W. Zhang, C. Wang, A. J. Appleby, F. E. Little, Solid State Ionics, Vol. 150, 383-389 (2002).
[232] E. K.W. Lai, P. D. Beattie, F. P. Orfino, E. Simon, Electrochimica Acta, Vol. 44, 2559-2569 (1999).

emeraldine base (Figure 4.1) to cast free standing films. PANI in the emeraldine base form is an insulator and can be transformed into the electronically conductive emeraldine salt by proton doping, also termed the protonation process, in which the material is made electrically conductive by an internal redox reaction through protonation of the imine nitrogen sites [233].

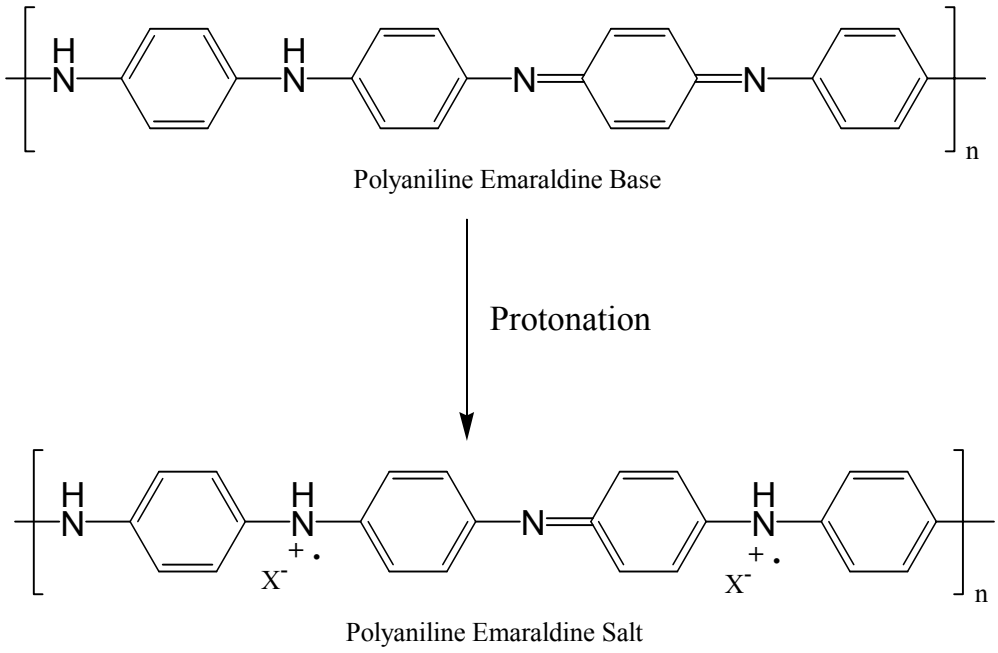

Figure 4.1: Structures of polyaniline emaraldine before and after protonation where X is the dopant cation

Sulfonated poly(arylene ether sulfone) has high thermal and mechanical stability and also shows good stability against acids, bases and oxidants. The synthesis and characterization of poly(arylene ether sulfone) [234] and sulfonated poly(arylene ether sulfone) random copolymers and their membrane characteristics for proton exchange membrane fuel cells have been extensively studied by McGrath's et al. [235,236,237, 238,239,240,241,242], where the

[233] S. Stafström, J. L. Brédas, A. J. Epstein, H. S. Woo, D. B. Tanner, W. S. Huang, A. G. MacDiarmid, Physical Review Letters, Vol. 59, 1464-1467 (1987).

[234] S. Wang, J. E. McGrath, "Synthesis of Poly(arylene ether)s" in Synthetic Methods in Step-Growth Polymers, T. E. Long and M. Rogers (Eds), pp. 327-374, John Wiley and Sons, NY, (2003).

[235] Y. S. Kim, F. Wang, M. Hickner, S. Mccartney, Y. T. Hong, T. A. Zawodzinski, J. E. McGrath, Journal of Polymer Science, Part B: Polymer Physics, Vol. 41, 2816-2828 (2003).

salt form of poly (arylene ether sulfone) is abbreviated as BPS while the acid form isabbreviated as BPSH. The chemical structure of BPS is shown in Figure 4.2.

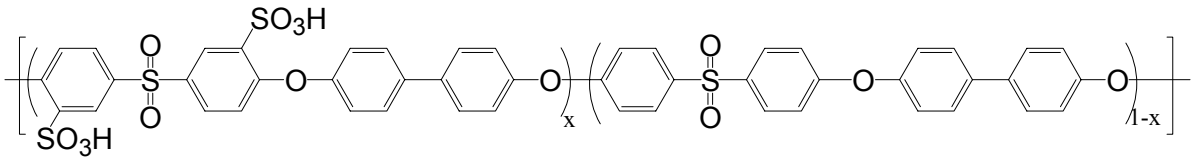

Figure 4.2: Chemical structure of sulfonated poly (arylene ether sulfone) (BPSH)

4.2.2 Preparation of Polyaniline/BPS-35 Composite Films

PANI emaraldine base and BPS-35 at various weight percents were separately dissolved in NMP by stirring vigorously overnight at room temperature. Prior to mixing solutions, the PANI/NMP solution was sonicated for 8-10 hours and the BPS-35/NMP solution was filtered using a 45 μm PTFE syringe filter. The PANI/NMP solution was then added drop wise into BPS-35/NMP solution and stirred for 8 hours. The PANI/BPS-35 solution was cast into square aluminum molds having inner dimensions of 9cm x 9cm and placed into a vacuum oven. The temperature of the vacuum oven was increased stepwise from 60 °C to 150 °C for 24 hours resulting in solvent-free composite films (see Figure 4.3). The flexible films were rinsed several times with distilled water and then doped by immersing them into 1M sulfuric or hydrochloric acid solution anywhere from 1 minute to 22 hours.

---

[236] F. Wang, M. Hickner, Q. Ji, W. Harrison, J. B. Mecham, T. A. Zawodzinski, J. E. McGrath, Macromolecular Symposia, Vol. 175, 387-396 (2001).
[237] F. Wang, M. Hickner, Y. S. Kim, T. A. Zawodzinski, J. E. McGrath, Journal of Membrane Science, Vol. 197, 231-242 (2002).
[238] W. L. Harrison, F. Wang, J. B. Mecham, V. A. Bhanu, M. Hill, Y. S. Kim, J. E. McGrath, Journal of Polymer Science Part A: Polymer Chemistry
Vol. 41, 2264-2276 (2003).
[239] Y. S. Kim, M. J. Sumner, W. L. Harrison, J. S. Riffle, J. E. McGrath, B. S. Pivovar, Journal of the Electrochemical Society, Vol. 151, A2150-A2156 (2004).
[240] Y. S. Kim, M. A. Hickner, L. Dong, B. S. Pivovar, J. E. McGrath, Journal of Membrane Science, Vol. 243, 317-326 (2004).
[241] M. J. Sumner, W. L. Harrison, R. M. Weyers, Y. S. Kim, J. E. McGrath, J. S. Riffle, A. Brink, M. H. Brink, Journal of Membrane Science, Vol. 239, 199-211 (2004).
[242] M. A. Hickner, H. Ghassemi, Y. S. Kim, B. R. Einsla, J. E. McGrath, Chemical Reviews, Vol. 104, 4587-4612 (2004).

It was observed that better film properties was obtained if the PANI and BPS were predissolved separately, and then slowly mixed.

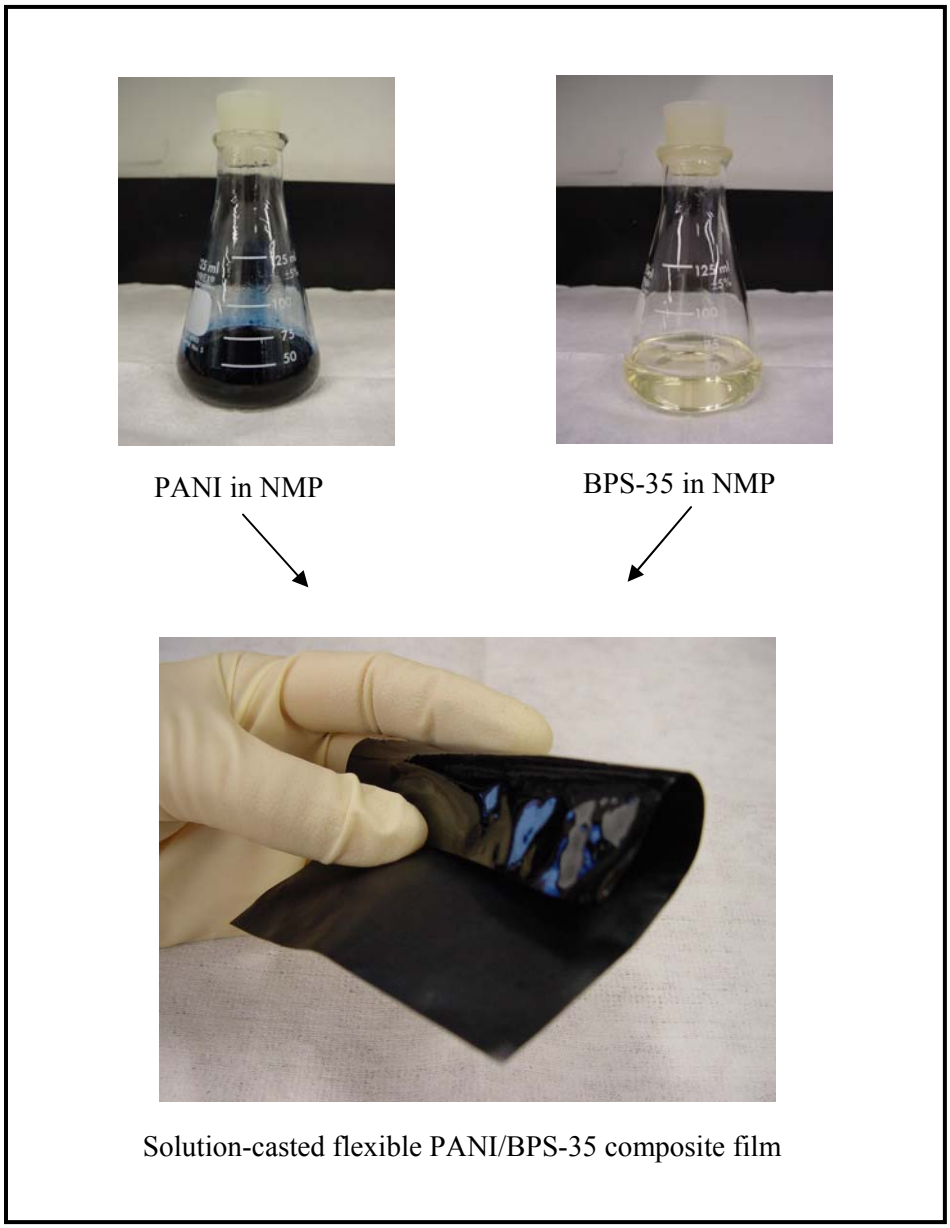

Figure 4.3: Preperation of PANI/BPS-35 composite film

4.3 Characterization

4.3.1 Conductivity

DC conductivity measurements were performed at room temperature using a Mitsubishi Chemical Laresta-EP MCP-T360 type four point probe. Error resulting from film anisotropy and geometry was minimized by measuring the conductivity at least five different spots on the film for both the air and mold sides. The average of those measurements is presented in this study.

The effects of relative humidity and temperature on the conductivity of composite films were also examined. The PANI/BPS-35 films were first inserted into the conductivity cell [243] and then placed in the ESPEC SH-240 temperature and humidity controlled oven. The electrical conductivity of the films was measured at three different temperatures (24, 44, and 80 °C), and two different humidity levels (50 and 70% RH) using an Agilent 34401A multimeter. An experimental schematic is shown in Figure 4.4.

[243] T. A. Zawodzinski, M. Neeman, L. O. Sillerud, S. Gottesfeld, Journal of Physical Chemistry, Vol. 95, 6040-6044 (1991).

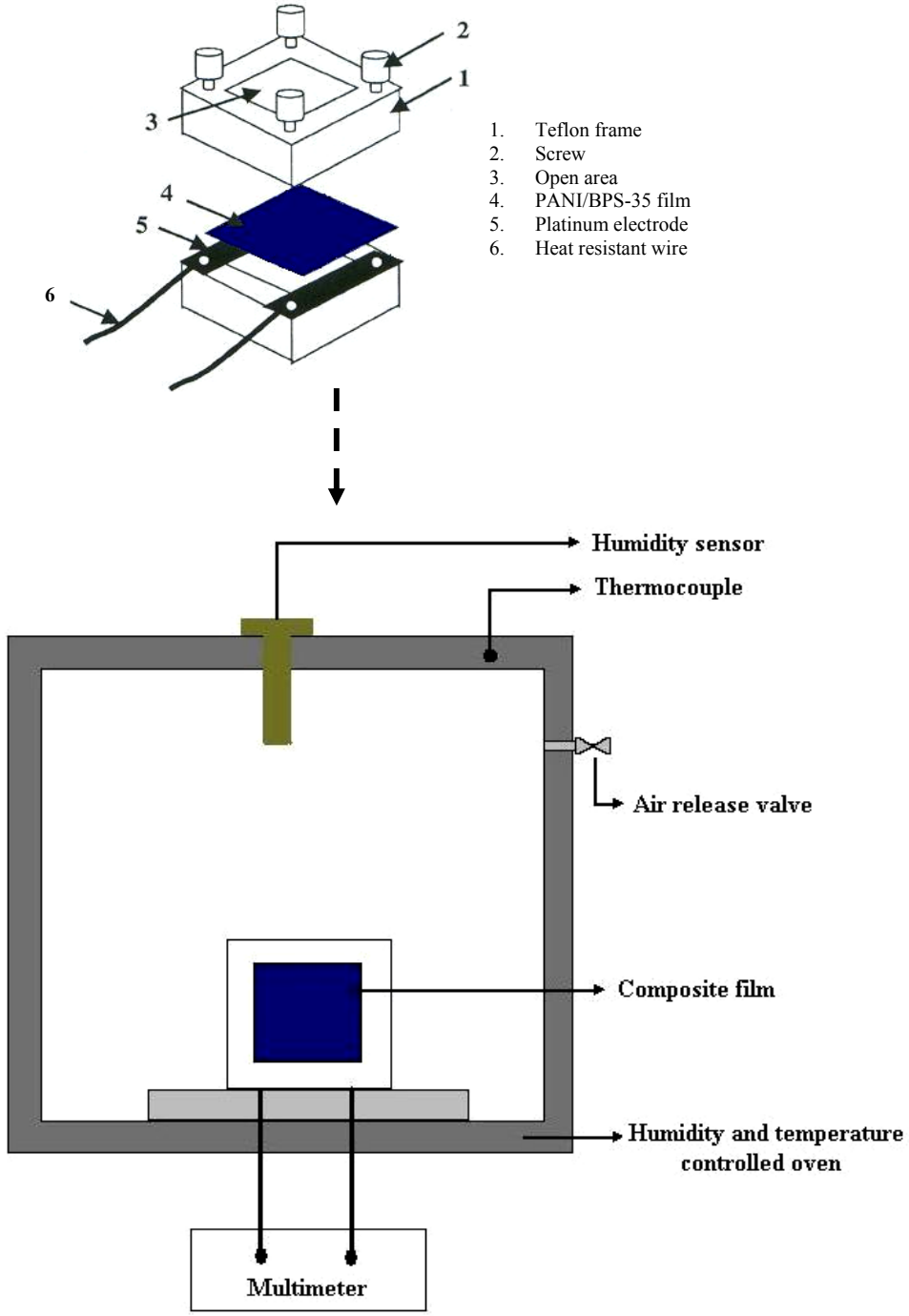

Figure 4.4: Experimental setup for relative humidity and temperature dependent conductivity measurements

The resistivity data were converted into conductivity data using;

$$R = \rho \frac{L}{A} \quad where\ \rho = \frac{1}{\sigma} \tag{4.1}$$

where R is the resistance, σ is the conductivity, ρ is the resistivity, L is the length and A is the cross sectional area of the sample. The rough data were analyzed using the Design-Expert statistical software. A 2-level factorial model was used to determine the relative humidity and temperature effects on DC conductivity.

The temperature dependent conductivity measurements were also performed in order to understand the dominant conductivity mechanism. The temperature range between -40 and 200 °C were scanned using a computer controlled oven. Two point probe technique was used to measure the resistance of the PANI/BPS-35 composite films and the data were converted into conductivity again using Eqn. (4.1).

4.3.2 Vacuum Evaporation System

Edward Auto 306 vacuum evaporation system has been used in this study to make metal contacts on the PANI/BPS-35 composite films.

4.3.3 Tensile Testing

The mechanical properties of BPS-35 and PANI/BPS-35 composite films with different PANI loading were studied at room temperature using a TA.XT Plus Texture Analyzer (Texture Technology Corp) at a strain rate of 0.017 mm/s. The Young's modulus, tensile strength, and elongation at break values were identified for dry and fully hydrated (swollen) samples.

4.3.4 Water Absorption

Doped composite films were dried at 110 °C under vacuum and weighed. The films were then soaked in DI water for 24 hours. The surface water on the swollen films was removed using a paper towel and the samples weighed again. This procedure was repeated three times. The water uptake of the composite films was calculated using following equation [244];

$$Water\ uptake = \left[\frac{W_{wet} - W_{dry}}{W_{dry}} \right] x100 \qquad (4.2)$$

where W_{wet} and W_{dry} are the weight of swelled and dry composite films, respectively.

4.3.5 Fourier Transform Infrared (FTIR) Analysis

The FTIR spectra of PANI/BPS-35 composite films with various PANI loadings were obtained using a Nicolet Impact 400 FT-IR spectrometer to confirm the functional groups within the copolymers.

4.3.6 Thermogravimetry Analysis (TGA)

The thermo-oxidative properties of both the BPSH-35 copolymers and PANI/BPS-35 composite films were analyzed using a TA Instruments TGA Q 500. Vacuum dried thin films (5 to 10 mg) were evaluated over the range of 40 to 600 ^{o}C at a heating rate of 10 ^{o}C/min under an inert nitrogen atmosphere.

[244] Jeffrey B. Mecham, Ph.D. Dissertation, Chemistry Department, Virginia Polytechnic Institute and State University, 2001.

4.3.7 Scanning Electron Microscopy (SEM)

The morphology of the fracture surface of composite films was examined by LEO 1550 SEM at 5 kV. Samples were fractured at liquid nitrogen and gold sputtered prior to observation.

4.4 Results and Discussions

4.4.1 Room Temperature DC Conductivity

Free standing PANI/BPS-35 films were doped in aqueous protonic acid solution to convert the polyaniline emeraldine base into the salt form to make the films electrically conductive, where BPSH-35 contributes to the ionic conductivity. The electrical conductivity of the composite films strongly depends on doping conditions including dopant type and doping time [245]. The composite films doped with sulfuric acid had one order of magnitude lower resistivity when compared to films doped with hydrochloric acid (Figure 4.5). One can conclude that counter ion of the dopant has an effective control mechanism of the electrical properties of the composite films.

[245] A. Pud, N. Ogurtsov, A. Korzhenko, G. Shapoval, Progress in Polymer Science, Vol. 28, 1701-1753 (2003).

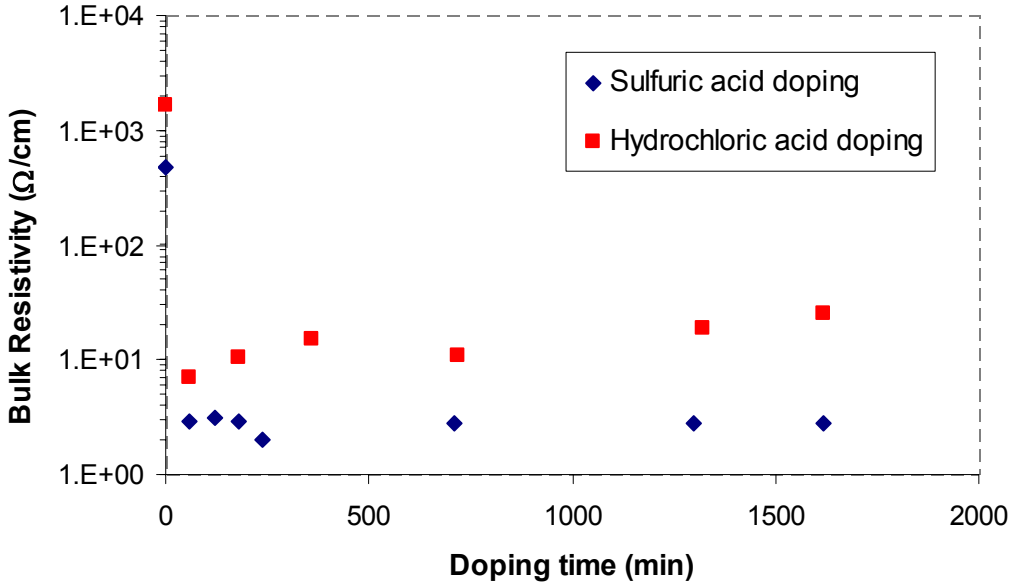

Figure 4.5: Bulk resistivity versus doping time plot for 40 wt% PANI containing composite films doped with sulfuric acid or hydrochloric acid

A relatively wide range of doping time was investigated for each dopant. Electrical conductivity appeared after one minute of doping, indicating relatively fast protonation kinetics. Regardless of dopant type, two to three hours of doping time was enough to equilibrate the resistivity of all of the PANI/BPS-35 composite films (Figure 4.6 and 4.7). Since BPS has hydrophilic regions resulting from disulfonated moieties, which absorb water, the quantity of absorbed water depends on the degree of disulfonation and the acidification method. The water uptake of BPSH-35 (35 mole percent disulfonated copolymer) was 20 weight percent when it was acidified with 1M sulfuric acid at room temperature for 3.5 hours. We believe that BPSH assists the doping process by transporting dopant into the bulk due to its described water uptake property.

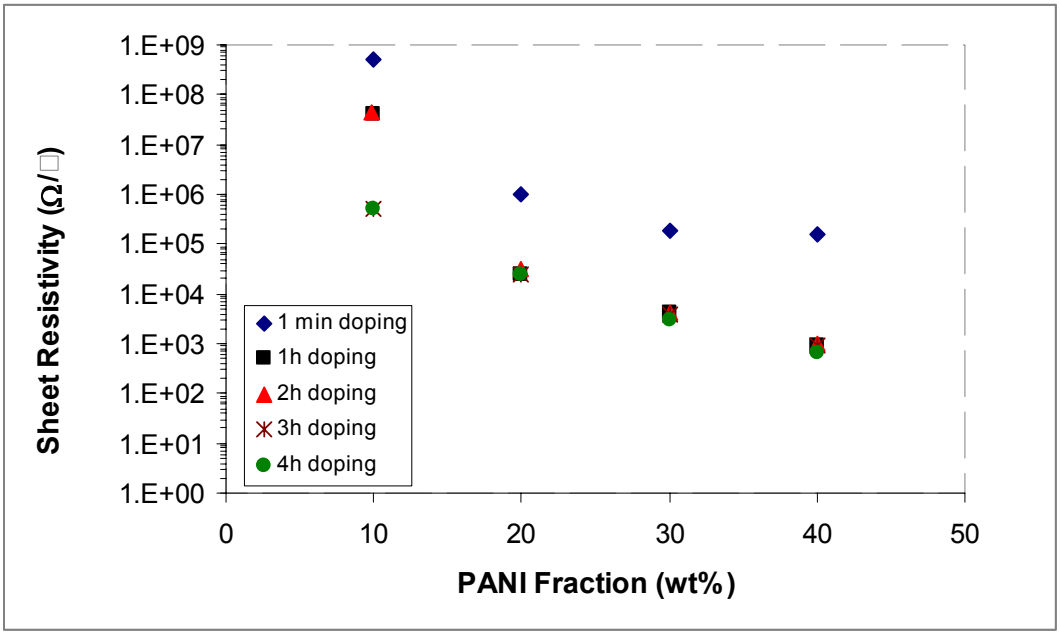

Figure 4.6: Sheet resistivity versus PANI fraction plot for composite films doped in 1M sulfuric acid solution for various doping times

Figure 4.7 reveals the room temperature DC conductivity of the composite films for various PANI loading. The electrical conductivities of a series of composite films having from 10 to 40 weight percent PANI were in the range of $2x10^{-7}$ – $2x10^{-3}$ S/cm for only one minute of doping with a sulfuric acid solution. However, the same composite films possessed higher conductivities ($2.3x10^{-6}$-0.6 S/cm) for longer doping times (1-4 hours). Figure 6 also indicates that maximum conductivities reported above changed slightly after 15 weight percent PANI loading. Hence, the threshold conductivity was reached at around 15 wt% PANI loading and 2-3 hours doping time.

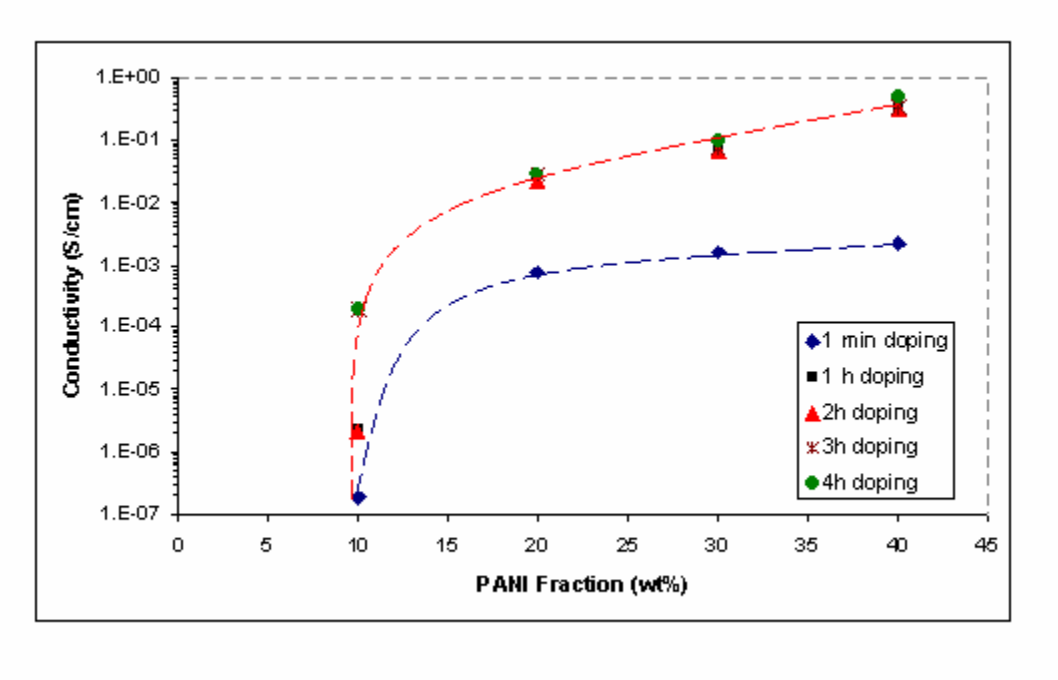

Figure 4.7: Conductivity versus PANI fraction plot for composite films doped in 1M sulfuric acid solution at various doping times

Other researchers have reported PANI composites using various insulating matrices, such as poly(vinyl alcohol) (PVA), poly(vinyl chloride) (PVC), polyacrylonitrile (PAN) as well as the commercial ionomer Nafion® [31-36] (Table 4.1). PANI/BPS-35 composite film is a new promising material in this area from two perspectives. First, the electrical conductivities are high enough for a broad range of applications. Second, the polymer blend method used in this study is superior to chemical and electrochemical synthesis given consideration of time/cost parameters.

Table 4.1: Room temperature DC conductivies of various polyaniline containing composite films

Composite	Preparation Method	PANI Content (wt %)	Conductivity (S/cm)	Reference
PANI-PVA[i]	Chemical synthesis	8.0 - 29.08	$6.1x10^{-6}$- 1.32	[246]
PANI-PAN[ii]	Electrochemical synthesis	-	0.1	[247]
PANI-PVA	Chemical synthesis	5 - 38	0.2 - 2.5	[248]
PANI/nylon 6	Diffusion and chemical oxidative polymerization	1.5 – 4.4	$1.5x10^{-5}$-$3.5x10^{-2}$	[249]
PANI/PVC[iii]	Chemical mixing	60	$1.47x10^{-2}$	[250]
PANI/Nafion®	Chemical mixing	20	10^{-2}	[251]
PANI/BPS-35	Chemical mixing	10-40	$1.9x10^{-4}$-$6.1x10^{-1}$	current study

[i] Polyaniline-poly(vinyl alcohol), [ii] Polyacrylonirile, [iii] Polyviyl Chloride

[246] R. Gangopadhyay, A. De, G. Ghosh, Sythetic Metals, Vol. 123, 21-31 (2001).

[247] Y. H. Park, C. R. Park, Synthetic Metals, Vol. 118, 187-192 (2001).

[248] A. Mirmohseni. G. G. Wallace, Polymer, Vol. 44, 3523-3528 (2003).

[249] S. W. Byun, S. S. Im, Polymer, Vol. 39, 485-489 (1998).

[250] R. K. Gupta, R. A. Singh, Materials Chemistry and Physics, Vol. 86, 279-283 (2004).

[251] C. Barthet, M. Guglielmi, Journal of Electroanalytical Chemistry, Vol. 388, 35-44 (1995).

4.4.2 Relative Humidity-Temperature Effect on DC Conductivity

Electrical conductivities of the composite films were tested under both atmospheric and highly oxidative conditions. It was observed that there was almost no conductivity change for the composite films tested at room temperature under atmospheric conditions over a six month period. The oxidative conditions were provided by controlling the humidity and temperature simultaneously. Table 4.2 indicates the conductivity of 20 weight percent PANI containing composite film at different relative humidity and temperature conditions.

Table 4.2: Conductivity of 20% wt PANI-containing composite films for different temperatures and relative humidity levels

Relative Humidity (%)	Temperature (^{o}C)	Conductivity (mS/cm)
50	24	17
70	24	19
50	44	23
70	44	25
50	80	44
70	80	53

The influence of humidity and temperature on conductivity was analyzed using Design-Expert software for a two-level factorial mode. The three-dimensional plot extracted from computer analysis shows the conductivity versus relative humidity/temperature relationship (Figure 4.8). The room temperature conductivity slightly increased when the relative humidity increased from 50% to 70%. This increase became more significant at higher temperatures. However, the influence of temperature on conductivity was dominant over relative humidity. The conductivity increment from 17 mS/cm to 44

mS/cm was observed when the temperature increased from 24 to 80 °C at 50 % RH. The maximum conductivity was 53 mS/cm at 80 °C and 70 % RH. As expected, the temperature dependence of PANI/BPS-35 composite films was similar to that of conventional crystalline semiconductors.

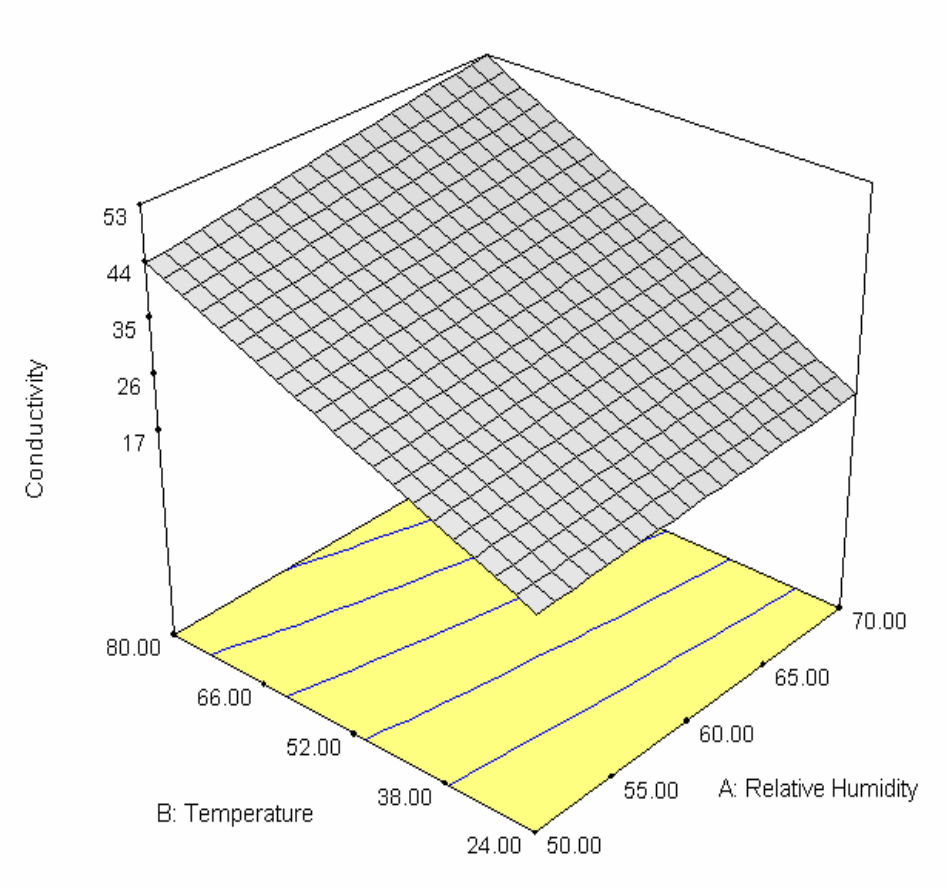

Figure 4.8: 3D Design-Expert™ plot of conductivity versus relative humidity and temperature for 20 wt% PANI containing composite film

4.4.3 Temperature Dependent DC Conductivity

Electrical properties of polymeric or organic materials can be written as a function of time, temperature, ambient atmosphere, potential and direction [252]. Temperature dependency of electrical conductivity of polymeric materials has similarities with that of inorganic semiconductors. Therefore there has been attempts in literature to explain the conduction mechanism in organic materials using existing solid state theory [253, 254]. The conductivity of organic semiconductor changes exponentially with temperature and data generally fit the hoping mechanism [255]. The charge carriers in organic semiconductors, which are soliton pairs (bipolarons), can hop to the next chain isoenergetically with a certain probability and the mobility of these hopping particles depends on the diffusion of them in the polymer matrix. Since the diffusion is a thermally activated process, mobility can be expressed as

$$\mu = \mu_0 \exp\left(-E_a / k_B T\right) \quad . \tag{2.3}$$

Where, μ is the mobility, μ_0 is the pre-exponential function, E_a is the activation energy, k_B is the Boltzmann's constant and T is temperature. Figure 4.9 shows the DC conductivity (σ_{DC}) of 20 wt% PANI containing composite film as a function of temperature. Conductivity is about $2x10^{-2}$ S/cm at room temperature and decreases as temperature lowered, indicating semiconductor-like behavior. A weaker temperature dependency is obtained for higher temperatures. One can say that there is no evidence of metal-like behavior in the temperature range of 223-473 K for the composite film having 20 wt% PANI loading.

[252] D. A. Seanor, Electrical Properties of Polymers, Academic Press Inc., London, 1982.

[253] V. Luthra, R. Singh, S. K. Gupta, A. Mansingh, Current Applied Physics, Vol. 3, 219-222 (2003).

[254] E. Riande, R. Diaz-Calleja, Electrical Properties of Polymers, Marcel Dekker Inc., New York, 2004.

[255] C. O. Yoon, M. Reghu, D. Moses, A. J. Heeger, Y. Cao, T.-A. Chen, X. Wu, R. D. Rieke, Synthetic Metals, Vol. 75, 229-239 (1995).

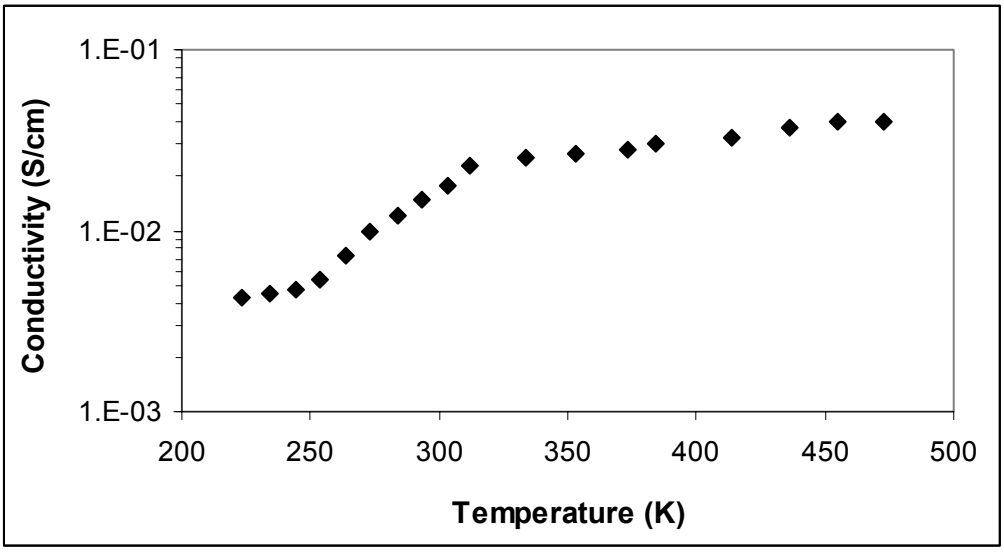

Figure 4.9: Temperature dependence of DC conductivity for 20 wt% PANI containing composite film

The DC conductivity-temperature plots of composite films follow the Arrhenius behavior, but with two activation energies. The activation energy, calculated from the slope of log (σ_{DC}) versus 1000/T graph, is 0.113 eV below 300 K and 0.047 eV above 300 K. It is evident from the Figure 4.10 that Mott's three-dimensional variable range hopping model is a reasonable model to explain the conductivity mechanism of the PANI/BPS composite film. According to this model DC conductivity can be written as;

$$\sigma_{DC}(T) = \sigma_0 \exp\left[-\left(\frac{T_0}{T}\right)^{1/4}\right] \tag{4.4}$$

and T_o is;

$$T_0 = \lambda\alpha^3 / k_B N(E_F) \tag{4.5}$$

where λ is a dimensionless constant, α is the inverse rate of the fall of the wave function, k_B is the Boltzmann's constant, and $N(E_F)$ is the density of states at the Fermi level. The value of T_0 for the temperature range 223-303 K is 4.52×10^7 K.

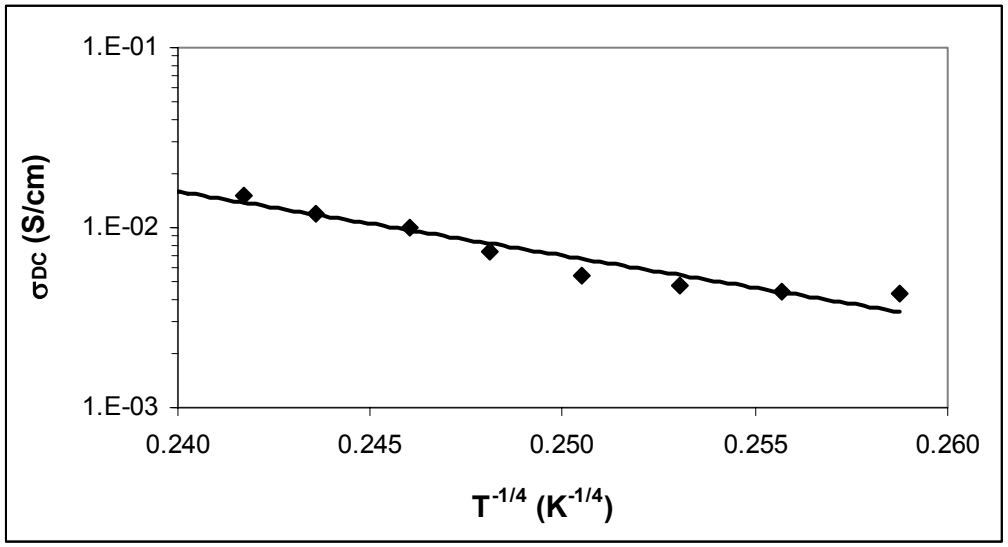

Figure 4.10: Variation of DC conductivity as a function of $T^{-1/4}$ for 20 wt% PANI containing composite film

4.4.4 Metal/PANI-BPS Junctions

Metal-semiconductor junction is a useful building block for many electronic devices. When a metal and a semiconductor touch each other, due to the energy-band discontinuity at the interface a potential barrier forms. According to Schottky-Mott theory the height of this barrier depends on the work function and electron affinity of metal and semiconductor [256]. If this potential barrier is negligibly small, an Ohmic contact forms between semiconductor and metal. Otherwise, a Schottky barrier or rectifying contact forms. Schottky contacts make good diodes, but for getting signals into and out of a semiconductor device an Ohmic contact is needed.

Besides conventional inorganic semiconductors, electrically conductive polymers such as polyaniline, polypyrolle, polythiophene have received much attention in the fabrication of Schottky diodes [257, 258, 259, 260, 261, 262, 263]. Table 4.3 summarizes the some semiconductor

[256]E. H. Rhoderick, R. H. Williams, Metal-Semiconductor Contacts, Plenum Press, New York, 1988.
[257] P. S. Abthagir, R. Saraswathi, Journal of Applied Polymer Science, Vol.81, 2127-2135 (2001).

polymer diodes with different ideality factors and barrier heights. Rectification properties of polymer diodes depend on the preparation and doping properties of the semiconductor polymers.

Table 4.3: Ideality factors and barrier heights of polymer Schottky diodes having various configurations

Device Configuration	Ideality Factor (n)	Barrier Height [ϕ_b(eV)]	Reference
Aluminum-Polyaniline-Platinum	3.26	0.78	[93]
Aluminum-Polyaniline/PVC*-Platinum	2.71	0.86	[93]
Gold-Polyaniline	2.8	0.66	[94]
Gold-Polypyrolle-Aluminum	1.2	0.97	[89]
Gold-Polypyrolle-Indium	2.1	0.89	[89]
Gold-P3HT**-Aluminum	4.6	0.36	[95]
Gold-P3HT**-Titanium	3.3	0.18	[95]

*PVC (poly(vinyl chloride)) **P3HT (poly-3-hexyl-thiophene)

[258] R. Singh, D.N. Srivastava, R.A. Singh, Synthetic Metals, Vol. 121, 1439-1440 (2001).
[259] G. Liang, T. Cui, K. Varahramyan, Solid-State Electronics, Vol. 47, 691-694 (2003).
[260] L. Huang, T. Wen, A. Gopalan, F. Ren, Materials Science and Engineering, Vol. B104, 88-95 (2003).
[261] R. K. Gupta, R. A. Signh, Materials Chemistry and Physics, *In Press*, *Corrected Proof*, (2004).
[262] S. Angappane, N. R. Kini, T. S. Natarajan, G. Rangarajan, B. Wessling, Thin Solid Films, Vol. 417, 202-205 (2002).
[263] G. Lloyd, M. Raja, I. Sellers, N. Sedghi, R. D. Lucrezia, S. Higgins, B. Eccleston, Microelctronic Engineering, Vol. 59, 323-328 (2001).

In this study, the junction properties of aluminum/PANI-BPS system have been investigated. Approximately 200 nm thick aluminum layer was thermally evaporated on 20 wt% PANI containing composite film. The rectification behavior of junction of Al/PANI-BPS at room temperature can be seen in Figure 4.11. The rectification ratio at ±1.25 V is 19.

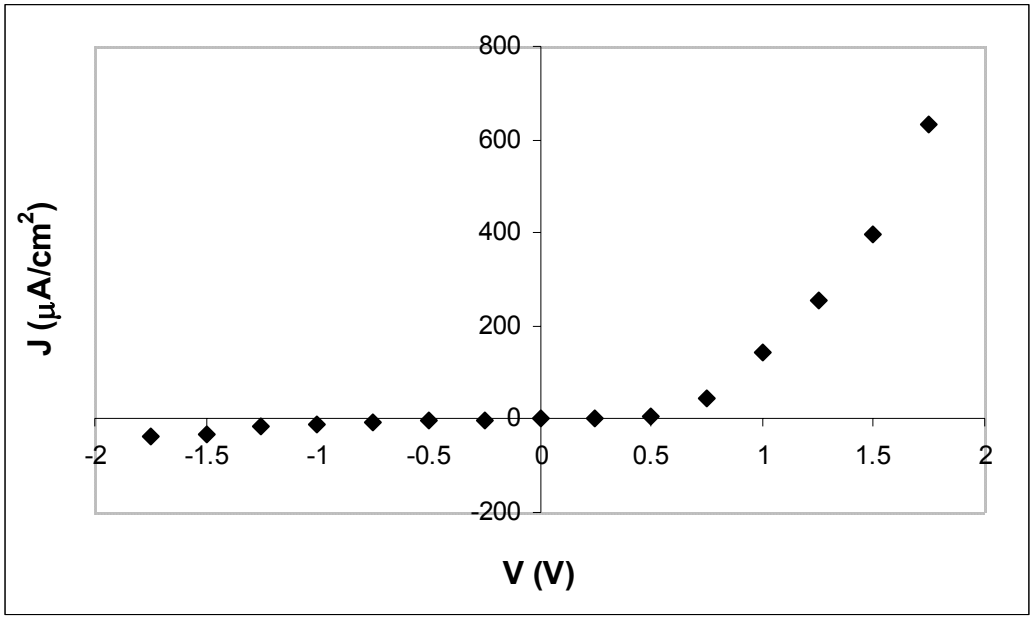

Figure 4.11: Current density/voltage characteristic of junction of Al/PANI-BPS

Junction properties of Au/PANI-BPS have also been investigated. Instead of vacuum evaporation of gold, inkjet printable conducting nanoclusters were deposited on PANI/BPS composite film (see Figure 4.12). The preparation of conductive nanocluster ink and device fabrication processes has been discussed in Chapter 2.

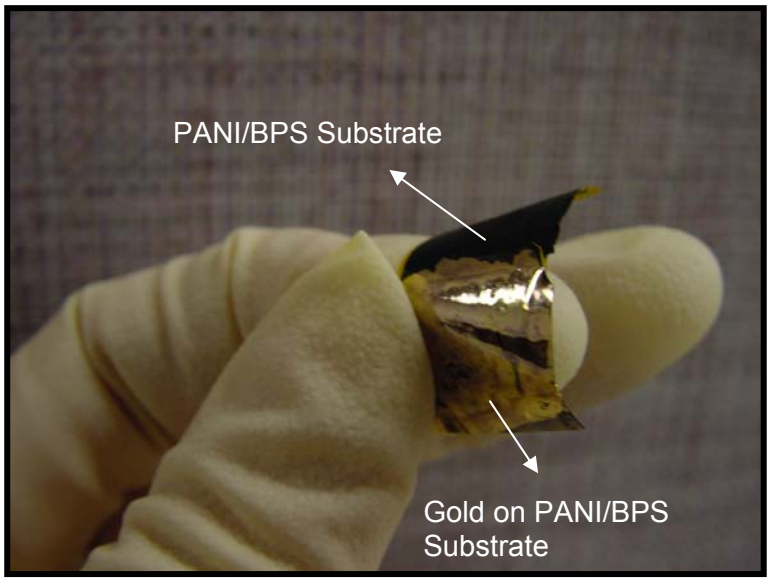

Figure 4.12: Au/PANI-BPS Junction

Temperature dependence of junction of Au/PANI-BPS can be seen in Figure 4.13. The I-V curves are not exactly the same with the metal-inorganic semiconductor Schottky diode. Symmetry has been obtained between forward and reverse bias. This is probably due to the narrow depletion layer width at the interface. It is obvious that Au contact on PANI/BPS does not show ohmic behavior and it provides a Schottky barrier with a small rectification ratio.

The value of Richardson constant, calculated from y intercept of J_S/T^2 versus 1/T plot, is $1.1x10^{-6}$ mA/T^2cm^2. This value is much smaller than the Richardson constant for the free electron (120 A/K^2cm^2). The slope of the same graph gives us the barrier height ϕ_B, which is 0.07 V. The low potential barrier is probably the reason of the small rectification ratio.

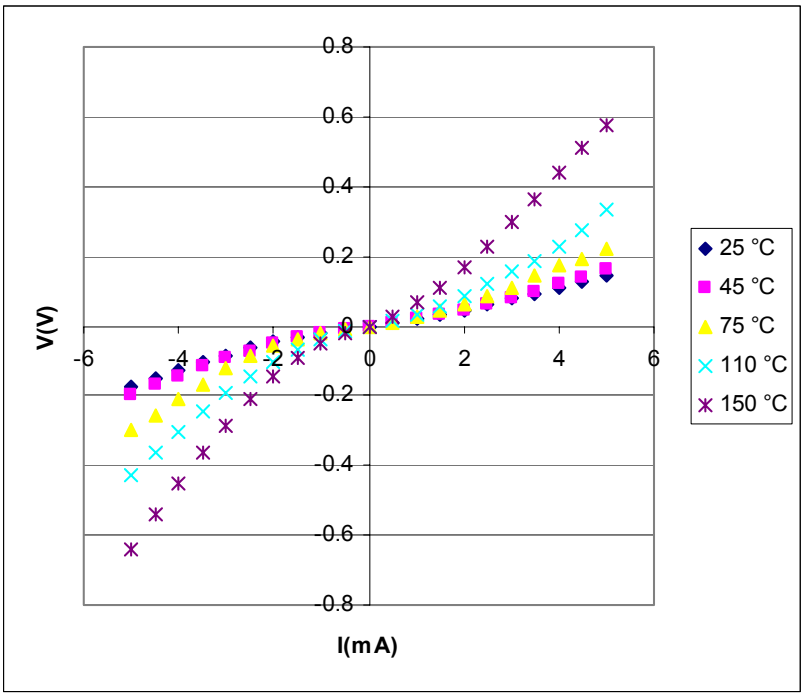

Figure 4.13: Temperature dependence of I-V characteristics of Au/(PANI/BPS) Schottky diode

4.4.5 FTIR Analysis

FTIR analyses of BPSH-35 copolymer, sulfuric acid doped polyaniline, and both undoped and doped 20 weight percent PANI containing composite films can be seen in Figure 8. BPSH copolymer has two characteristic peaks at 1030 and 1098 cm^{-1} due to the symmetric and asymmetric stretching of SO_3H groups [21] (Figure 4.14a). The peaks at 1497 and 1574 cm^{-1} were labeled as benzenoid and quinoid moieties of sulfuric acid doped PANI, respectively. The peak at 1136 cm^{-1} was assigned to aromatic C-H in-plane bending (Figure 4.14b). FTIR spectra of doped composite films (Figure 4.14d) contained the characteristic peaks of BPSH-35 copolymer as well as a peak at 1544 cm^{-1} possibly due to shifting of the PANI peak at 1497 cm^{-1}. This peak could be attributed to the strong interaction -most possibly hydrogen bonding- between SO_3 and NH moieties. On the other hand, the interaction described above was not observed for the undoped composite film (Figure 2.13c).

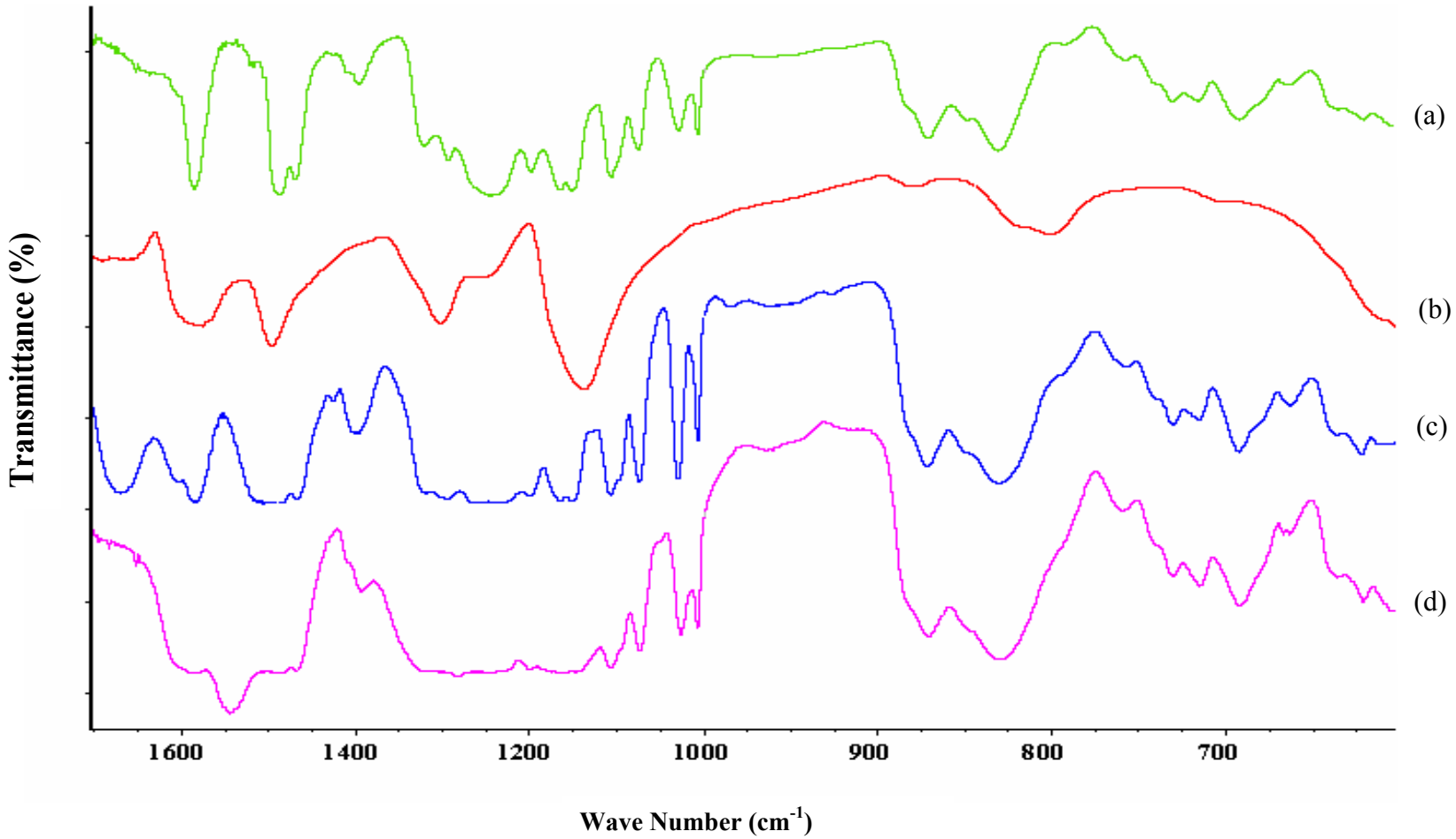

Figure 4.14: FTIR spectra of (a) BPSH-35, (b) sulfuric acid doped PANI, (c) undoped PANI/BPS-35 film (20%), (d) sulfuric acid doped PANI/BPS-35 film (20%)

4.4.6 Thermal and Mechanical Properties

The thermal stabilities of the composite films at different PANI loadings were compared with the control BPSH-35 copolymer. Both BPSH copolymer and the composite films showed high thermal stability which was more than enough for many applications (Figure 4.15).

The BPSH-35 copolymer was first desulfonated and then main chain degradation occurred due to a typical thermal decomposition process. Interestingly, an increase in thermal stability was observed for 20 weight percent sulfonation, suggesting a specific, strong interaction between the BPSH copolymer and PANI. The 1, 5 and 10 percent weight loss temperature comparisons of the BPSH-35 and composite films can be seen in Figure 4.16. The 10 percent weight loss temperature of 20 weight percent PANI containing composite films, where threshold conductivity has been reached, was about 395 °C, which represents an approximately 85 °C improvement compared to BPS copolymer (neat). Conversely, the composite films containing 40 weight percent PANI showed the opposite trend in that desulfonation occurred at lower temperatures compared to other composite films as well as the BPSH-35 copolymer. One can conclude that there were not enough sulfonic acid moieties available to complex the PANI well. Hence, the composites containing higher weight percent PANI showed thermal decomposition at lower temperatures than analogous composite with lower PANI loading levels.

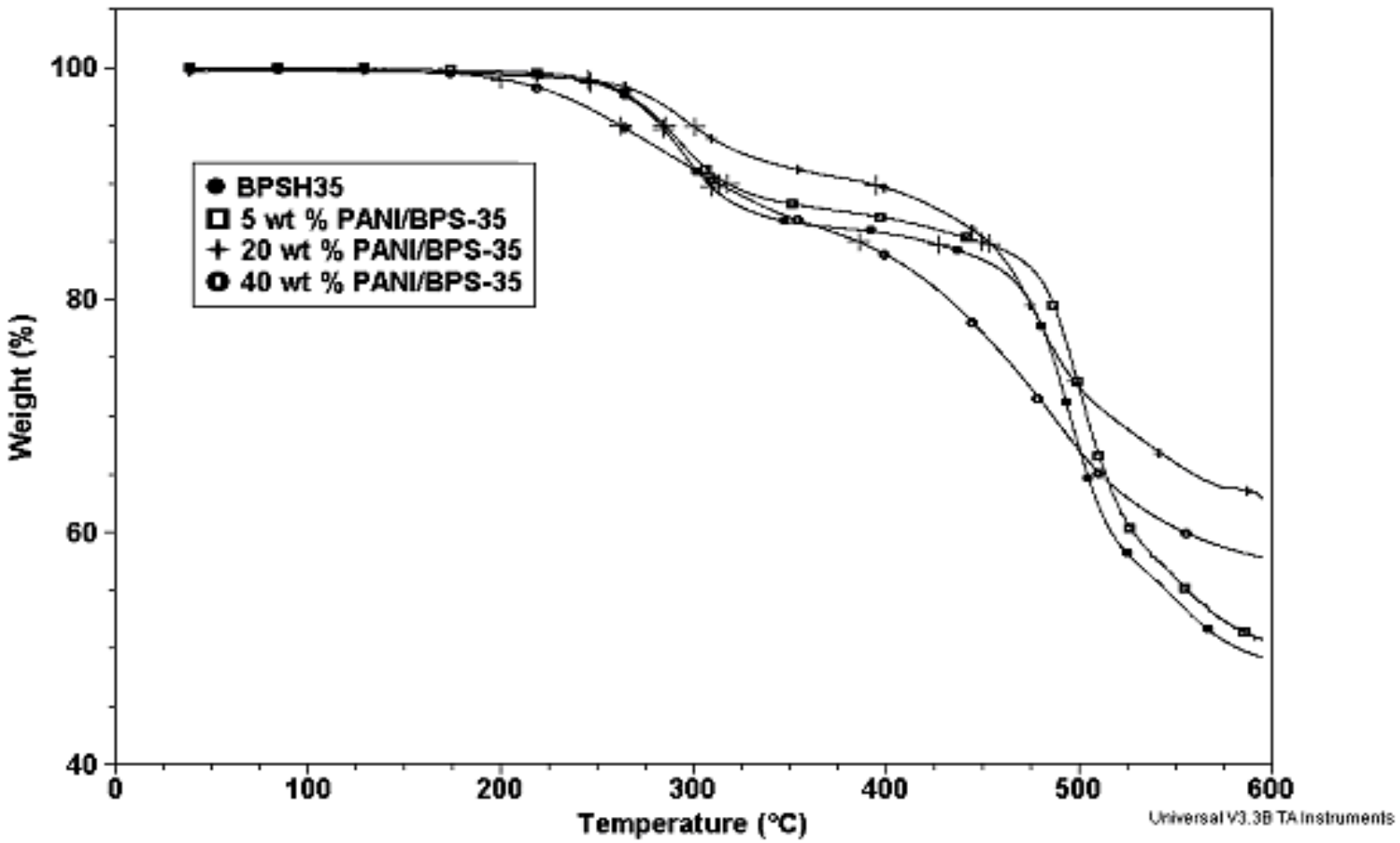

Figure 4.15: TGA curves of BPSH-35 and PANI/BPS-35 composite films with various PANI loadings

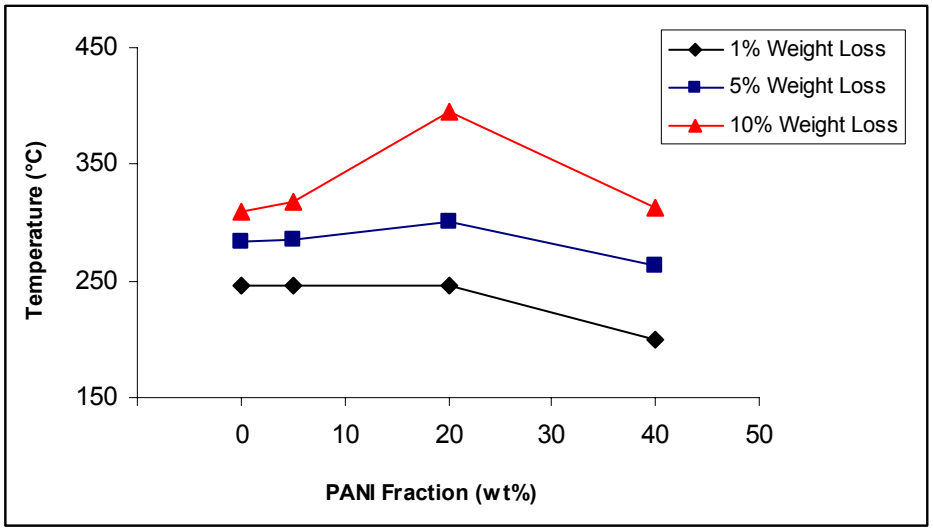

Figure 4.16: 1, 5 and 10 percent weight loss temperatures of BPSH-35 (0 % PANI fraction) and PANI/BPS-35 composite films with various PANI loadings

Mechanical ductility is a desirable property for the conductive composites in order to utilize them in the industry. However, the ductile to brittle transition can possibly occur depending on several factors such as the type and weight fraction of conductive filler as well as the molecular structure of the supportive matrix material. It has been demonstrated that BPSH copolymers are highly thermo oxidatively stable and mechanically ductile [27]. Figure 4.17 shows the stress strain behavior of dry BPSH copolymer and PANI/BPS-35 films at different PANI loadings.

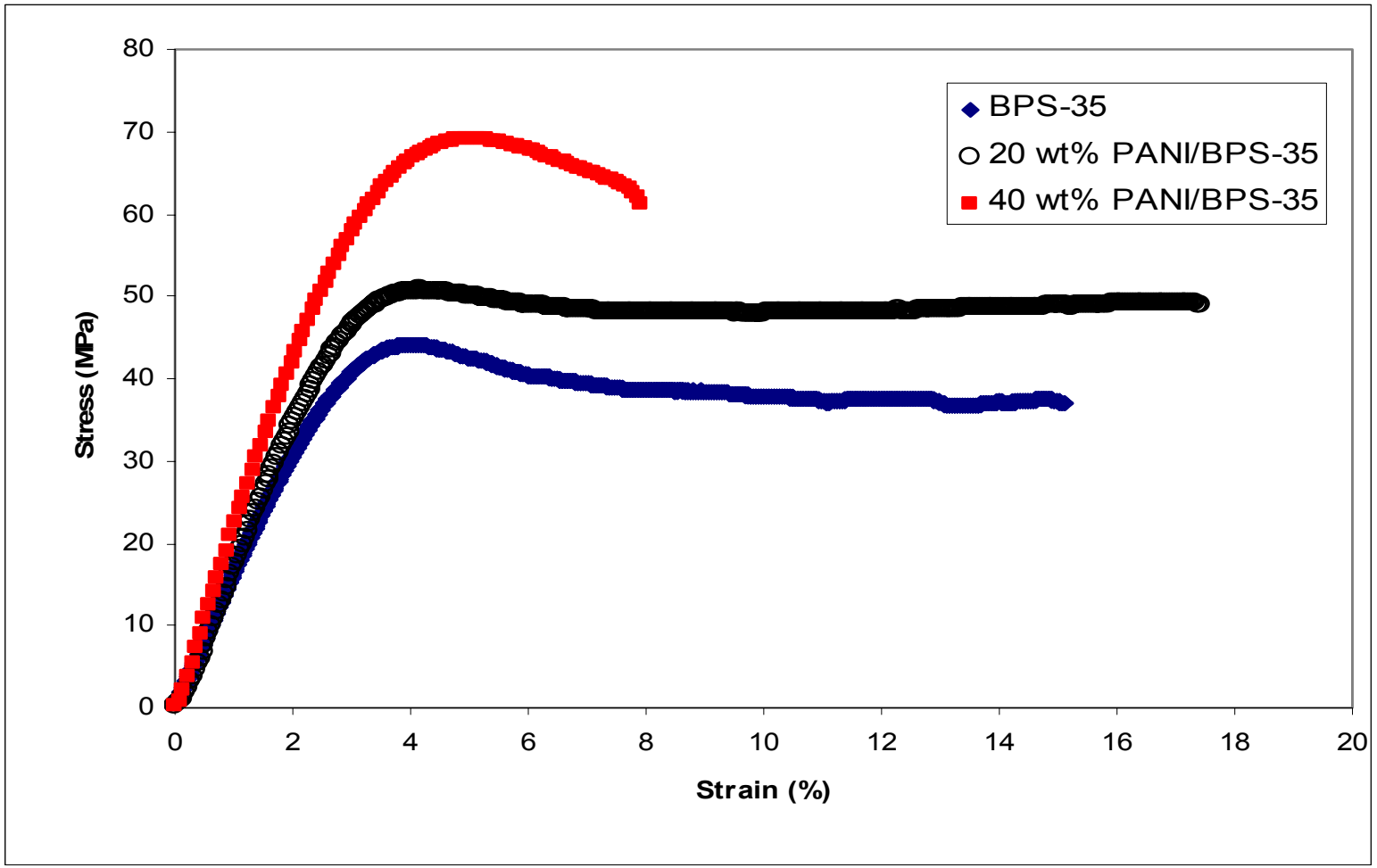

Figure 4.17: Stress versus strain graph for <u>dry</u> PANI/BPS-35 composite films having various PANI loadings

The BPSH and 20 weight percent PANI containing composite film exibited similar mechanical properties. However, it was observed that the PANI reinforced the composite without reducing the ductility at this composition. Related data can be seen in Table 4.4. The ductile to brittle transition was observed to occur when the PANI loading increased from 20 to 40 percent. The proposed interaction between the conductive filler (PANI) and the supporting matrix (BPSH) afforded good mechanical toughness and ductility without reducing the electrical conductivity with 20 weight percent PANI in the composite film. Similar mechanical tests were performed for the fully hydrated samples (Figure 4.18). The water uptake of the composite films decreased with increased PANI loading. The fully hydrated samples followed similar mechanical behavior as dry samples under load. The ductile to brittle transition was also observed as the PANI loading changed from 20 to 40 weight percent. However, fully hydrated samples were more ductile due to the plastization effect (Table 4.4).

Table 4.4: Mechanical properties and water uptake data for PANI/BPS-35 composite films

Sample condition	PANI Fraction (wt %)	Tensile Strength (MPa)	Young's Modulus (GPa)	Elongation at break (%)	Water Uptake (%)
dry	0	44	1.4	15	-
	20	51	1.9	17	-
	40	69	2.1	8	-
wet	0	30	1.0	44	25
	20	40	1.3	27	20
	40	41	1.4	11	14

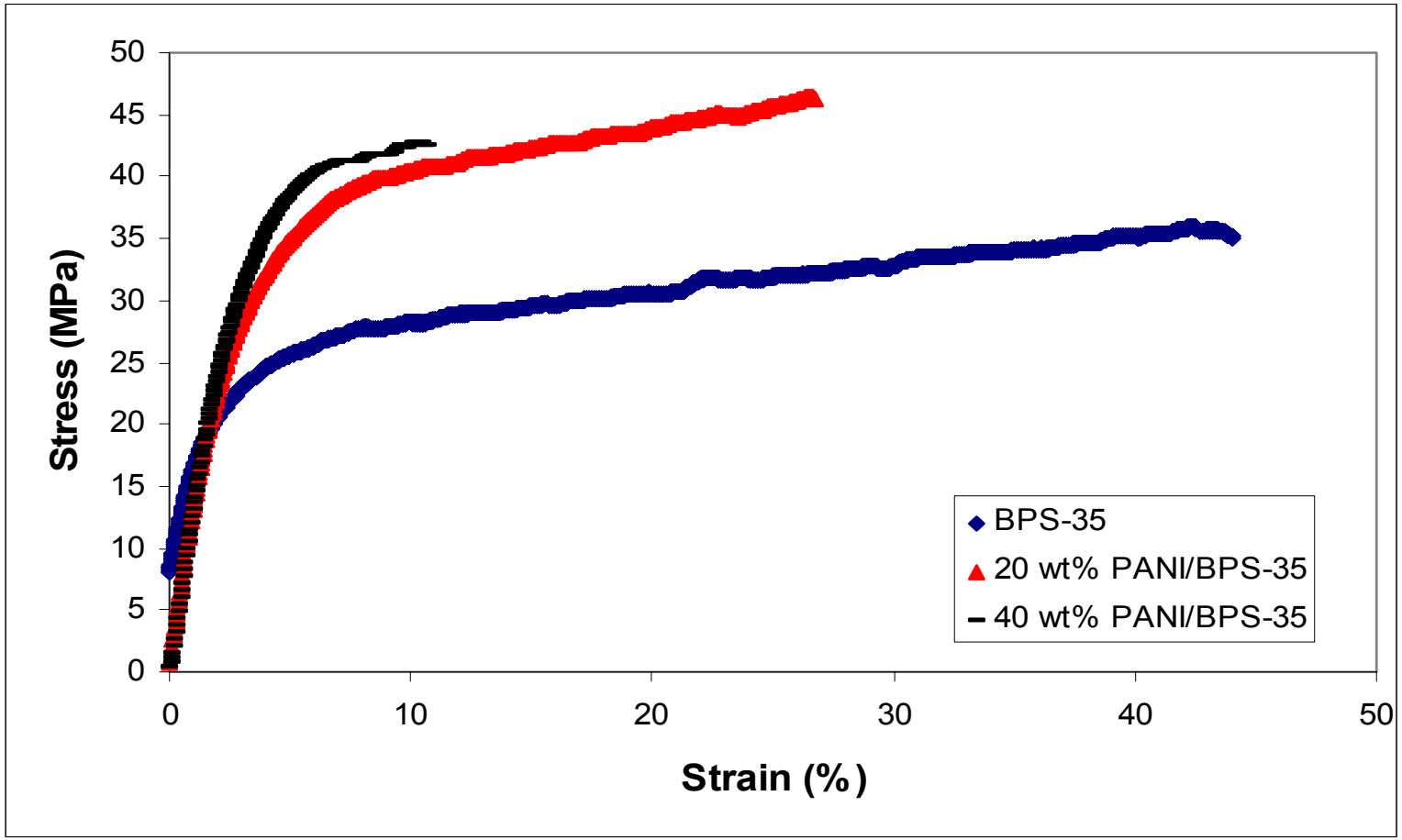

Figure 4.18: Stress versus strain graph for <u>fully hydrated</u> PANI/BPS-35 composite films having various PANI loadings

4.4.7 Morphology

SEM technology was used to investigate the morphology of PANI/BPS-35 films. The detailed morphology study of BPS having different sulfonation percent were done by the McGrath et al. [264] and cluster-like structure with diameter 10-25 nm was assigned as the hydrophilic sulfonic acid groups. The domain size of these clusters depends on the degree of sulfonation. Similar cluster-like structure of sulfonated groups can be seen in Figure 4.19a. By addition of PANI, domain size of sulfonated groups increased to 100-200 nm (Figure 4.19b). This increase in domain size can be explained by the migration of PANI through the sulphonated groups due to the chemical interaction. Previously discussed FTIR and TGA studies support the existence of this strong interaction between PANI and sulphonated groups in BPS copolymer.

[264] M. A. Hickner, H. Ghassemi, Y. S. Kim, B. R. Einsla, and J. E. McGrath, Chemical Review, Vol. 104, 4587-4612 (2004).

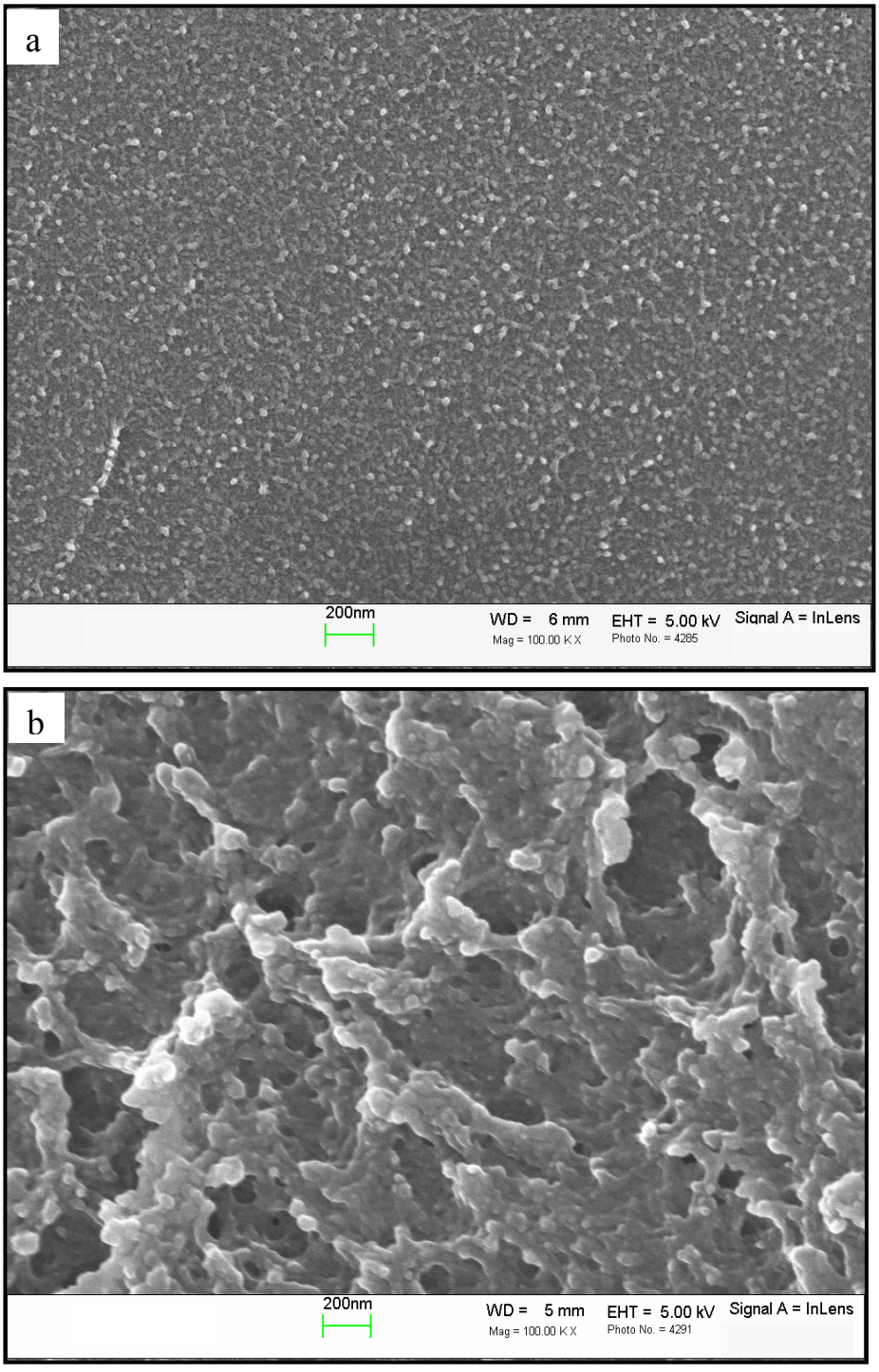

Figure 4.19: Fracture scanning electron microscope pictures of (a) BPS(35), (b) doped PANI/BPS(35) composite film with 40 wt % PANI

4.5 Conclusions

During this study, thermoxidatively stable, ductile PANI/BPS-35 composite films with adjustable electrical conductivity were prepared. These composite films are promising candidates for many applications that require electrical conductivity with mechanical stability. Composite films were doped using aqueous solutions of both sulfuric and hydrochloric acids. Higher conductivities were obtained for the composites doped with sulfuric acid. The conductivity values, which would be useful for a wide range of applications, were achieved after only 1 min doping. Sulfonated poly (arylene ether sulfone) having 35 mole percent ionic content helped the doping process due to its water uptake properties. Conductivity of the composite films equilibrated after 2-3 hours of doping and a maximum conductivity of 0.6 S/cm was achieved.

The influence of relative humidity and temperature on conductivity was investigated using a two point probe technique. The conductivity increased slightly at room temperature with increasing relative humidity, which revealed a greater influence at higher temperatures (80 °C). However, the influence of the temperature on conductivity was dominant to relative humidity. The temperature dependent DC conductivity studies showed that Mott's three-dimensional hopping method can be used to explain the conduction mechanism of PANI/BPS composite films.

Fourier transform infrared spectroscopy (FTIR) was used for structural confirmation of sulfonated poly (arylene ether sulfone), PANI and composite films. The FTIR spectra of the doped and undoped composite films differed greatly, suggesting a molecular interaction between the supportive matrix and conductive filler.

Thermogravimetric (TGA) analysis indicated that the 20 weight percent PANI-containing composite films had better thermal stability compared to the unfilled BPSH supportive matrix which reinforced the PANI conductive quite well. The 10 percent weight loss temperature of 20 weight percent PANI loaded composite film was 395 °C. It is hypothesized that the thermal stability of the 40 weight percent PANI composite films

decreased due to the insufficient amount of ionic content which leads to weaken the interaction among the phases.

Tensile tests were conducted for both dry and fully hydrated composite films, and the sulfonated poly (arylene ether sulfone) copolymer. The composite films were very ductile and tough with when BPS was loaded with up to 20 weight percent PANI. Beyond this point the ductile to brittle transition was observed. The fully hydrated composite films were more ductile and showed similar ductile to brittle transitions at higher PANI loadings (40 wt %). The Young's modulus of 1.9 and 1.3 GPa were observed for dry and wet 20 weight percent PANI containing composite films, respectively.

CHAPTER 5

Solution Processable Organic Semiconductors: Device Fabrication and Characterization

5.1 Introduction

As emphasized in Chapter 1, the traditional photolithographical manufacture of electronic devices requires long and expensive production steps. Recently, new techniques such as microcontact printing, screen printing, ink-jet printing and line patterning have been developed to produce low cost disposable electronic devices. These methods do not only reduce the number of fabrication steps but also eliminate the need for high-vacuum processing, such as chemical vapor deposition and plasma etching. The possibility of using different substrates, e.g. flexible polymers, is another important advantage of these new techniques.

The same methods explained in Chapter 2 and 3 can be used to selectively deposit water-based organic semiconductor and therefore build functional devices on flexible substrates. In this chapter, the line patterning and inkjet printing of a p-type organic semiconductor, Poly-3-4-ethyleneoxythiophene/poly-4-sytrensulfonate, on flexible substrates has been introduced. Using these two fabrication techniques, basic electronic components have been manufactured on overhead transparency and polyimide films. In the next section line patterned polymer resistors and field effect transistors will be

investigated. The inkjet printed polymer thin films will be introduced in the following section.

5.2 Line-Patterning of Poly-3-4-ethyleneoxythiophene/poly-4-sytrensulfonate

Poly-3-4-ethyleneoxythiophene/poly-4-sytrensulfonate (PEDOT/PSS), which is one of the intrinsically conductive polymers, is used in this study as active material. In late 80s, the precursor of PEDOT/PSS, which is ethylenedioxithiophene (PEDOT), was chemically polymerized at Bayer AG research laboratories [265]. This polymer has a high conductivity (~300 S/cm) and high stability in oxidized state [266]. However, the insolubility of PEDOT limits its application. In early 90s, Bayer company developed a new polymer by adding the water soluble electrolyte, which is poly(styrene sulfonic acid), during the polymerization of PEDOT. This process results in a water soluble conducting polymer with high stability and good film-forming properties. The physical properties of PEDOT/PSS dispersion used in this study can bee seen in Table 5.1. For simplicity, PEDOT/PSS[a] and PEDOT/PSS[b] will be used in this chapter for aqueous dispersion of Baytron P and Baytron PHC V2 respectively.

Table 5.1: Physical properties of PEDOT/PSS dispersions

Commercial Name	*Mean particle size (nm)*	*Viscosity (cP)*	*Solid Content (%)*	*Sheet Resistivity (Ωcm)*
Baytron P	80	80	1.3	1
Baytron PHC V2	100	120	1.3	0.15

[265] Bayer AG, European Patent 339 340, 1988
[266] M. Dietrich, J. Heinze, G. Heywang, F. Jonas, Journal of Electroanalytical Cehmistry, Vol. 369, 87-???, 1994

5.2.1 Line Patterned Resistors

Figure 5.1 shows the various geometries produced by the line patterning on overhead transparency. It is observed that the film of PEDOT/PSS remained strongly adhere to the transparency surface after sonication, passing a laboratory Scotch-tape test.

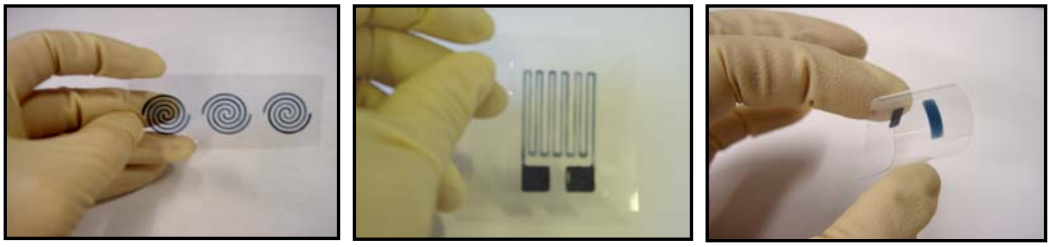

Figure 5.1: Line patterned PEDOT/PSS on 3M transparency

The first functional device manufactured in this chapter using PEDOT/PSS via line patterning is a resistor. The resistor is the oldest and the simplest electrical device. The name "resistor" comes from the material property of resisting electric current flow. In 1826, the German physicist Georg Simon Ohm found the relationship between voltage (V) and current (I) to vary with the cross-sectional area (A), length (L) and material properties of the conductor (ρ). This relationship between voltage and current is called Ohm's law

$$V = RI \quad and \quad R = \rho \frac{L}{A} \ , \tag{5.1}$$

where the unit of the voltage is volt (V), that of resistance and current are ohm (Ω) and amper (A), respectively. Figure 1.25 (a) shows the linear and symmetric I-V characteristics of a linear resistor. The slope of this graph gives the conductance having unit of Siemens (S), which is equal to the reciprocal of the resistance. Figure 5.2 (b) indicates the circuit representation of a resistor. For the case R=0 circuit is called short circuit and for the case $R \rightarrow \infty$ the circuit reduces to an open circuit. The power rating is an important parameter for choosing a resistor. Most of the electrical power absorbed by the

resistor is converted into heat. If a resistor is operated beyond the rated power level, it will overheat and degrade. The absorbed power for a linear resistor can be written as

$$P = VI = I^2 R = \frac{V^2}{R} \quad . \tag{5.2}$$

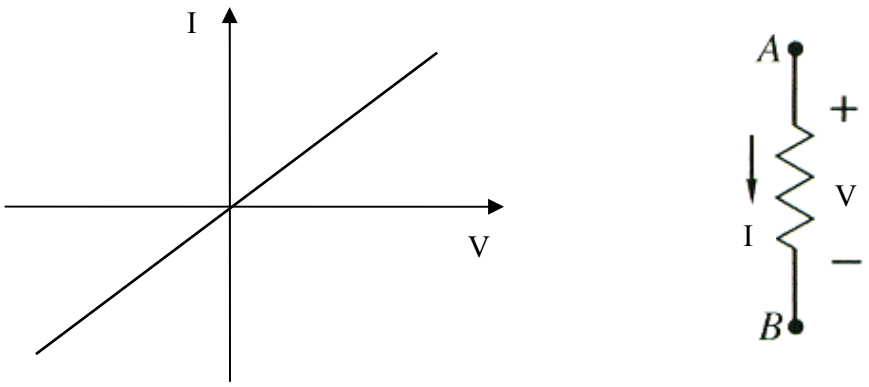

(a) (b)

Figure 5.2: (a) I-V characteristics of a linear resistor, (b) circuit representation of a resistor

Polymer thin film resistors were fabricated on 3M transparency as described in section 3.1.1. After deposition of the polymer, samples were dried under the heating lamp at approximately 80°C. The length of the resistors kept constant while the width and the thickness vary. The thickness of the resistor was controlled by the number of polymer layers on the substrate (see Figure 5.3). Silver epoxy was used to make electrical contacts on the polymer resistors. I-V characterization of polymer thin film resistors was done by using Keithley 236 I-V source-measure unit.

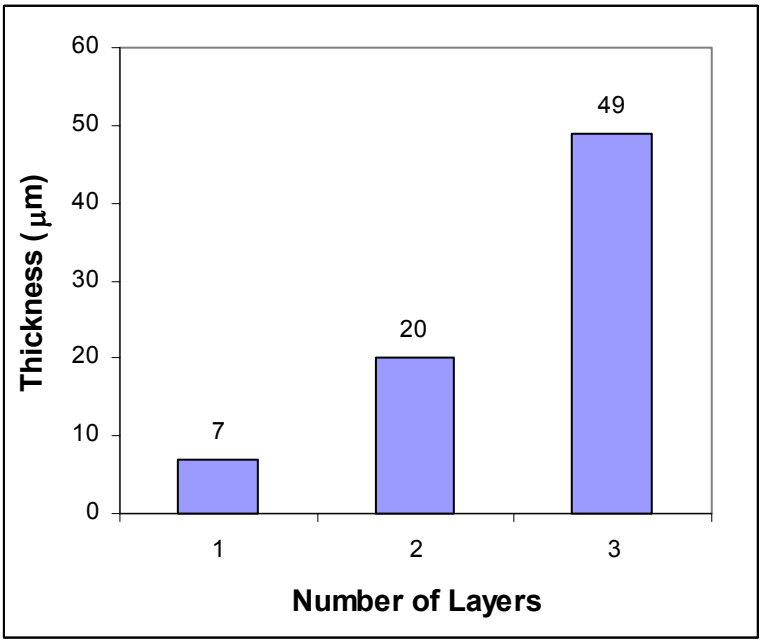

Figure 5.3: Thickness versus number of layers plot for line patterned polymer resistors (active material is PEDOT/PSS[a])

As shown in Figure 5.4 (a), polymer resistors show ohmic characterization and as expected the resistance decreases with increasing the thickness (Figure 5.4 (b)). Table 5.2 summarizes the resistance and conductivity data of line patterned polymer resistors where the PEDOT/PSS[a] is active material

Table 5.2: Resistivity, conductivity and thickness data for line patterned resistors

Number of layers	R (kΩ)	σ (S/cm)	thickness (μm)
1	58	5.54E-02	7
2	25	4.50E-02	20
3	8	5.74E-02	49

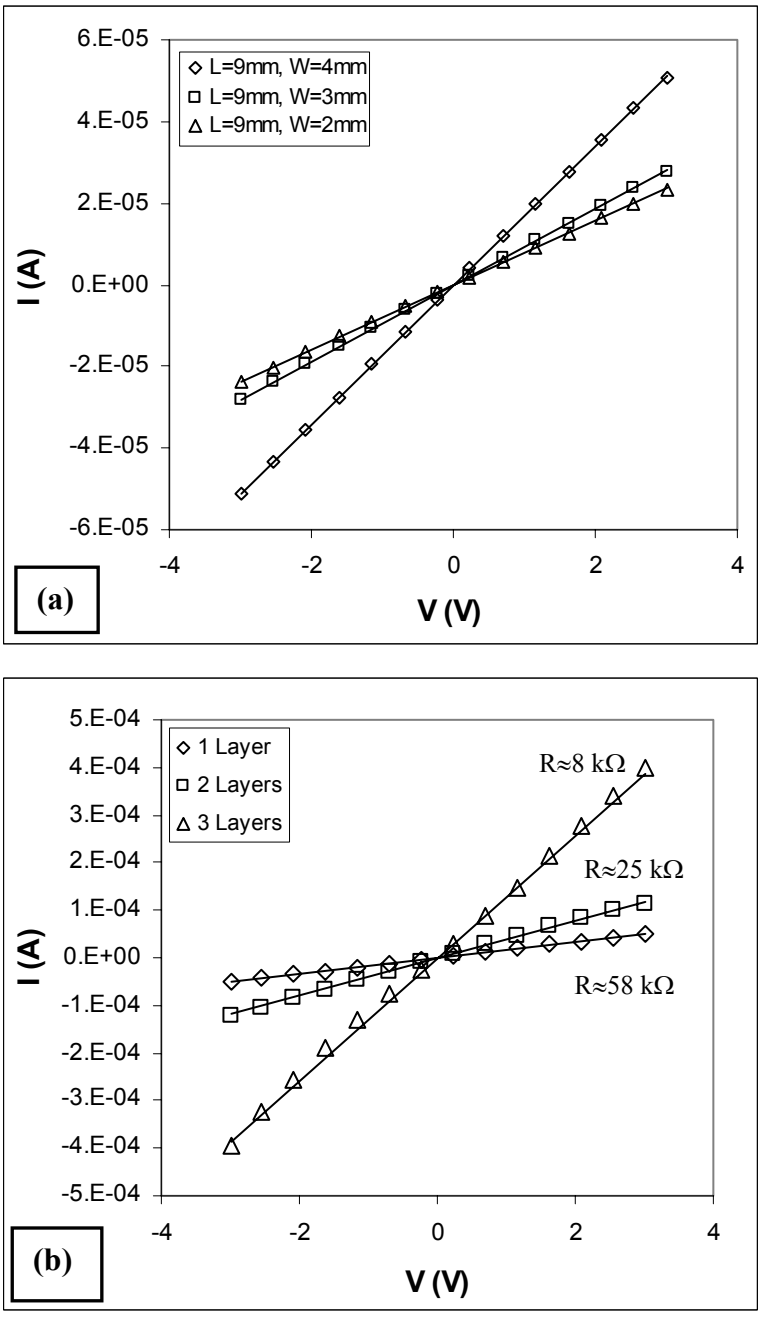

Figure 5.4: Current versus voltage plots of line patterned polymer resistors (a) One layer of Baytron P (b) Baytron P with L=9mm, W=4mm

The effect of the annealing on conductivity was examined. The polymer resistors were annealed at 90 °C for 30 min under vacuum. It is observed that the annealing enhanced the electrical conductivity slightly. The slight change indicates the almost all of the solvent was successfully removed during the fabrication step.

The polymer resistors were also fabricated using PEDOT/PSS[b] as the active material. Like polymer resistors made by PEDOT/PSS[a], PEDOT/PSS[b] resistors showed ohmic behavior. However higher conductivities were observed compared to the line patterned resistors using Baytron P. As seen in the Table 5.3 the conductivity of PEDOT/PSS[b] resistors is approximately 60 times higher than that of PEDOT/PSS[a].

Table 5.3: Resistance and conductivity data of Baytron PHC V2 resistors with different geometries and after annealing process at 90°C under vacuum for 30 min

Sample ID	L (cm)	W (cm)	thickness (μm)	R (Ω)	σ (S/cm)
A	0.9	0.4	14	463	3.5
B	0.9	0.3	14	725	3.0
C	0.9	0.2	16	877	3.2

5.2.2 Ethylene Glycol Treatment

It has been reported that the electrical, optical, and morphological properties of PEDOT/PSS change by adding organic solvents into the aqueous solution or by treating the solid film of PEDOT/PSS with those solvents [267, 268,269]. Pettersson et al [209] prepared thin films from aqueous PEDOT/PSS dispersion and also from the aqueous

[267] J. Y. Kim, J. H. Jung, D.E. Lee, J. Joo, Synthetic Metals, Vol. 126, 2002, 311-316
[268] L. A. A. Pettersson, S. Ghosh, O. Inganäs, Organic Electronic, Vol. 3, 2002, 143-148
[269] S. K. M. Jönsson, J. Birgerson, X. Crispin, G. Graczynski, W. Osikowicz, A. W. Denier van der Gon, W. R. Salaneck, M. Fahlman, Synthetic Metals, Vol. 139, 2003, 1-10

dispersion containing 65% sorbitol by weight to PEDOT/PSS solid. They found that PEDOT/PSS thin films have uniaxial anisotropy with the optic axis parallel to the surface normal. Sorbitol addition results in decrease in the anisotropy in the polymeric material and increase in electrical conductivity from 0.94 S/cm to 56 S/cm. This optical and electrical change is attributed to reorientation of polymer chains to more macroscopically random state and also a large inter-chain conduction. Jönsson et al made a study about the effects of solvent on the morphology and sheet resistivity of PEDOT/PSS films [210]. They spin coated both the PEDPT/PSS dispersion and PEDOT/PSS blended with sorbitol, N-methylpyrrrolidinone and isopropanol. The conductivity of PEDOT/PSS pristine films enhanced from ~0.1 S/cm to 48 S/cm by solvent addition. The AFM images of both heated PEDOT/PSS-pristine and PEDOT/PSS-solvent films showed that the maximum grain size and maximum height variation decreased by solvent addition. Therefore, Jönsson et al proposed that excess PSS is cleaned from the surface of PEDOT/PSS grains in the film resulting in better connection between charge carrying species. Recently, Ouyang et al[270] has reported that conductivity of PEDOT/PSS films increased by a factor of ~358 and ~500 after treated with DMSO and ethylene glycol (EG) respectively. They attributed this drastic increase in conductivity to conformational change in PEDOT/PSS structure. They proposed that Raman spectroscopic study of same group indicated that PEDOT chain changes from a benzoid to a quinoid structure following EG treatment.

The effect of the EG treatment on line patterned resistors was investigated in this section. After deposition of PEDOT/PSS on the 3M transparency, samples were dried at 50 °C approximately 30 min. Then resistance and thickness measurements were performed via Hewlett Packard 34401 type multimeter and Mitutoyo Digimatic micrometer respectively. A second heating was performed at 90 °C under vacuum for again 30 min. Finally the PEDOT/PSS resistors were immersed into the EG for 5 minutes and then dried under vacuum at 100 °C for 30 minutes to evaporate the excess EG. It is observed that conductivity of the PEDOT/PSS resistors (both from Baytron P and Baytron PHC V2) increased slightly with annealing process. However, after EG treatment the conductivity of PEDOT/PSS[a] resistors increased approximately 900 times and reached

[270] J. Ouyang, Q. Xu, C-W Chu, Y. Yang, G. Li, J. Shinar, Polymer, Vol.45, 2004, 8443-8450

51 S/cm. The maximum conductivity for line patterned resistors from Baytron PHC V2 is approximately 150 S/cm after EG treatment (see Table 5.4).

Table 5.4: Electrical properties of line patterned resistors

Samples	Resistance (Ω)	Sheet Resistivity (Ω/□)	Conductivity (S/cm)
PEDOT/PSS[a] pristine	$2x10^5$	$4.44x10^4$	$5.63x10^{-2}$
PEDOT/PSS[b] pristine	600	$2.00x10^2$	5.56
Annealed PEDOT/PSS[a] pristine	$1.5\ x10^5$	$3.33x10^4$	$7.5x10^{-2}$
Annealed PEDOT/PSS[b] pristine	500	$1.67x10^2$	6.67
Annealed PEDOT/PSS[a]-EG treated	238	52.9	51
Annealed PEDOT/PSS[b]-EG treated	26	8.67	147

[a] Baytron P, [b] Baytron PHC V2

5.2.3 Line Patterned Field Effect Transistors

Field effect transistors (Figure 5.5) were fabricated as described in literature [271]. First gate and source-drain electrodes were line patterned on overhead transparency by PEDOT/PSS. Then, a drop of the epoxy is placed on the gate electrode and finally source-drain electrode placed on top of it at 90°C. Epoxy provides an insulator layer between gate and source-drain electrodes. It has been reported that a doped conducting polymer consists of a metallic "island" surrounded by low conducting "beaches". Applied

[271] A. G. MacDiarmid, Synthetic Metals, Vol. 125, 11-22 (2002).

electric field chances the conductivity of the beaches and hence the extent of electrical percolation in the source-drain PEDOT/PSS electrode. Because of this affect the bulk conductivity of channel changes.

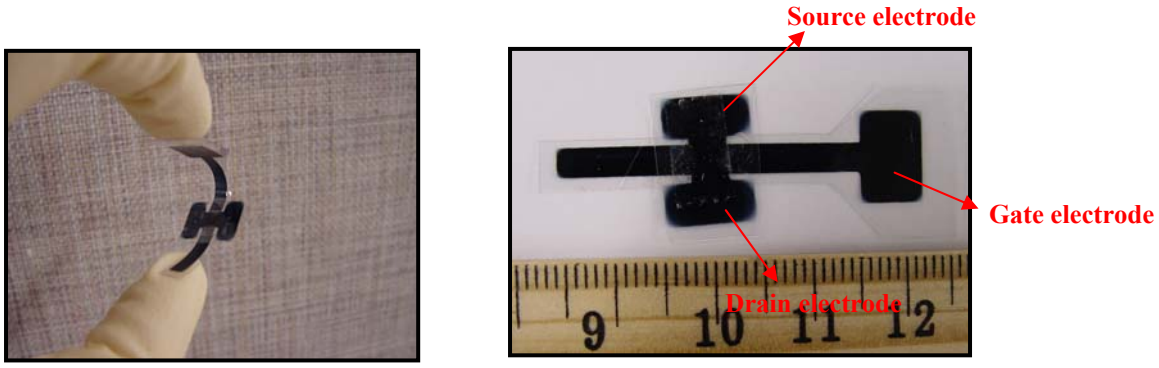

Figure 5.5: Polymer FET on transparency

When the positive voltage applied to the gate electrode, electrons will be induced into the channel at the interface between the insulator and PEDOT/PSS layer due to the capacitance effect. The induced electrons will recombine with the holes in the channel. As a result of this recombination, the drain current decreases. The thickness of the insulator region has a very pronounced effect on the field from gate electrode. Figure 5.6 indicates the source-drain current versus source-drain voltage graph.

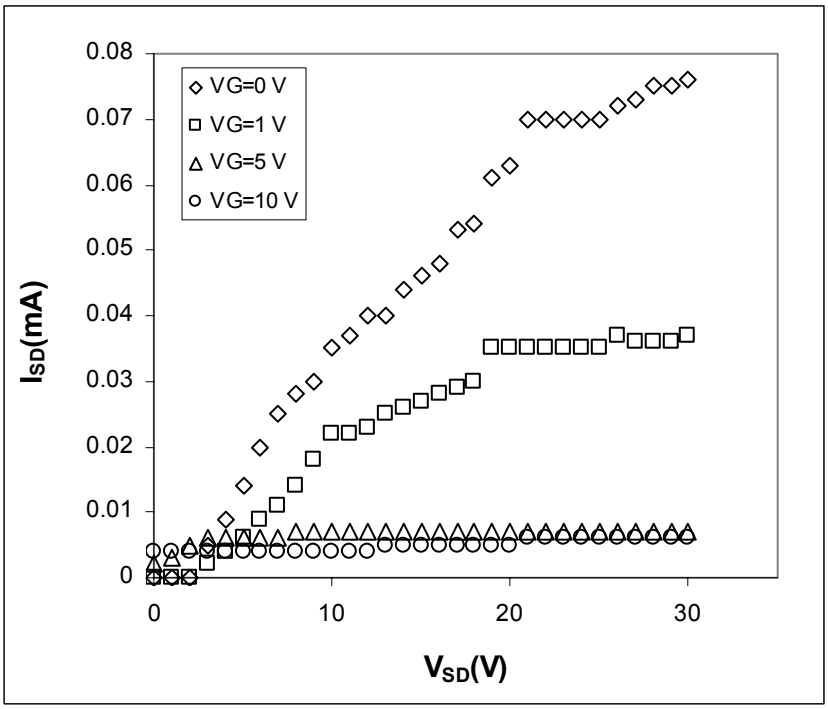

Figure 5.6: Source-drain current versus source-drain voltage graph for different gate voltages

As seen in Figure 5.7, the polymer FETs have the characteristics of p-channel field effect transistor. It is observed that channel conductance decreased and channel resistance increased with increasing the gate voltage because of the recombination of majority carriers (holes) in the channel with the induced electrons (Table 5.5).

Table 5.5: Channel conductance and resistance for different gate voltages

V_G(V)	g_{SD}(μS)	R_{SD}(kΩ)
0	2.9	345
1	1.5	667
5	1.1	909

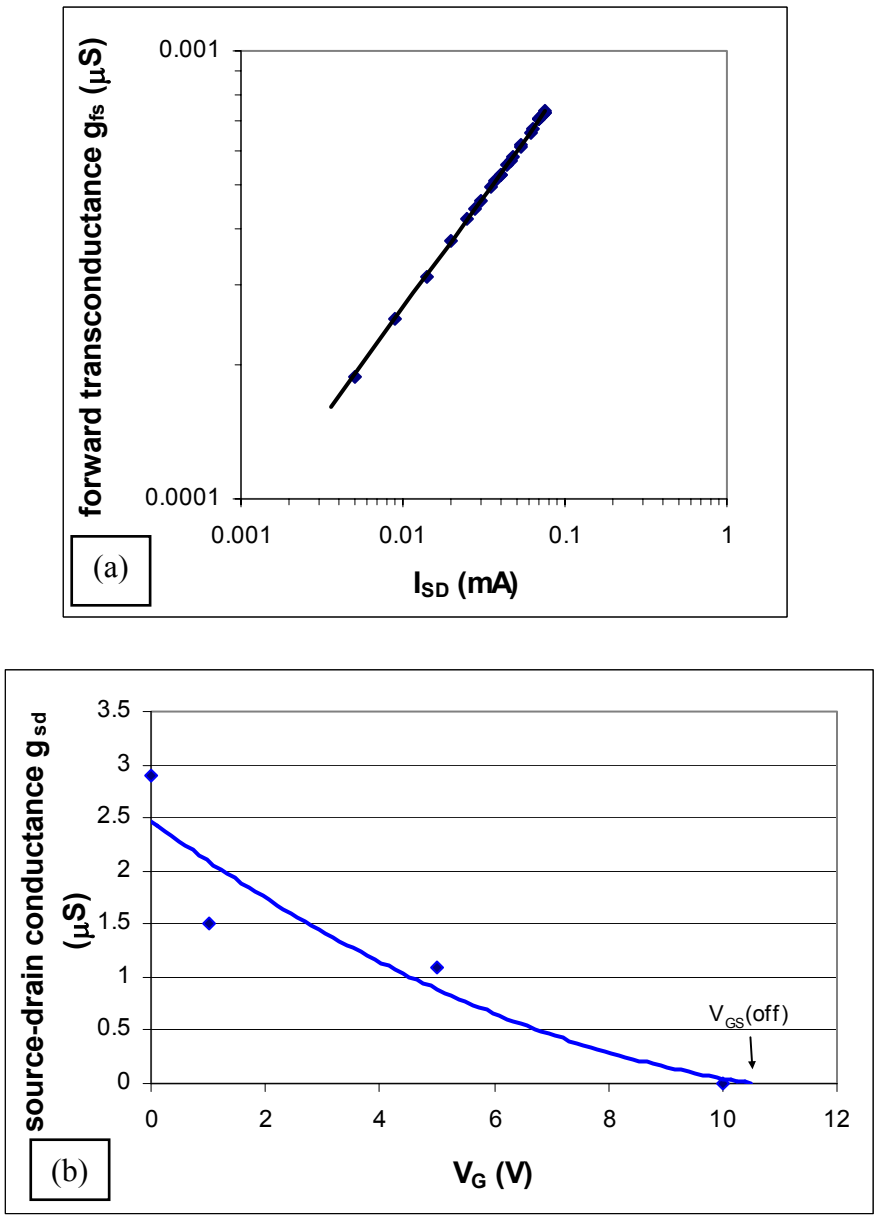

Figure 5.7: (a) Forward transconductance versus source-drain current graph, (b) source-drain conductance versus gate voltage graph

Preliminarily studies showed that the polyaniline also has similar electrical characterizations with PEDOT/PSS. Therefore it may possible to use different conducting

polymers as gate and source-drain electrode. Using different types of conducting and semiconducting polymers may provide the means to design different types of FETs and increase the efficiency.

So far the line patterned resistors and field effect transistors on mechanically flexible substrates have been discussed. Baytron P and Baytron PHC V2 have been used as active material to build functional devices. The effects of making multiple layers of active material and ethylene glycol treatment on electrical performances of line patterned resistors have been examined. Line patterned field effect transistors and some electrical characterizations have also been introduced. The next section describes the inkjet printing of PEDOT/PSS. Inkjet printing provides very good control of thickness and resolution of patterned active material. Experimental details and results of this study are presented in the following section.

5.3 Inkjet Printing of PEDOT/PSS

As explained in Chapter 1 and 2, inkjet printing technique, has been gaining more attention because of its unique features, such as its simplicity of fabrication, compatibility with different substrates, availability of non-conducting and no-mask patterning, low temperature processing, and low cost [114-117, 197-202].

In this study, Lexmark inkjet printer modified to print semiconductor and insulator ink on flexible substrates. Modification can be done by just replacing the regular printer ink with polymer solution. No further modification is required for alcohol or water based functional inks. Approximately 80 μm wide PEDOT/PSS lines were printed on paper (see Figure 5.8) using modified Lexmark Z515 color inkjet printer, which uses the thermal technology. The Lexmark Z515 inkjet printer reaches print speeds of 12ppm black, 7ppm color with 2400 X 1200 and 4800 X 1200 dpi resolutions, respectively. The sheet resistivity of PEDOT/PSS line on paper was about $2x10^6$ Ω/□. The Lexmark inkjet printer works best with the water based inks, since the ink cartridge is not compatible with organic solvents such as toluene and N-Methylpyrollidinone.

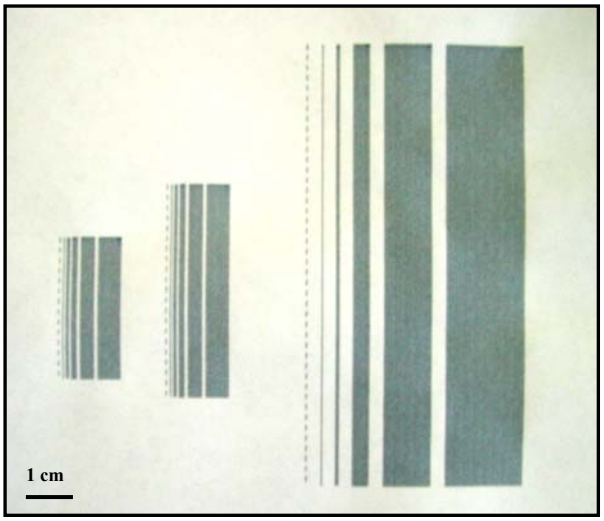

Figure 5.8: Picture of inkjet printed PEDOT/PSS lines on paper

Using the Lexmark Z515 color inkjet printer, polymer resistors with various dimensions were printed on polyimide substrate. Baytron P was used as the active material. I-V measurements were performed using Keithley 236 IV source-measure unit. Prior to resistor fabrication, electrical contacts were inkjet printed by using silver MO ink. The details about the silver MO ink and inkjet printing conditions has been given in Chapter 2. The voltage versus current graph for inkjet printed PEDOT/PSS on polyimide substrate can be seen in Figure 5.9. In order to increase the PEDOT/PSS loading on the surface multiple-layer lines were inkjet printed. As expected when the number of passes increased the conductivity of printed lines also increased. The resistance of PEDOT/PSS lines formed in 5 and 20 passes lines was 375 and 130 kΩ for, respectively.

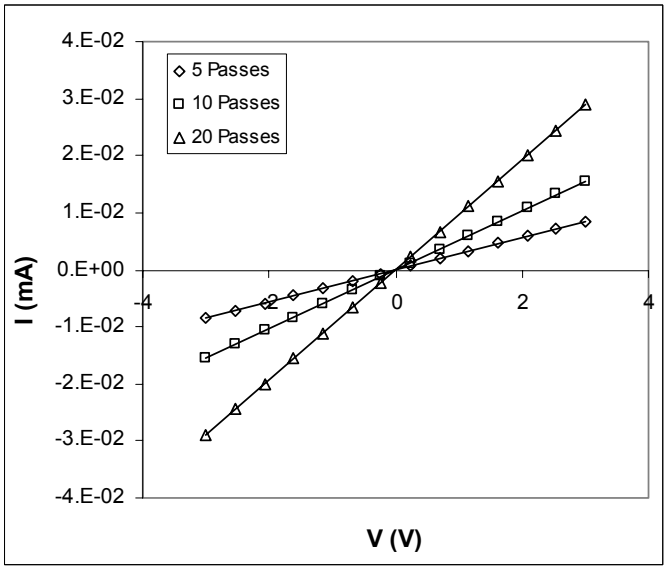

Figure 5.9: Current versus voltage graph for inkjet printed PEDOT/PSS

The effect of annealing on resistance of inkjet printed PEDOT/PSS lines was investigated. Inkjet printed PEDOT/PSS lines from 15 lines were annealed at 90 °C under vacuum for 30 minutes. As seen in Figure 5.10, the resistance of polymer lines decreased approximately 20% after annealing. Further annealing did not change the resistivity significantly.

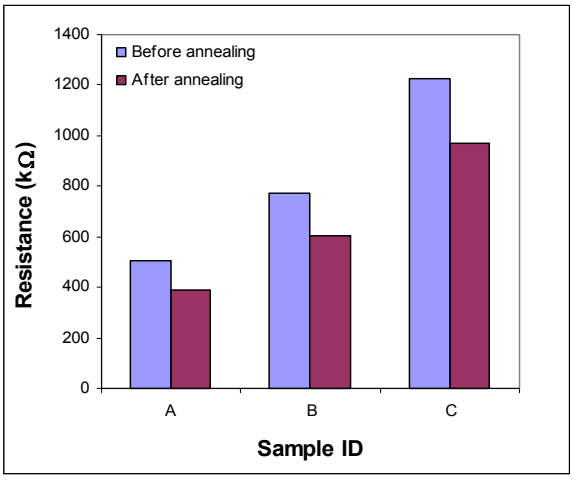

	Sample ID		
	A	B	C
L (mm)	10	10	10
W (mm)	5	3	2

Figure 5.10: The effect of annealing on resistivity of inkjet printed PEDOT/PSS lines

The effect of ethylene glycol treatment was also investigated. Inkjet printed PEDOT/PSS lines were immersed in ethylene glycol for 5 minutes. Like line patterned PEDOT/PSS resistor, it was observed that ethylene glycol treatment enhanced the conductivity of inkjet printed polymer lines. Table 5.6 summarizes the resistance of inkjet printed PEDOT/PSS lines from 15 passes before and after annealing and after ethylene glycol treatment. The resistance of PEDOT/PSS lines decreased approximately 350 times after ethylene glycol treatment.

Table 5.6: Resistance of 10 mm long inkjet printed PEDOT/PSS lines from 15 passes

W(mm)	R^{*} (kΩ)	R^{**} (kΩ)	R^{***} (kΩ)
5	505	388	1.56
3	775	602	2.23
2	1224	971	3.22

*Before Annealing, **After Annealing, ***After EG treatment

5.4 Conclusions

Polymer-based resistors and field effect transistors have been fabricated using line patterning and inkjet printing methods. The polymer resistors showed ohmic characteristics and as expected the resistance decreased with increase in the thickness of active material. The resistance of line patterned and inkjet printed PEDOT/PSS (Baytron P) has enhanced 900 and 350 time with ethylene glycol treatment. Line patterned field effect transistors showed typical characteristics of p-channel field effect transistor. The channel conductance decreased and channel resistance increased with increase in the gate voltage because of the recombination of majority carriers (holes) in the channel with the induced electrons. The promising performances of polymer resistors and field effect transistors and also the simplicity and low cost of their fabrication methods reported in

this chapter, would make it possible to integrate them into more complicated electronic structures to build disposable electronic devices on mechanically flexible substrates.

CHAPTER 6

CONCLUSIONS AND SUGGESTED FUTURE WORK

The primary objective of this study was to investigate the cost effective fabrication methods of solution processable metals and semiconductors on mechanically flexible substrates. Solution processable materials provide a means for the direct patterning of active material on various flexible substrates including plastics, paper and fabric. This is envisioned to open a new era in electronics. Solution processable metals and semiconductors make it possible to fabricate foldable, ultra thin and light displays, integrated circuits on plastics, photonic textiles serving as displays, intelligent shoes that can control the cushioning level using sensors and more other products which are ready to take place in the markets. Relatively large scale and inexpensive fabrication methods are among the advantages of organic or flexible electronics over the traditional inorganic or rigid electronics.

Successful direct deposition of silver, gold, and copper on flexible substrates via inkjet printing, line patterning and mask printing methods have been demonstrated in this dissertation. Conductive silver inks for inkjet printing were prepared from solution of (1,5-cyclooctadiene)(hexafluroacetyl-acetonato)silver(I) organometal compound in butanol. 0.5 mm wide silver lines were printed on polyimide substrates using a resolution

of 2217 dpi. The addition of silver nano powder into the butanol based ink increased the conductivity of printed lines. A surface resistivity as low as 0.1 Ω/□ was obtained in this study.

Inkjet printing of gold nanoclusters enabled the rapid and room temperature deposition of conductive ink on flexible substrates. Inkjet printed gold nanoclusters were converted into metallic form by heat treatment. The melting and coalescence of gold nanoclusters occurred around 140-200 °C, which is well below the melting point of bulk gold. The conductivity of inkjet printed lines from a single pass was about $1x10^5$ S/m. A suggestion for future work would be the fabrication of passive circuit elements such as interconnects, inductors, capacitors, and electrodes on very large area and mechanically flexible substrates using both silver and gold ink formulations, which have been presented in this dissertation.

Alternative selective metallization methods were also examined in this study. Determination of low-cost and low-tech metallization of flexible substrates was the main purpose. Therefore, different experimental methodologies for different metals and substrate materials have been developed. Silver, gold and copper thin films have been deposited on polyester, polyether imide, polyimide and overhead transparency films via electroless deposition and patterned via line patterning and mask printing methods. This novel patterning method was elegantly simple, very cost effective, and adaptable into mass production like roll-to-roll process. The electrical conductivity of line patterned metals was very close to that of bulk materials.

Thermoxidatively stable, ductile, and electrically conductive composite films from polyaniline and sulfonated poly(arylene ether sulfone) have been introduced. These composite films can be used as flexible electrode material, precursor of humidity and chemical sensors, and also electromagnetic shielding material. We presented a simple chemical route to prepare composite materials having a tunable electrical conductivity. The conductivity of composite films can be arranged from insulating level to upper semiconductor level by changing the amount of polyaniline in the composite. The DC

conductivity measurement studies under high temperature and high humidity showed that composite films were very stable to oxidative conditions. Temperature dependent conductivity measurements showed that Mott's three-dimensional hoping method can be used to explain the conductivity mechanism of PANI/BPS films.

Fourier transform infrared spectroscopy and thermogravimetric analysis indicated a molecular interaction between the supportive matrix (BPS) and conductive filler (PANI). Ductile and tough composite films were obtained with Young's modulus up to 2.1 and 1.4 GPa for dry and wet PANI/BPS-35 composite films, respectively. Overall, the 20 wt% PANI containing composite films performed best, which was attributed to the ionic content available to interaction of PANI. These composite films could be promising candidates for many applications that require a combination of electrical conductivity with mechanical stability.

Finally, the line patterning method was used to fabricate polymer resistors and field effect transistors on flexible substrates. A commercially available organic semiconductor, Poly-3-4-ethyleneoxythiophene/poly-4-sytrensulfonate (PEDOT/PSS), was used as the active material. The effect of building multiple layers and ethylene glycol treatment on conductivity was examined. The conductivity of polymer resistors from 3 layers of PEDOT/PSS increased from $5x10^{-2}$ to 51 S/cm with ethylene glycol treatment. Line patterned PEDOT/PSS field effect transistors showed typical characteristics of p-type transistor. Inkjet printing also used to transfer PEDOT/PSS on paper and transparency films. The sheet resistivity of inkjet printed polymer resistors were about $2x10^{5}$ Ω/□. That value was lowered approximately 350 times by ethylene glycol treatment.

Basic circuit elements such as resistors, field effect transistors and interconnects were fabricated on the flexible substrates. Solution based, cost effective, and rapid manufacturing techniques have been investigated. Various metals and semiconductors have been successfully deposited from their solutions. Suggested future work would include the integration of individual circuit elements into functional devices and also the fabrication of multiple layered circuit devices. Adaptation of solution based flexible

electronic fabrication methods given in this study into fabrics and manufacturing of wearable electronics mentioned earlier could be other possible future work following this dissertation.

APPENDIX A

QUANTUM APPROACH TO POLYMERIC ELECTRONIC STRUCTURE

The main aim of this section is to explain basic theory of the electronic structure of polymeric solids and also to make a connection between the polymeric solids and the crystalline solids so the band theory and the conduction mechanism of the polymeric systems can be understood. Many different theoretical models and approximations are being used to determine the electronic properties of polymers. The Born-Oppenheimer approximation, which will be explained in following section, ab initio calculations, the Hartree-Fock approximation and the SSH model are the most common ones due to their advantages and the drawbacks of different schemes, and physical significance of the results and applicability to calculation of metal-polymer interfaces.

1. Born-Oppenheimer Approximation

The Born-Oppenheimer approximation allows us to calculate the π-electron states in polymers by regarding the fixed nuclear configuration. In other words, the key idea in this approximation is that nuclei are much heavier than the electrons and therefore move much slower [272]. Thus, the electrons are the primary dynamic objects, which determine the chemical bonding and transport properties of interest. Thus, the Hamiltonian depends

[272] W. R. Salaneck, S. Stafström, J.-L. Brédas, Conjugated Polymer Surfaces and Interfaces, Cambridge University Press, New York, 1996.

only on the nuclear coordinates ***R***. Within the Born-Oppenheimer approximation the electronic Hamiltonian, H_e can be written as

$$H_e\{r,R\} \equiv H_{e-e}\{r\} + V_{n-e}\{r,R\}$$

where

$$H_{e-e}\{r\} = \sum_i \frac{p_i^2}{2m_e} + \sum_{j>i} \frac{e^2}{|r_j - r_i|}$$

and

$$V_{n-e}\{r,R\} = -\sum_{\alpha,i} \frac{Z_\alpha e^2}{|R_\alpha - r_i|} \quad , \qquad \text{(A.1)}$$

where subscripts *e-e* and *n-e* indicate the electron-electron and nuclei-electron interactions, respectively. R_α and Z_α are the coordinates and the charge of the αth nucleus and finally r is the coordinate of the electrons. The electron-electron Coulomb repulsion in equation (1.1) is such that this differential equation is non-separable. It is therefore impossible to obtain an exact solution of the Schrödinger equation for the Hamiltonian in equation (1.1) without further approximations.

In order to understand the Born-Oppenheimer approximation better, one can think of the molecules as a collection of particles of different masses, which are connected by springs to each other. If this system is held fixed and then released simultaneously, a force ***F*** between two particles having masses m_1 and m_2 ($m_1 << m_2$) contributes an acceleration

$$a_1 = F/m_1 \quad and \quad a_2 = F/m_2 \quad . \qquad \text{(A.2)}$$

Depending on the masses, the acceleration of the lighter particle will be much larger than that of heavy particle. This means that after a reasonable time period, the average velocity of the light particles (electrons) will be larger than that of the heavy particles (nuclei). This basic mechanics is the idea behind the Born-Oppenheimer approximation, of course within the analogy of macroscopic states to the microscopic molecules.

The Born-Oppenheimer approximation can be formulated in a series of steps. The first step is to write the Hamiltonian and Schrödinger equation in terms of the electronic eigen functions and electronic energies. If the electronic Hamiltonian is as in (1.1), then the Schrödinger equation can be written as

$$H_e\psi_\varepsilon^e(r_i;R_\alpha)=E_\varepsilon^e(R_\alpha)\psi_\varepsilon^e(r_i;R_\alpha) \quad , \tag{A.3}$$

where ε represents the quantum numbers of the set of electrons. As mentioned earlier, the Born-Oppenheimer approximation assumes a geometrically fixed nuclear position meaning that nuclei do not move during a time interval characteristic of the motion of the electrons in their orbits. Therefore, the electronic Schrödinger equation can be solved for some fixed set of nuclear coordinates. Generally a new set of solutions and new wave functions and energies can be found for a different fixed nuclear coordinate set. Because of the electron-nucleus interactions in the electronic Hamiltonian, the electronic energy qualifies as part of the potential energy of nuclear motion.

The second step is the combination of a particular electronic state with the coulomb nuclear repulsion terms. In this case, one should write the time-independent nuclear Schrödinger equation as

$$H^n(R_\alpha)\psi_{\varepsilon\nu}^n(R_\alpha)=E_{\varepsilon\nu}\psi_{\varepsilon\nu}^n(R_\alpha) \quad , \tag{A.4}$$

where H^n is the nuclear Hamiltonian, $\psi_{\varepsilon\nu}^n$ is the nuclear wave function and $E_{\varepsilon\nu}$ is the nuclear energy. The energy $E_{\varepsilon\nu}$ is constant for a particular electronic state (ε) and for a specific quantum number (ν) is required to specify a nuclear quantum state.

The third and the last step is to write the stationary-state wave function of the molecule as the products of the solutions to the electronic and nuclear wave functions

$$\psi_{\varepsilon\nu}(r_i;R_\alpha)=\psi_\varepsilon^e(r_i;R_\alpha)\psi_{\varepsilon\nu}^n(R_\alpha) \quad . \tag{A.5}$$

The molecular Schrödinger equation can then be written as

$$\begin{aligned} &\left(T_e + T_n + V_{ee} + V_{en} + V_{nn}\right)\Psi_E = E\Psi_E \\ &where, \\ &\Psi_E = \psi^e\psi^n \end{aligned} \quad , \tag{A.6}$$

where T and V represent the kinetic and potential energy operators respectively. After a few simple mathematical arrangements, one can write the Schrödinger equation as

$$\left(T_n + E^e + V_{nn}\right)\psi^e\psi^n = E\,\psi^e\psi^n \quad . \tag{A.7}$$

Equation (1.34) can be rewritten using the commutator

$$\psi^e_\varepsilon\left(T_n + V_{nn} + E^e\right)\psi^n + \left[T_n, \psi^e\right]\psi^n = E\,\psi^e\psi^n$$

$$\begin{aligned} &where, \\ &T_n\psi^e - \psi^e T_n \end{aligned} \quad . \tag{A.8}$$

If the commutator is zero, one can separate the wave function into electronic and nuclear parts as

$$\psi_E = \psi^e\psi^n \quad . \tag{A.9}$$

Therefore, it is possible to say that the Born-Oppenheimer approximation is valid only for zero or small commutators compared to the other terms in equation (1.8). Otherwise, this approximation fails. In order to obtain a more precise solution, one can use time-independent perturbation theory [273]. The Hamiltonian can be written as

$$H\left(r_i, R_\alpha\right) = H^e\left(r_i\right) + H^{en}\left(r_i, R_\alpha\right) + H^n\left(R_\alpha\right) \quad . \tag{A.10}$$

[273] Blaizot, J-P., *Quantum Theory of Finite Systems*, MIT Press, Cambridge, Massachusetts, 1986.

As assumed previously, if $H^{en}(r_i,R_\alpha)$ is zero, the Hamiltonian would be separable into electronic and nuclear parts. Unfortunately, there is no particular evidence for $H^{en}(r_i,R_\alpha)$ to be zero or small. The Born-Oppenheimer approximation indicates the wave function can be written as

$$\psi_{\varepsilon\nu}(r_i,R_\alpha)=\psi_\varepsilon^e(r_i,R_\alpha)\psi_{\varepsilon\nu}^n(R_\alpha) \tag{A.11}$$

with

$$E_{\varepsilon\nu} = E_{\varepsilon\nu}^n \quad . \tag{A.12}$$

It is possible to expand the molecular wave function as

$$\psi_{\varepsilon\nu} = \psi_\varepsilon^e\psi_{\varepsilon\nu}^n + \psi_{\varepsilon\nu}^{(1)} + \psi_{\varepsilon\nu}^{(2)} + \cdots \quad . \tag{A.13}$$

Similarly

$$E_{\varepsilon\nu} = E_{\varepsilon\nu}^n + E_{\varepsilon\nu}^{(1)} + E_{\varepsilon\nu}^{(2)} + \cdots \quad . \tag{A.14}$$

Therefore, the Schrödinger equation in equation (1.28) becomes

$$\begin{aligned} H[\psi_\varepsilon^e\psi_{\varepsilon\nu}^n + \psi_{\varepsilon\nu}^{(1)} + \psi_{\varepsilon\nu}^{(2)} + \cdots] = \\ [E_{\varepsilon\nu}^n + E_{\varepsilon\nu}^{(1)} + E_{\varepsilon\nu}^{(2)} + \cdots][\psi_\varepsilon^e\psi_{\varepsilon\nu}^n + \psi_{\varepsilon\nu}^{(1)} + \psi_{\varepsilon\nu}^{(2)} + \cdots] \quad . \end{aligned} \tag{A.15}$$

By using the equation (1.37), the first term in the left hand side of the above equation can be written as

$$\begin{aligned} H\psi^e\psi^n &= (H^e + H^{en})\psi^e\psi^n + H^n\psi^e\psi^n \\ &= E^e\psi^e\psi^n + \psi^e H^n\psi^n + [H^n,\psi^e]\psi^n \\ &= \psi^e(H^n + E^e)\psi^n + [T_n,\psi^e]\psi^n \\ &= E^n\psi^e\psi^n + [T_n,\psi^e]\psi^n \quad . \end{aligned} \tag{A.16}$$

One can obtain an approximate first-order equation by substituting equation (1.16) into equation (1.42) and keeping only first order terms

$$[T_n,\psi_\varepsilon^e]\psi_{\varepsilon\nu}^n + H\psi_{\varepsilon\nu}^{(1)} = E_{\varepsilon\nu}^n\psi_{\varepsilon\nu}^{(1)} + E_{\varepsilon\nu}^{(1)}\psi_\varepsilon^e\psi_{\varepsilon\nu}^n \quad . \tag{A.17}$$

According to the closure property and the orthonormality relation, eigenfunctions of wave equations must satisfy the following two equations

$$\sum_{\varepsilon} \psi_{\varepsilon}^{e}(r_i, R_\alpha)^{*} \psi_{\varepsilon}^{e}(r_i', R_\alpha) = \delta(r_i - r_i') \quad ,$$

and

$$\int \psi_{\varepsilon}^{e}(r_i, R_\alpha)^{*} \psi_{\varepsilon'}^{e}(r_i, R_\alpha) d\tau_e = \delta_{\varepsilon\varepsilon'} \quad ,$$

where $d\tau_e = dr_1 dr_2 \ldots dr_{N_e}$. (A.18)

Similar relations should hold for the nuclear wave functions. If one expands the wave function in the set of product functions of electronic and nuclear wave functions, an expansion coefficient will appear in front of the product. Assuming all expansion coefficients are small (<<1), then the first order correction to the wave function will be smaller than that of zeroth-order term. Hence, the Born Oppenheimer approximation is a good approximation to the molecular wave function. The details of the expansion coefficient calculation can be found in reference [274]. The Born-Oppenheimer approximation fails when the electronic energy levels are degenerate or nearly degenerate. As seen in Figure A.1 at $R=R_1$ the electronic levels are separated by energy gaps, so the expansion coefficient is small enough to write the wave function separately in terms of electronic and nuclear wave functions. However, at $R=R_2$ a near degeneracy in the electronic energy occurs. At this value of R, the expansion coefficient is large and the Born-Oppenheimer approximation fails [275].

[274] M. A. Morrison, T. L. Estle, N. F. Lane, Quantum Statea of Atoms, Molecules, and Solids, Prentice-Hall Inc, new Jersey, 1976.
[275] M. A. Morrison, T. L. Estle, N. F. Lane, Quantum States of Atoms, Molecules, and Solids, Prentice-Hall Inc, New Jersey, 1976.

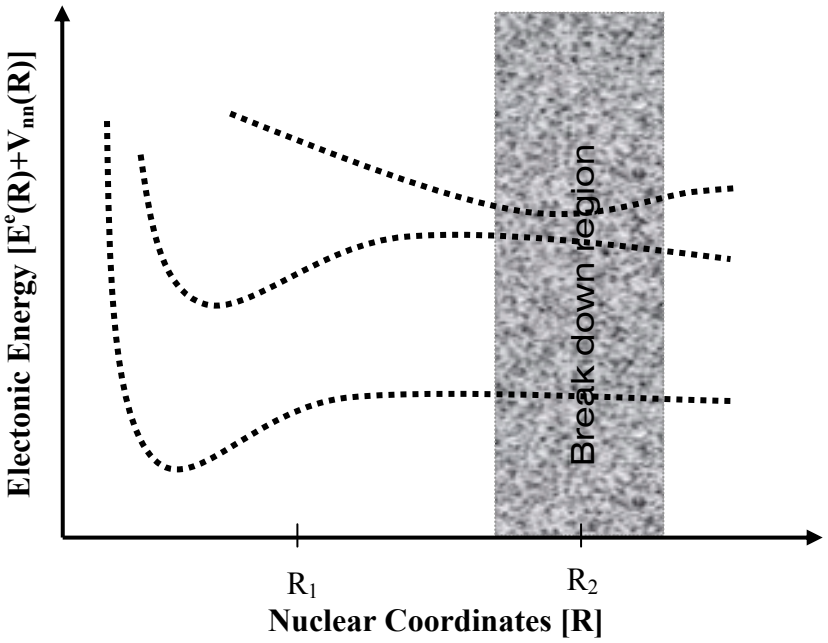

Figure A.1: Schematic of the breakdown of the Born-Oppenheimer approximation.

2. AB Initio Calculations

Energy band structure and band gap and even the structural properties of the conducting polymers can be calculated by using the ab initio evaluations [276, 277]. To solve the Schrödinger equation, the ab initio technique uses the special orthogonalized basis wave functions and realistic atomic potentials to calculate interaction integrals [278].

The exact solution of the Schrödinger equation for many electron systems (N>1) is impossible, since the wave function ψ cannot be separated for these systems. There are several approximations developed by different scientists, such as Kinoshita and Pekeris [279, 280], Hylleraas [281] etc. The Hartree-Fock approximation, which gives the approximate

[276] E. Yurtsever, M. Yurtsever, Synthetic Metals, Vol. 101, pp 335-336, 1999.
[277] R. V. Bantaculo, A. C. Alguno, R. M.Vequizo, A. S. Dahili, H. Miyata, E. W. Ignacio, A.M. Bacala, Proceedings Of The 17th Philippine Chemistry Congress, XavierSports and 2001.
[278] J. Mort, G. Pfister, Electronic Properties of Polymers, John Wiley and Sons, New York, 1982.
[279] T. Kinoshita, Quantum Electrodynamics, Advanced Series on Directions in High Energy Physics - Vol. 7, World Scientific, Singapore, 1990.

total wave functions for many-electron systems, can be applied to the atomic, molecular and solid-state systems [282] to find an approximated solution for the Schrödinger equation. In the next section the details of the Hartree-Fock approximation will be given.

3. Hartree-Fock Approximation

New developments in computational quantum chemistry allow applying the approximate independent-electron theories to the full Hamiltonian for a wide range of molecules and chemical compounds. There are two approximations typically employed to think about the multielectron atoms. The first is the isolated electron approximation and the other is the central field approximation. Hartree made a systematic version of the central approximation. He described the Hamiltonian for N-electron systems as

$$H = \sum_{i=1}^{N}\left[-\frac{\hbar^2}{2m_e}\nabla_i^2 - \frac{Ze^2}{r_i} + V_i^S(r_i)\right] \quad , \qquad \text{(A.19)}$$

where $V_i^S(r_i)$ is a spherical symmetric screening potential, including the spherical average of the potentials e^2/r_{ij} over the motion of all electrons (here j=1,2,…N, i≠j). After substituting the potential $V_i^S(r_i)$ in equation (1.19), the Hartree equation is obtained as

$$\left[-\frac{\hbar^2}{2m_e}\nabla_i^2 - \frac{Ze^2}{r_i} + \sum_{i\neq j}\left\langle \psi^H_{(nlm_l)_j}\left|\frac{e^2}{r_{ij}}\right|\psi^H_{(nlm_l)_j}\right\rangle\right]\psi^H_{(nlm_i)_i}(r_i) = E^H_{(nlm_i)_i}\psi^H_{(nlm_i)_i}(r_i) \quad \textit{where} \quad i = 1,2,...,N \; . \qquad \text{(A.20)}$$

---

[280] C. L. Pekeris, Physical Review, Vol. 127, 509-511 (1962).
[281] E. A. Hylleraas, *Mathematical and Theoretical Physics*, Wiley-Interscience, New York, 1970.
[282] F. F. Charlotte, The Hartree-Fock Method for Atoms, John Wiley & Sons, New York, 1977.

Once equation (1.20) has been solved, the expectation value of the Hamiltonian with respect to this wave function will give the approximate energy of the atom.

Although Hartree theory gives a good approximation of the atomic energy (~7% agreement with experimental results [18]), it is impossible to obtain accurate results while ignoring the spin of the electrons. This problem can be solved by using the Hartree-Fock approximation. However, in this case it is not easy to guess the form of the screening potential. Therefore, $V_i^S(r_i)$ should still be taken as the spherical average of the potentials e^2/r_{ij} over the motion of all electrons.

The Hartree-Fock approximation must satisfy three basic criteria. First, a Hartree-Fock approximation ψ must satisfy the anti-symmetry conditions. The anti-symmetry term comes from the spin of the electron. An electron can have two different spin quantum numbers, 1/2 and -1/2. Therefore, according to "anti-symmetry conditions" the wave function ψ can be written as

$$p_{ij}\psi = -\psi \qquad for\ all\ i, j \le N, i \ne j \quad . \tag{A.21}$$

To solve the Schrödinger equation, the Hartree-Fock method first replaces the Hamiltonian, H, by one which has a solution. So,

$$H \approx \hat{H} = \sum \left\{ -\frac{1}{2}\nabla_i^2 - \frac{Z}{r_i} + V(r_i) \right\}, \tag{A.22}$$

where the single particle potential V is used instead of the interactions between the electrons. Furthermore, it is possible to write a new wave function Φ, which is separable. Hence, the Schrödinger equation can be written as

$$\left[-\frac{1}{2}\nabla_i^2 - \frac{Z}{r_i} + V(r_i) \right]\phi(i) = E_i\phi(i) \quad . \tag{A.23}$$

The wave function Φ can be separated into radial, angular and spin parts in spherical coordinates. By adding an anti-symmetrizing operator A it is possible to write the wave function Φ as the Slater determinant

$$\Phi = \frac{1}{(N!)^{1/2}} \begin{vmatrix} \phi_1(1) & \phi_1(2) & \cdots & \phi_1(N) \\ \phi_2(1) & \phi_2(2) & \cdots & \phi_2(N) \\ \vdots & & & \\ \phi_N(1) & \phi_N(2) & \cdots & \phi_N(N) \end{vmatrix} \quad . \tag{A.24}$$

The Hartree-Fock method solves the problem of defining approximate many-electron wave functions. This method assumes that the wave function Ψ must consist of sums of products of N spin-orbitals of the form

$$\phi_{nlm_l m_s}(r,\theta,\varphi,\sigma) = \left(\frac{1}{r}\right) P(nl...;r) Y_{lm_l}(\theta,\varphi)\chi_{m_s} \quad , \tag{A.25}$$

where $\{n_j l_j m_{l_j} m_{s_j}\}$ are the quantum numbers, *P(nl;r)* is the radial, $Y_{lm_1}(\theta,\varphi)$ is the spherical harmonic and χ_{m_s} is the spin function. Another assumption for Hartree-Fock method is the orthogonality. In other words, spin-orbitals should form an orthogonal set

$$\int \phi_{nlm_l m_s}(1)\phi_{n'l'm_{l'}m_{s'}}(1)d\tau_1 = \delta_{nn'}\delta_{ll'}\delta_{m_l m_{l'}}\delta_{m_s m_{s'}} \quad , \tag{A.26}$$

where δ_{ij} is the Kronecker delta function, which is defined as

$$\begin{aligned} \delta_{ij} &= 0, \quad i \neq j \\ &= 1, \quad i = j \end{aligned} \quad . \tag{A.27}$$

The last requirement of the Hartree-Fock approximation is that the wave function Ψ must be an eigenfunction of the total angular momentum operators L^2, L_z as well as the total spin operators S^2 and S_z, that is

$$\begin{aligned} L^2\Psi &= L(L+1)\Psi \qquad S^2\Psi = S(S+1)\Psi \\ L_z\Psi &= M_L\Psi \qquad\quad S_z\Psi = M_S\Psi \end{aligned} \quad . \tag{A.28}$$

With regard to the above conditions, the Hartree-Fock equations can be written as,

$$\left[-\frac{\hbar^2}{2m_e}\nabla_i^2-\frac{Ze^2}{r_i}\right]\psi^{HF}_{(nlm_i)_i}(r_i)+$$

$$\sum_{\substack{j=1\\ j\neq i}}^{n}\left\{\psi^{HF}_{(nlm_i)_i}(r_i)\left\langle\psi^{HF}_{(nlm_i)_j}(r_j)\left|\frac{e^2}{r_{ij}}\right|\psi^{HF}_{(nlm_l)_j}\right\rangle\right.$$

$$\left.-\psi^{HF}_{(nlm_i)_i}(r_i)\delta_{m_{s_i}}\delta_{m_{s_j}}\left\langle\psi^{HF}_{(nlm_i)_j}(r_j)\left|\frac{e^2}{r_{ij}}\right|\psi^{HF}_{(nlm_l)_j}\right\rangle\right\}=$$

$$E^{HF}_{(nlm_i)_i}\psi^{HF}_{(nlm_i)_i}(r_i) \quad . \qquad \text{(A.29)}$$

These equations properly account for spin-pairing and result in lower energies and in better agreement with measurements. The detailed derivation of the Hartree-Fock equation will not be given in this chapter, since it is beyond the scope of this study.

3.1 Examples of Hartree-Fock Calculations for Polymers

The electronic structures and band-gaps of polymers, modeled using Hartree-Fock, Hückel, and Density Functional theories, have been reported [26-32]. The first ab initio calculation for the energy band structure of polyacetylene was reported by Andrė and Leroy [283]. After their calculation many different scientists performed ab initio calculations for polyacetylene and for other conducting polymers [284, 285, 286]. A. K. Bakhshi investigated the electronic structure and conduction properties of oxygen and nitrogen containing polymers, such as polypyrrolo[3,4-C]pyrrole (PPPY) and

[283] J. M. Andrė and G. Leroy, Theoretical Chemistry Acta, Vol.9, 123 (1967).
[284] A. Yamashiro, A. Ikawa, H. Fukutome, Synthetic Metals, Vol. 85, 1061-1064 (1997).
[285] S. A. Jansen, T. Duong, A. Major, Y. Wei, L. T. Sein Jr., Synthetic Metals, Vol. 105, 107-113 (1999).
[286] A. K. Bakhshi, G. Gandhi, Solid State Communications, Vol. 129, 335-340 (2004).

polyfurano[3,4-C]furan (PFFU) [287]. Table A.1 gives the summary of A. K. Bakhshi's work on the electronic properties of various polymers calculated based on ab initio calculations.

Table A.1: Calculated electronic properties (eV) of some polymers

Polymer	Ionization Energy	Electron Affinity	Band Gap	Reference
Polythiophene[3,4-C] thiophene (PTTP)	7.048	5.076	1.972	
Polypyrrolo[3,4-C] pyrrolo (PPPY)	6.693	2.294	4.399	
Trans-polyacetylene	8.482	1.968	6.514	
Cis- polyacetylene	8.990	1.858	7.131	
Polypyrrole	8.826	-0.275	9.102	
Polythiophene (PTP)	9.499	1.362	8.137	

There has been an effort also for theoretical modeling of the structural and electronic properties of oligomers [33-35]. S. Millefiori et al. [288], J. B. Logowski [289], and G. Moro et al. [290] used the Hartree-Fock theory to calculate the bond lengths and excitation energies of selenophene, phenylene vinylene, and thiophene oligomers, respectively.

4. Hückel and SSH Models

Organic conducting polymers have a framework of alternating double, σ-bonds, and single, π-bonds. Since the π-electrons are less bound to the core of the polymer

[287] A. K. Bakhshi, Journal of Molecular Structure (Theochem), Vol. 361, 259-268 (1996).
[288] S. Millefiori, A. Alparone, Synthetic Metals, Vol. 95, 217-224 (1998).
[289] J. B. Lagowski, Journal of Molecular Structure (Theochem), Vol. 589-590, 125-137 (2002).
[290] G. Moro, G. Scalmani, U. Cosentino, D. Pitea, Synthetic Metals, Vol. 108, 165-172 (2000).

backbones than σ-electrons, it is reasonable to assume that π-electrons are involved in both physical and chemical processes and play an important role in determine the electrical and optical properties of the polymers. Hückel theory is based on this idea and describes the molecule using a Hamiltonian for π-orbitals and all other interactions except those orbitals are neglected [291]. The simplicity of the Hückel theory ignores all other interactions except nearest neighbor interactions. In practice, Hückel orbits form an orthonormal set. Examples and details of this theory can be found in many textbooks [292, 293, 294]. Here only the Hückel π-band structure of regular polyacetylene consisting of a single π orbital per unit cell (Figure A.2 (a)) and two π orbitals per unit cell will be given.

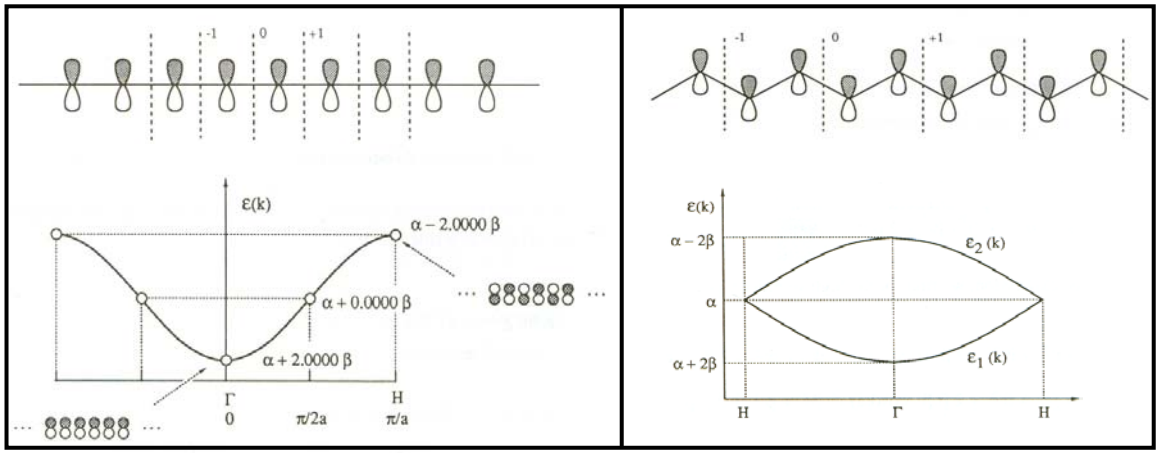

(a) **(b)**

Figure A.2: Hückel π-band structure of polyacetylene (a) a single π orbital per unit cell (b) two π orbitals per unit cell (Reproduced by the permission of World Scientific) [291]

Another model to describe the electronic structure of the conjugated polymers uses Su-Schrieffer-Heeger (SSH) Hamiltonian approach [295]. This model takes into account the electron-phonon interactions as well as electron-electron interactions in the conjugated

[291] J-M André, J. Delhalle, J-L Brédas, Quantum Chemistry Aided Design of Organic Polymers, World Scientific, Singapore, 1991.
[292] C. A. Coulson, R. B. Mallion, *Hückel Theory for Organic Chemist*, Academic Press, London, 1978.
[293] Arvi Rauk, *Orbital Interaction Theory of Organic Chemistry*, John and Sons Inc., New York, 1994.
[294] L. Salem, The Molecular Orbital Theory of Conjugated Systems, W. A. Benjamin, New York, 1966.
[295] J. L. Bréda, R. R. Chance, Conjugated Polymeric Materials: opportunitie in Electronics, Optoelectronics and Molecular Electronics, NATO ASI Series, Series E: Applied Sciences-Vol. 182, 1990.

polymers. The electron-phonon interaction leads to the Peierls transition. Figure A.3 shows the Peierls transition for polyacetylene [296].

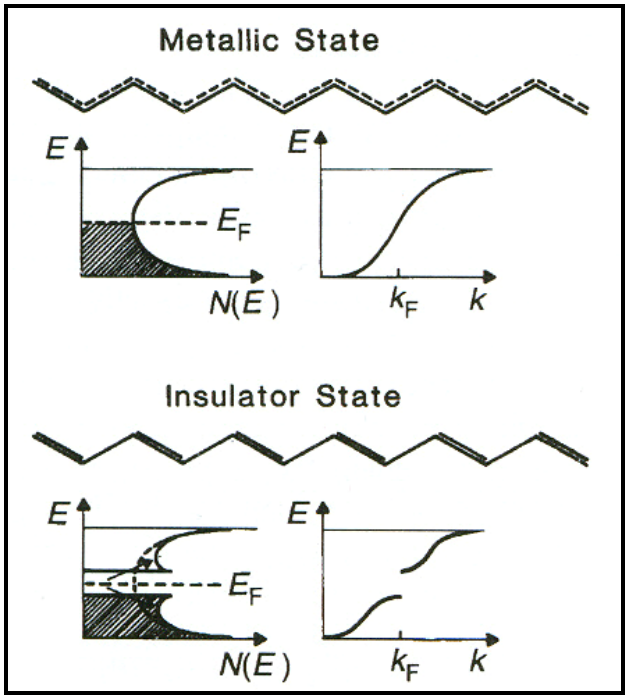

Figure A.3: Peierls distortion for polyacetylene (Reproduced by the permission of WILEY) [297].

Basically, Peierls distortion, which is also known as the dimerization, can be characterized by the bond length alternation between single and double bonds. If the bond length of a single bond is *a* and that of double bonds is *b* for alternating carbon bonds in trans-polyacetylene, the relative difference of the bond lengths gives the bond-alternation parameter, p given as

$$p = \frac{a-b}{(a+b)/2} \quad . \tag{A.30}$$

[296] T. A. Skotheim, Handbook of conducting Polymers, Vol. 2, Marcel Dekker Inc., New York, 1986.
[297] H. S. Nalwa, Handbook of Organic Conductive Molecules and Polymers, Vol. 2, John Wiley & Sons, New York, 1997.

Since a double bond is shorter than a single bond, p is greater than zero in this case. The bond-alternation parameter will change sign with existence of a conjugational defect (soliton). In Figure A.8, a hypothetical metallic state can be seen. In this state the π-electrons are completely delocalized and they do not form bonds. Depending on the temperature, an opening in the energy band occurs making the polymer a semiconductor. This metal-to-semiconductor transition is known also as the Peierls transition. Extensive studies of the dynamics of solitons have been performed using the Su-Schrieffer-Heeger approach [298]. In order to understand the SSH theory, it is better to write SSH Hamiltonian for polyacetylene first. The SHH Hamiltonian of polyacetylene in terms describing the coordinate for the CH group along the molecular symmetry can be expressed as

$$H_{SSH} = -\frac{M}{2}\sum_n u_n^2 + \frac{K}{2}\sum_n \left(u_n - u_{n+1}\right)^2 - \sum_{n,s}\left[t_0 + \alpha\left(u_n - u_{n+1}\right)\right]\left(c_{n+1,s}^{\dagger}c_{n,s} + c_{n,s}^{\dagger}c_{n+1,s}\right) \quad , \qquad \text{(A.31)}$$

where M is the mass of the CH group, u_n is the configuration coordinate for displacement of the nth CH group along the molecular symmetry axis, K is the elastic constant of the σ-bond, $4t_0$ is the width of the π band, and $c_{n,s}^{\dagger}$ and $c_{n,s}$ are the annihilation and creation operators for a π electron on site n with spin s, respectively. The first two terms of equation (A.31) represents the kinetic energy of the system, the second term is the elastic energy of the system and the third term is the electron hopping term. For the perfect dimerized structure of polyacetylene, the displacements take the form

$$u_n = \pm(-1)^n u_0 \quad , \qquad \text{(A.32)}$$

where n=0 indicates the origin or starting point, and + and - signs represent the opposite directions from the soliton. The Peierls gap (2Δ) for the polyacetylene can be written as

$$2\Delta = 16t_0 \exp\left[-\left(1+\frac{1}{2\lambda}\right)\right] \quad \text{where} \quad \lambda = 2x^2/(\pi t_0 K) \quad . \qquad \text{(A.33)}$$

[298] W. P. Su, J. R. Schrieffer, A. J. Heeger, Physical Review Letters, Vol.42, 1698-1701 (1979).

APPENDIX B

TRANSPORT PROPERTIES OF CONDUCTING POLYMERS

There are different transport mechanisms for conducting polymers depending on the morphology and the doping level of the polymer. Generally, charge transport mechanisms are based on the motion of radical cations or anions, which are created by oxidation or reduction, along a polymer chain. Therefore, it is better to describe the concepts of soliton, polaron, and bipolaron before identifying the electrical conductivity and transport mechanisms of conjugated polymers.

1. Solitons, Polarons, and Bipolarons

Solitons or "kinks" can be thought as the defects in the polymer structure. It is better to examine this topic by regarding polyacetylene, which is the simplest among conjugated polymers with alternating carbon and hydrogen bonds [299]. Consider the two energetically equivalent bond isomer forms obtained from one another simply by exchanging the single and double bound. This type of polyacetylene is called the all-trans form, which is the thermodynamically most stable form [ ]. When two energetically equivalent bond isomer forms touch each other, a cation or anion defect is created on the polyacetylene backbone. Since this defect creates a boundary between two equal energy moieties, it can move in either direction without affecting the energy of the backbone.

[299] H. S. Nalwa, Handbook of Organic Conductive Molecules and Polymers, Vol. 2, John Wiley & Sons, Chichester, 1997.

The name of "soliton" comes from that of mathematical solitary waves, which describes the motion of this defect [300, 301].

Solitons can be neutral, or negatively or positively charged. A negatively charged soliton results from adding an electron to a soliton. Similarly when the soliton loses an electron a positively charged soliton is formed. The interactions between the chains result in an attractive interaction between the solitons. Because of this interaction, solitons move toward each other and at some distance form one common defect called a polaron. Polarons have both charge and spin. Obviously, when oppositely charged solitons interact, they will annihilate. Interchain interactions will push the solitons together and the electrostatic force keeps them apart. Therefore, as a result of these forces solitons will be stabilized at a point and this final defect is called a bipolaron. Figure B.1 indicates all of these defects for trans-polyacetylene [297].

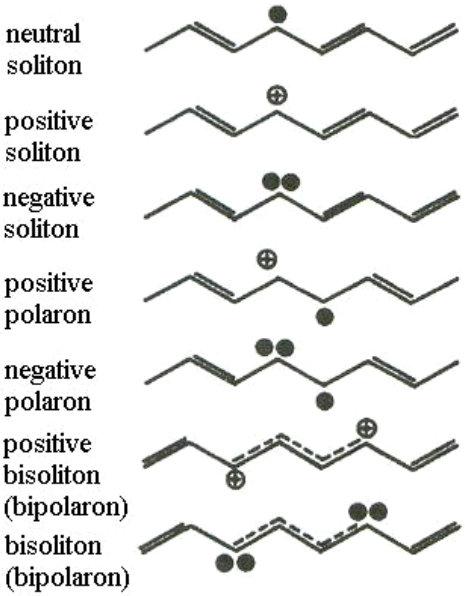

Figure B.1: Complex conjugational defects in trans-polyacetylene (Reproduced by the permission of WILEY) [297].

[300] J. I. Kroschwitz, Electrical and Electronic Properties of Polymers: A State-of-the-Art Compendium, John Wiley & Sons, New York, 1988.

[301] A. J. Hegeer, The Journal of Physical Chemistry B, Vol. 105, 8475-8491 (2001).

2. Theory of Bloch-Type Conduction

The conductivity of the delocalized or coherent wave functions can be explained by Bloch-type conduction. On the other hand, for nonperiodic polymers, such as randomly doped polyacetylene, the conduction mechanism cannot be explained with the Bloch theorem, since most of the states are localized. For this case, the notion of the hopping mechanism, which be explained in the next section, can be applied.

If the widths of the valance and conduction bands of a polymer are much greater than the thermal energy at room temperature ($\Delta E/k_BT>>1$), the transport properties can be explained by the deformation potential approximation. This approximation was introduced by Bardeen and Shockley [302]. According to their theory, the shifts in the valance and conduction band can be written in terms of deformation potential constants (D_c, D_v) and dilatation (Δ) as

$$\delta\varepsilon_{c,l} = D_c\Delta, \quad \delta\varepsilon_{v,u} = D_v\Delta \ , \tag{B.1}$$

where the subscripts v,l and c,u indicates the upper edge of the valance band and lower edge of the conduction band, respectively. The electric current density (j) is linearly proportional to the electric field (E) for the macroscopic response of the electrons. The proportionality constant gives the conductivity as

$$j = \sigma E \ . \tag{B.2}$$

The electrical conductivity can be written in terms of band gap ΔE, Boltzmann constant k_B and temperature T as

$$\sigma(T) = \sigma_0 \exp\left(-\Delta E/2k_BT\right) \ . \tag{B.3}$$

By assuming both electrons and holes are present in a semiconductor, the pre-exponential function σ_0 becomes

$$\sigma_0 = \frac{2e^2\hbar c_l}{\pi}\left(\frac{1}{m_e^* D_c^2} + \frac{1}{m_h^* D_v^2}\right) \ , \tag{B.4}$$

[302] J. Bardeen, W. Shockley, Physical Review, Vol. 80, 72-80 (1950).

where c_l is the longitudinal elastic constant, m_e^* and m_h^* are effective masses of an electron and a hole, respectively.

For some wide band gap polymers, such as DNA and proteins, transport properties have been reported [303]. The bandwidth and drift mobility of the adenine stack was calculated as 0.246 eV and 156 cm^2/Vs, respectively, using the Bloch type transport theory [55]. If the bandwidth of the polymer is comparable with the thermal energy, the scattering effect throughout the whole conduction and valance band should be taken into account to calculate the transport properties. For the narrow-band polymers, since the perturbing Hamiltonian is used to determine the electronic band structure of the solid, the calculation of the transport parameters is complex. In this case, the Bloch –type conductivity depends on the equilibrium charge carrier distribution, scattering matrix elements and the trial wave function.

3. Theory of Hopping Conduction

As explained in section 1.2, solitons are the discontinuities in the pattern of alternating single and double bonds. Motion of a soliton discontinuity along the polymer chain is not responsible for the charge transport. However, an inter chain soliton hoping mechanism could contribute to electrical conduction [304].

There are two main studies explaining the charge transport in polymers using hoping mechanism. Mele et al. [305] introduced a model in which the electron could hop between states produced by solitons pinned at dopant sites to yield observed conductivities. One year after Mele et al., Kivelson introduced an alternative model for transport mechanism in polyacetylene [306]. This model is also based on the hoping between soliton sites, but it

[303] J. J. Ladik, Quantum Theory of Polymers as Solids, Plenum Press, New York, 1988.

[304] A. B. Kaiser, Reports on Progress in Physics, Vol. 64, 1-49 (2001).

[305] E. J. Mele, M. J. Rice, Physical Review B, Vol. 23, 5397-5412 (1981).

[306] S. Kivelson, Physical Review B, Vol. 25, 3798-3821 (1982).

is only valid for low doping levels. It requires the presence of a neutral soliton, which can hop to a charged soliton site with small activation energy. Although this model has its own problems, it works well for lightly doped trans-polyacetylene.

There are number of other theories explaining the charge transport in a polymer chain, but most of them failed to describe the inter-chain charge transport, which is the rate limiting step. In general, for all conducting polymers, the electrical conductivity can be written in terms of the concentration of the solitons (C) and the hopping probability of the two solitons separated by x carbon atoms [P(x)] as

$$\sigma = C\int P(x)dx \quad . \tag{B.5}$$

Equation (1.90) indicates that the soliton pairs (bipolarons) can hop to the next chain isoenergetically with a certain probability. This probability is a function of vibrational overlap and the probalities of finding a second charge soliton and unocc (1.6) on the other chain. The mobility of a hopping particle depends on the diffusion of these particles in the polymer matrix and can be written as

$$\mu = eD/k_BT \quad where \quad D = (1/2)\nu L^2 \quad , \tag{B.6}$$

where e is the charge of an electron, D is the diffusivity, ν is the hop frequency and L is the mean hop length. Since the diffusion is a thermally activated process, mobility can be expressed as

$$\mu = \mu_0 \exp(-E_a / k_BT) \quad . \tag{B.7}$$

Thermal energy k_BT decreases as temperature decreases indicating that there are fewer nearby states with assessable energies. Hence the mean range of hopping increases by decreasing the temperature. This idea leads to a more general from of the hoping conductivity, which can be expressed by Mott's law given as

$$\sigma(T) = \sigma_0 \exp\left[-\left(\frac{T_0}{T}\right)^{\gamma}\right] \quad . \tag{B.8}$$

Here, the value of γ changes depending on the hopping range. For example, it is equal to 1/4 for hopping in three dimensions and 1/2 for one-dimensional hopping. If the thermal energy is sufficiently high for hopping in the nearest neighbors, equation (1.8) reduces the simple activated form with γ=1.

One dimensional hoping has been emphasized as the major conductivity mechanism in conducting polymers [307, 308], in which the polymer chains traverse disordered regions to connect crystalline conductive islands. In other words, it can be thought that doped conducting polymer consists of a metallic "island" surrounded by low conducting "beaches" [309]. Tunneling can occur between metallic islands, if the metallic regions are large enough that the electrostatic charging energy is much smaller than the thermal energy. In this case the conductivity can be written as a function of temperature as

$$\sigma(T) = \sigma_t \exp\left[-\left(\frac{T_t}{T + T_s}\right)\right] \quad , \qquad \text{(B.9)}$$

where the σ_t is pre-exponential constant, T_t is the temperature at which the thermal voltage fluctuation is large enough to overcome a simple parabolic barrier and the ratio T_t/T_s determines the tunneling for the low temperature limits.

[307] A.J. Epstein, W.-P. Lee, V.N. Prigodin, Synthetic Metals, Vol. 117, 9-13 (2001).

[308] C.O. Yoon, M. Reghu, D. Moses, A.J. Heeger, Y. Cao, T.-A Chen, X. Wu, R.D. Rieke, Synthetic Metals, Vol. 75, 229-239 (1995).

[309] A. G. MacDiarmid, Synthetic Metals, Vol. 125, 11-22 (2002).

VITA

Nurdan Demirci Sankır was born in Bilecik, Turkey. She graduated with highest honors from primary to high school and joined the highest-ranking university, Middle East Technical University, in Turkey. She received both B.S. and M.S. degree in Physics from the same university. She completed the Solid-State Physics program during her B.S. education. She was interested in semiconductors and related technologies and studied theoretical aspects of metal-semiconductor contact resistance and measurement techniques in her M.S. education. In fall of 2002, she enrolled at Virginia Polytechnic Institute and State University for her Ph.D. in Materials Science and Engineering department. She worked under the guidance of Prof. Richard O. Claus and studied on the flexible electronics and related process technologies. She was awarded the Alfred E. Knobler Scholarship during her MEng and Ph.D. studies at Virginia Tech. She will join NanoSonic Inc. as research scientist after completing her doctoral degree.